UNIVERSIDADE FEDERAL DE GOIÁS (UFG)/

UNIVERSIDADE FEDERAL DE CATALÃO (UFCAT) em implantação

PROGRAMA DE PÓS-GRADUAÇÃO EM ENGENHARIA DE PRODUÇÃO

UNIDADE ACADÊMICA DE ENGENHARIA (FENG)

AREA DE CONCENTRAÇÃO EM ENGENHARIA DE OPERAÇÕES E PROCESOSS INDUSTRIAIS

ANALYSIS AND OPTIMIZATION OF THE TIG-MIG/MAG PROCESS VARIABLES ON THE WELDING BEAD GEOMETRY PARAMETERS

EVANIELLY GUIMARÃES CORREIA

Catalão – GO

2021

UFG

UNIVERSIDADE FEDERAL DE GOIÁS
UNIDADE ACADÊMICA ESPECIAL DE ENGENHARIA

TERMO DE CIÊNCIA E DE AUTORIZAÇÃO (TECA) PARA DISPONIBILIZAR VERSÕES ELETRÔNICAS DE TESES

E DISSERTAÇÕES NA BIBLIOTECA DIGITAL DA UFG

Na qualidade de titular dos direitos de autor, autorizo a Universidade Federal de Goiás (UFG) a disponibilizar, gratuitamente, por meio da Biblioteca Digital de Teses e Dissertações (BDTD/UFG), regulamentada pela Resolução CEPEC nº 832/2007, sem ressarcimento dos direitos autorais, de acordo com a Lei 9.610/98, o documento conforme permissões assinaladas abaixo, para fins de leitura, impressão e/ou download, a título de divulgação da produção científica brasileira, a partir desta data.

O conteúdo das Teses e Dissertações disponibilizado na BDTD/UFG é de responsabilidade exclusiva do autor. Ao encaminhar o produto final, o autor(a) e o(a) orientador(a) firmam o compromisso de que o trabalho não contém nenhuma violação de quaisquer direitos autorais ou outro direito de terceiros.

1. Identificação do material bibliográfico

[X] Dissertação [ ] Tese

2. Nome completo do autor

EVANIELLY GUIMARÃES CORREIA

3. Título do trabalho

ANALYSIS AND OPTIMIZATION OF THE TIG-MIG/MAG PROCESS VARIABLES ON THE WELDING BEAD GEOMETRY PARAMETERS

4. Informações de acesso ao documento (este campo deve ser preenchido pelo orientador)

Concorda com a liberação total do documento [X] SIM [ ] NÃO[1]

[1] Neste caso o documento será embargado por até um ano a partir da data de defesa. Após esse período, a possível disponibilização ocorrerá apenas mediante:
a) consulta ao(à) autor(a) e ao(à) orientador(a);
b) novo Termo de Ciência e de Autorização (TECA) assinado e inserido no arquivo da tese ou dissertação.
O documento não será disponibilizado durante o período de embargo.
Casos de embargo:
- Solicitação de registro de patente;
- Submissão de artigo em revista científica;
- Publicação como capítulo de livro;
- Publicação da dissertação/tese em livro.

Obs. Este termo deverá ser assinado no SEI pelo orientador e pelo autor.

Documento assinado eletronicamente por **Andre Alves De Resende**, **Professor do Magistério Superior**, em 17/12/2021, às 17:06, conforme horário oficial de Brasília, com fundamento no § 3º do art. 4º do Decreto nº 10.543, de 13 de novembro de 2020.

Documento assinado eletronicamente por **EVANIELLY GUIMARÃES CORREIA**, **Discente**, em

17/12/2021, às 17:41, conforme horário oficial de Brasília, com fundamento no § 3º do art. 4º do Decreto nº 10.543, de 13 de novembro de 2020.

A autenticidade deste documento pode ser conferida no site https://sei.ufg.br/sei/controlador_externo.php?acao=documento_conferir&id_orgao_acesso_externo=0, informando o código verificador **2584412** e o código CRC **636D8393**.

EVANIELLY GUIMARÃES CORREIA

ANALYSIS AND OPTIMIZATION OF THE TIG-MIG/MAG PROCESS VARIABLES ON THE WELDING BEAD GEOMETRY PARAMETERS

Dissertação apresentada ao Programa de Pós graduação em Engenharia de Produção da Universidade Federal de Goiás da unidade da Universidade Federal de Goiás (UFG) / Universidade Federal de Catalão (UFCAT) em implantação, como requisito para obtenção do título de **MESTRE EM ENGENHARIA DE PRODUÇÃO**. Área de Concentração: Engenharia de Operações e Processos Industriais. Linha de pesquisa: Engenharia e Desenvolvimento de Produtos e Processos.

Orientador: Prof. Dr. André Alves de Resende

Co-orientador: Prof. Dr. Rogério Santana Peruchi

Catalão – GO

2021

O PPG encontra-se vinculado à UFG, pois não houve ainda migração pela CAPES à UFCAT (criada pela Lei 13.634 de 20 de março de 2018, por desmembramento da Universidade Federal de Goiás-UFG).

Ficha de identificação da obra elaborada pelo autor, através do
Programa de Geração Automática do Sistema de Bibliotecas da UFCAT.

Correia, Evanielly Guimarães
ANALYSIS AND OPTIMIZATION OF THE TIG-MIG/MAG PROCESS VARIABLES ON THE WELDING BEAD GEOMETRY PARAMETERS / Evanielly Guimarães Correia. - 2021.
113, CXIII f.

Orientador: Prof. Dr. André Alves de Resende Resende; co-orientador Prof. Dr. Rogério Santana Peruchi.
Dissertação (Mestrado) - Universidade Federal de Catalão, Faculdade de Engenharia, Catalão, Programa de Pós-Graduação em Engenharia de Produção, Catalão, 2021.

1. TIG-MIG/MAG. 2. hybrid welding process. 3. welding bead geometry. 4. response surface. 5. optimization. I. Resende, André Alves de Resende, orient. II. Título.

CDU 658.5

UNIVERSIDADE FEDERAL DE GOIÁS

UNIDADE ACADÊMICA ESPECIAL DE ENGENHARIA

ATA DE DEFESA DE DISSERTAÇÃO

Ata nº **24** da sessão de Defesa de Dissertação de **EVANIELLY GUIMARÃES CORREIA**, que confere o título de Mestre em Engenharia de Produção, na área de concentração em Engenharia de Operações e Processos Industriais.

"Banca Examinadora de Qualificação/Defesa Pública de Dissertação/Tese realizada em conformidade com a Portaria da CAPES n. 36, de 19 de março de 2020, de acordo com seu segundo artigo: Art. 2o A suspensão de que trata esta Portaria não afasta a possibilidade de defesas de tese utilizando tecnologias de comunicação à distância, quando admissíveis pelo programa de pós-graduação stricto sensu, nos termos da regulamentação do Ministério da Educação."

Aos **trinta dias do mês de novembro do ano de dois mil e vinte um**, a partir das **08 horas e 30 minutos**, na Sala Virtual <https://meet.google.com/kpf-mvfq-kby?hs=224>, realizou-se a sessão pública de Defesa de Dissertação intitulada **"ANALYSIS AND OPTIMIZATION OF THE TIG-MIG/MAG PROCESS VARIABLES ON THE WELDING BEAD GEOMETRY PARAMETERS"**. Os trabalhos foram instalados pelo Orientador, **Professor Doutor ANDRÉ ALVES DE RESENDE (PPGEP/UFCAT)**, com a participação dos demais membros da Banca Examinadora: **Professor Doutor CARLOS ANTONIO RIBEIRO DUARTE (PPGEP/UFCAT)**, membro titular interno, cuja participação ocorreu através de videoconferência, do **Professor Doutor LOURIEL OLIVEIRA VILARINHO (UFU)**, membro titular externo, cuja participação ocorreu através de videoconferência e do Coorientador, **Professor Doutor ROGERIO SANTANA RERUCHI (UFPB)**, cuja participação ocorreu através de videoconferência. Durante a arguição os membros da banca **não fizeram** sugestão de alteração do título do trabalho. A Banca Examinadora reuniu-se em sessão secreta a fim de concluir o julgamento da Dissertação, tendo sido a candidata **aprovada** pelos seus membros. Proclamados os resultados pelo Professor Doutor ANDRÉ ALVES DE RESENDE, Presidente da Banca Examinadora, foram encerrados os trabalhos e, para constar, lavrou-se a presente ata que é assinada pelos Membros da Banca Examinadora, aos trinta dias do mês de novembro do ano de dois mil e vinte um.

TÍTULO SUGERIDO PELA BANCA

Documento assinado eletronicamente por **Andre Alves De Resende**, **Professor do Magistério Superior**, em 30/11/2021, às 10:05, conforme horário oficial de Brasília, com fundamento no § 3º do art. 4º do Decreto nº 10.543, de 13 de novembro de 2020.

Documento assinado eletronicamente por **Carlos Antonio Ribeiro Duarte**, **Professor do Magistério Superior**, em 30/11/2021, às 10:06, conforme horário oficial de Brasília, com fundamento no § 3º do art. 4º do Decreto nº 10.543, de 13 de novembro de 2020.

Documento assinado eletronicamente por **Louriel Oliveira Vilarinho**, **Usuário Externo**, em 30/11/2021, às 10:08, conforme horário oficial de Brasília, com fundamento no § 3º do art. 4º do Decreto nº 10.543, de 13 de novembro de 2020.

Documento assinado eletronicamente por **Rogério Santana Peruchi**, **Usuário Externo**, em 30/11/2021, às 10:09, conforme horário oficial de Brasília, com fundamento no § 3º do art. 4º do Decreto nº 10.543, de 13 de novembro de 2020.

A autenticidade deste documento pode ser conferida no site https://sei.ufg.br/sei/controlador_externo.php?acao=documento_conferir&id_orgao_acesso_externo=0, informando o código verificador **2503111** e o código CRC **FD53B44D**.

Aos meus pais, irmãs e esposo

AGRADECIMENTOS

Aos meus pais Edvando Nunes Guimarães e Marlene Guimarães Correia por todo apoio;

Ao meu esposo Felipe Rodrigues do Nascimento por toda dedicação e paciência não somente durante este período, mas ao longo de toda nossa vida;

Aos meus orientadores André Alves de Resende e Rogerio Santana Peruchi pela orientação que me guiou na execução deste trabalho.

CORREIA, E. C. **Analysis and optimization of the TIG-MIG/MAG process variables on the welding bead geometry parameters**. 113p. Master dissertation, Federal University of Goiás, Catalão, Goiás, 2021.

ABSTRACT

Research on TIG-MIG/MAG (Tungsten Inert Gas - Metal Inert Gas/Metal Active Gas) hybrid welding process has increased significantly. This increase is mainly due to Market needs, which are now pushing companies to invest in more competitive processes. The aim of this study is to evaluate the operational parameters of TIG-MIG/MAG hybrid process (TIG height, MIG/MAG contact tip to work distance, distance between the electrodes, torches angles and TIG current) over the weld bead geometry (weld width, high reinforcement height, penetration depth, toe angle and dilution rate). Statistical analysis was used to evaluate the variables and their relationship to the process. CCD (Central Composite Design), RSM (Response Surface Analysis), main effects and ANOVA were some of the techniques used in the examination. An optimization model was also proposed in this study and it was applied to a specific application of welding overlay. The optimization results showed that to achieve larger weld widths one can increase the distance between the electrodes and increase the TIG electrode height. Higher reinforcement is obtained by shortening the distance between the electrodes and reducing the TIG current and also setting the TIG height at about 4.5 mm and the MIG/MAG angle at about 35º. Shallower penetration depth is obtained by lessening the TIG current, the TIG electrode height and the distance between the electrodes. And increasing the MIG/MAG angle. To decrease the toe angle, the distance between the electrodes needs to be increased along with the TIG height and the MIG/MAG to angle set to about 30º. To minimize the dilution the distance between the electrodes must be shortened along with the TIG current. The MIG/MAG angle also impacts, it presents a curvature, and the value that best minimizes the dilution is set to about 35º. The results showed that varying the studied parameters it is possible to act on the weld bead geometry. The proposed statistical model proved to be effective, and its geometry prediction results were experimentally confirmed.

Keywords: TIG-MIG/MAG; hybrid welding process; welding bead geometry; response surface; optimization.

CORREIA, E. C. **Analysis and optimization of the TIG-MIG/MAG process variables on the welding bead geometry parameters**. 113p. Master dissertation, Federal University of Goiás, Catalão, Goiás, 2021.

RESUMO

Estudos sobre o processo hibrido TIG-MIG/MAG (Tungsten Inert Gas - Metal Inert Gas/Metal Active Gas) tem crescido significativamente. Este crescimento se dá principalmente em decorrência de novas exigências de mercado. O objetivo deste estudo é examinar os parâmetros operacionais do processo hibrido TIG-MIG/MAG (Altura do eletrodo TIG, extensão do arame MIG/MAG, distância entre os eletrodos TIG e MIG/MAG, ângulos das tochas e a corrente TIG) com relação aos aspectos referente a geometria do cordão de solda (largura da solda, altura do reforço, profundidade da zona fundida da solda, ângulo de convexidade e taxa de diluição). Analise estatística foi utilizada pra examinar as variáveis e seus relacionamentos. CCD (Central Composite Design), RSM (Response Surface Analysis), análise de efeitos principais e ANOVA são algumas das técnicas utilizadas. Neste estudo é proposto um modelo de otimização aplicado para uma aplicação especifica de solda de revestimento. Os resultados do modelo de otimização mostram que para atingir soldas com maiores larguras é necessário aumentar a distância entre eletrodos e aumentar a altura do eletrodo TIG. Para obter maior altura de reforço é preciso diminuir a distância entre os eletrodos, diminuir a corrente TIG, a altura do eletrodo TIG deve ser ajustada em cerca de 4.5 mm e o ângulo da tocha MIG/MAG deve ser por volta de 35º. Para obter menor profundidade da zona fundida de solda é necessário diminuir a corrente TIG, diminuir a altura do eletrodo TIG e diminuir a distância entre eletrodos, além de aumentar o ângulo da tocha MIG/MAG. Menores ângulos de convecção são obtidos com o aumento da distância entre eletrodos, aumento da altura do eletrodo TIG e o ângulo da tocha MIG/MAG deve ser ajustado para cerca de 30º. Para minimizar a diluição deve-se diminuir a distância entre eletrodos, diminuir a corrente do TIG, o ângulo MIG/MAG deve ser ajustado para cerca de 35º. Os resultados mostram que a é possível influenciar os resultados da geometria do cordão de solda através da variação dos parâmetros analisados neste estudo. O modelo estatístico proposto provou ser efetivo e os resultados previstos foram experimentalmente confirmados.

Palavras-chaves: TIG-MIG/MAG; processo de soldagem híbrido; geometria do cordão de solda; analise de superfície de resposta; otimização.

LIST OF FIGURES

LIST OF TABLES

LIST OF EQUATIONS

LIST OF ABREVIATIONS

ANOVA – Analysis of Variance;

ASM – American Society for Metals;

AWS – American Welding Society;

CCD – Central Composite Design;

D - dilution;

d – distance between electrodes;

DCEN - Direct-Current Electrode-Negative;

DCEP – Direct-Current Electrode-Positive;

DOE – Design of Experiments;

GMAW – Gas Metal Arc Welding;

GTAW – Gas Tungsten Arc Welding;

h1 – MIG/MAG height;

h2 – TIG height;

L – MIG/MAG wire extent;

MIG/MAG – Metal Inert Gas / Metal Active Gas;

P – Penetration Depth;

PA – Penetration Area;

R – Reinforcement Height;

RA – Reinforcement Area;

RSM – Response Surface Methodology;

TC – TIG current;

TIG – Tungsten Inert Gas;

W – Weld width;

Θ – Toe Angle;

Θ1 – MIG/MAG torch angle;

Θ2 – TIG torch angle.

LIST OF CONTENTS

CHAPTER I

INTRODUCTION

Cost reduction, high quality items and more agile and even flexible production systems are common topics under discussion. Each day managers and engineers are pushed to think of new ways of providing better quality to their products with as little investment as possible. On top of that, the foreseen future requires automatization and flexibility to their process.

Research on TIG-MIG/MAG hybrid welding process has increased significantly (TIG stands for *Tungsten Inert Gas* and MIG/MAG stands for *Metal Inert Gas/Metal Active Gas*). The process is also known as GTAW-GMAW (Gas Tungsten Arc Welding – Gas Metal Arc Welding*).* This process has sown some potential in recent research (CHEN et al., 2018; ZUO et al., 2018; HUANG et al., 2019; ZONG et al., 2019; COSTA & RESENDE, 2020; AZEVEDO & RESENDE, 2021). In alignment to that, the market is constantly looking for processes that bring more competitiveness.

TIG-MIG/MAG hybrid process is a new welding method comprised of a TIG assisting a MIG/MAG process (MENG et al. 2014). This combination shows advantages of both processes such as high efficiency (DING et al. 2015) and high weld quality (MISHINA et al., 2013 & DING et al., 2015). Meng et al. (2014) complement that the TIG arc in the TIG-MIG/MAG process acts as a pre-heat source to the base metal, which increases the weld width.

Mishima et al. (2014) numerically simulated the plasma property of TIG-MIG/MAG process based on the torch angle. They were able to find out that the as the torch angle increased, it passively impacted the temperature of the plasma between the electrodes and the current between electrodes. Chen et al. (2017) analyzed the effects of TIG-MIG/MAG process on magnesium alloys and their results were in favor of the process as it provided good quality weld bead at high Welding travel speed rates.

Huang et al. (2019) proposed a swing TIG-MIG/MAG hybrid process to solve problems of lack of sidewalls in narrow gap applications. They had a satisfactory sidewall penetration and reported improvements in the weld width and weld spread.

Welding parameters such as currents, torches angle, electrode distances, welding voltage, arc behavior, droplet transfer, welding travel speed and many other parameters have been investigated in the past years in order to assess the TIG-MIG/MAG hybrid welding process.

1.1 Justification

The justification of this work lies on the gaps that still exist in the TIG-MIG/MAG hybrid process research field. There is still more to learn about the parameters such as TIG electrode hight, torches angles, TIG current and electrode distances over the weld bead geometry parameters.

There is also very little statistical analyses available in the literature involved in the experiments conducted by the researchers of the area. This could provide more reliability on the information delivered about the process itself.

The intention of this work is to provide more visibility to this process to the industry by identifying better welding parameters, to offer some guidelines about the equipment settings and analyse its potentials to acquire a reliable and productive process.

1.2 Objectives

1.2.1 General objective

The general objective of this work is to evaluate the effects of the TIG-MIG/MAG hybrid process operational parameters, namely TIG height, MIG/MAG wire extension, distance between the electrodes, torches angles and TIG current, on the weld bead geometry characteristics (weld width, high reinforcement height, penetration depth, toe angle dilution rate).

To achieve this objective a series of steps were taken. Firstly, the behavior of the process parameters was examined, then, a mathematical model was built to numerically

represent the observed behavior. Finally, as the welding overlay is the process under investigation, the optimization model was built based on its desired geometry characteristics.

1.2.2 Specific objectives

The specific objectives of this study are:

a) to evaluate the variables of the TIG-MIG/MAG welding process (TIG height, MIG/MAG wire extension, distance between the electrodes, torches angles and TI current) over the weld bead geometry characteristics (weld width, reinforcement height, penetration depth, toe angle and dilution rate);
b) to propose an optimization model for the weld bead geometry in the TIG-MIG/MAG welding process;
c) apply the optimization model to a generic case of welding overlay.

CHAPTER II

LITERATURE REVIEW

2.1 TIG welding process

TIG welding process (Tungsten Inert Gas), also widely known as GTAW (Gas Tungsten Arc Welding), is the process used to unite practically all metal parts. The weld is formed by applying heat to the parts up to their fusion point and then bonding them together. A non-consumable tungsten electrode produce the weld through an electric arc that is placed in between the non-consumable electrode and the work piece. An inert shielding gas (typically argon, helium, or a combination of them) is used to protect the heat affected zone (HAZ) and the electrode from oxidation or other contamination (GROOVER, 2010). Figure 1 illustrates the process.

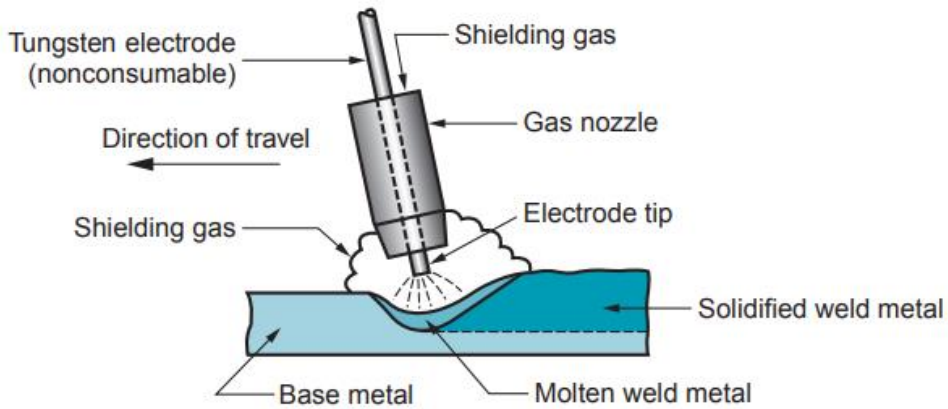

Figure 1 - Tungsten Inert Gas (TIG) process.

Source: (GROOVER, 2010).

The weld can be obtained with or without a filler metal. The latter is referred as autogenous weld. When using the filler metal, a separate rod or wire is melted by the heat of the arc, transferring the material to the weld pool. GTAW welding is primarily seen as a hand-held method, but it can also be mechanized, allowing a semi-automated or automated operation (GROOVER, 2010; DEGARMO et al. 2010).

2.1.1 TIG Equipment and materials

Figure 2 displays the most important equipment pieces of the TIG process: The torch (A), the shielding gas (C), the welding power source (D) and the cooling system (E). In addition, electrical cables, hoses for the gas and water supply (and as the figure show a water drain or return to circulator) and equipment to protect the torch from overheating are necessary.

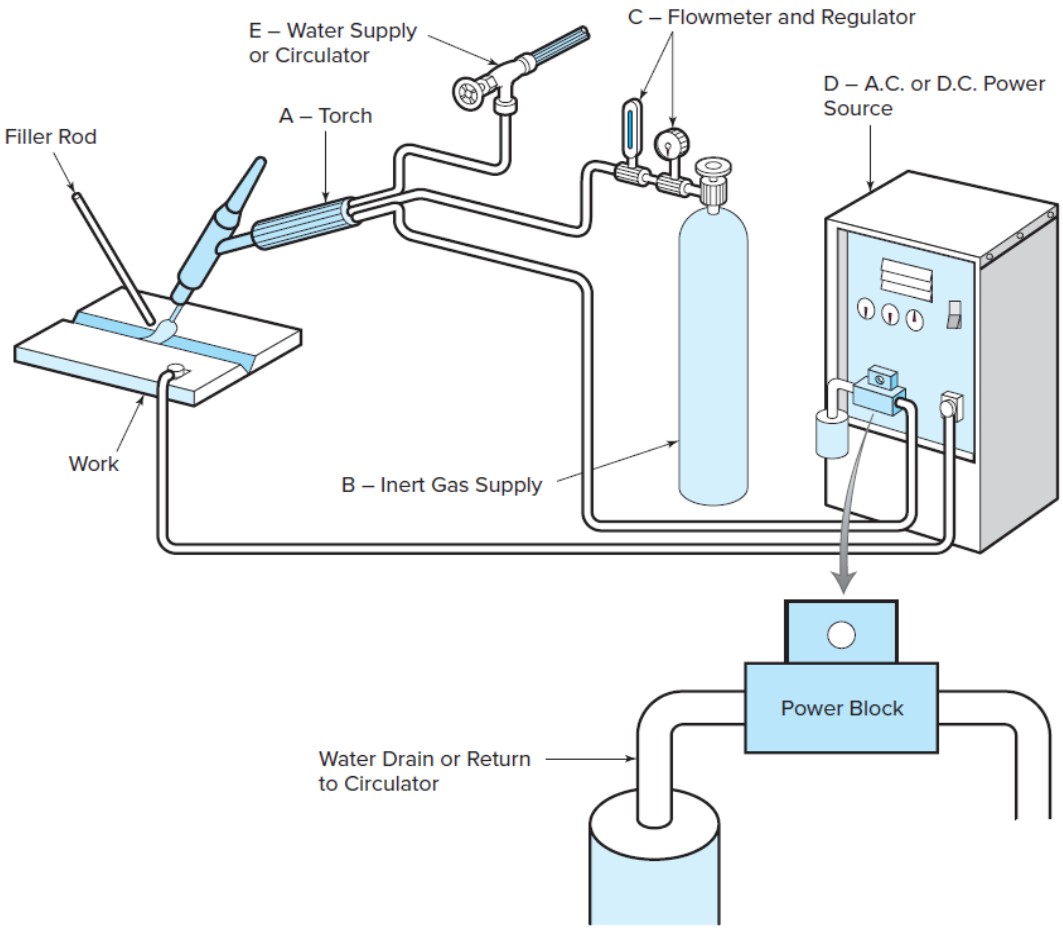

Figure 2 - TIG welding equipment.

Source: (BOHNART, 2017).

2.1.1.1 TIG torch

The torch (electrode holder) is a vital apparatus in the GTAW process. It is not only responsible for holding the non-consumable electrode, but also for feeding the welding zone with the current, the shielding gas and water (or air) supply. The water flows in and out of the holder through a tube connected to the water supply whereas the current flows through a cable connected to the power source. The shielding gas is also channelled in through a tube that is coupled to the shielding gas supply.

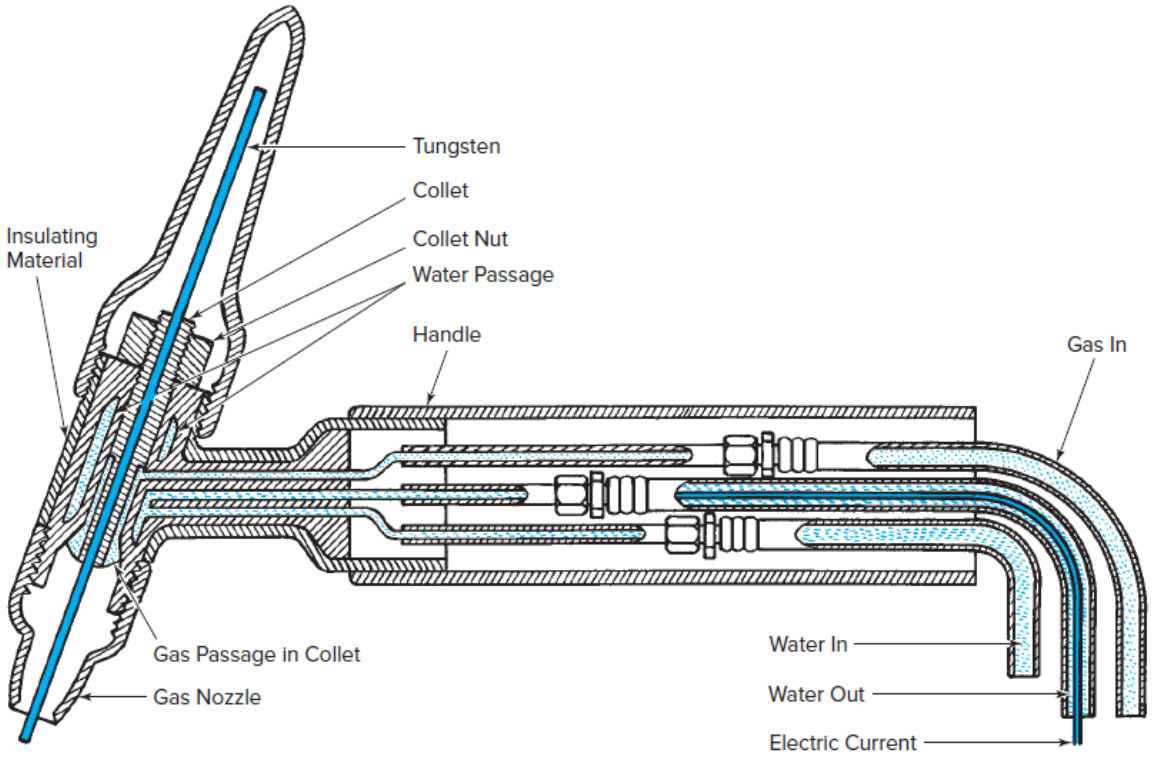

Figure 3 – Sectional view of the GTAW torch.

Source: (BOHNART, 2017).

2.1.1.2 Shielding gas

The shielding gas promotes a controlled environment for the welding to take place, providing protection to the electrode, the pool of molten metal, the arc and the neighbouring

heated areas (DAI et al., 2018). Argon and helium are the most common gases added to the GTAW process because both are chemically inert. That is, they do not interact with other materials to form compounds, which could affect the weld. They also provide a smooth and stable arc welding (BOHNART, 2017; DEGARMO et al. 2010).

A mixture of gases is used in an effort to harness the advantages of both materials. Helium, for example, can be added to obtain higher Welding travel speed and deeper penetration due to its capability of increasing the heat input. On the other hand, argon provides arc stability. Tazetdinov et al. (2013), for instance, developed a new method for arc welding in shielding gases with alternate pulsed supply of argon and helium. They were able to increase the welding precision, the strength properties, and leak lightness of the welded joints.

A proper system of gas flow control is required to provide a uniform flow of the gas throughout the entire welding process. Controlling the quantity of gas is essential. Too much gas, for instance, is inefficient and it makes the process more costly. Not enough gas does not provide effective protection to the welding area, allowing contamination to go into the welding area. Marinelli et al. (2019) combined high speed welding with low content of helium gas and the results have shown defects in the welding.

The correct gas flow rate depends on a series of factors such as the type of shielding gas being used, the type of the welding joint, the position of the welding torch, the speed of the welding. In addition, the size and shape of the welding nozzle and its distance from the part area, the size of the weld pool, the welding current and the air currents in the welding area also have an effect on the gas flow rate (BOHNART, 2017).

2.1.1.3 Power source

Figure 4 presents a scheme of how the power source is connected to the GTAW process. It consists of a direct current (DC) or alternate current (AC) power supply. It is then connected to the electrode holder through an electrode cable. An Ammeter is attached to the electrode cable. Another cable goes from the supply source to the work piece. A Voltmeter is established between the electrode cable and the work piece cable (DEGARMO et al. 2010).

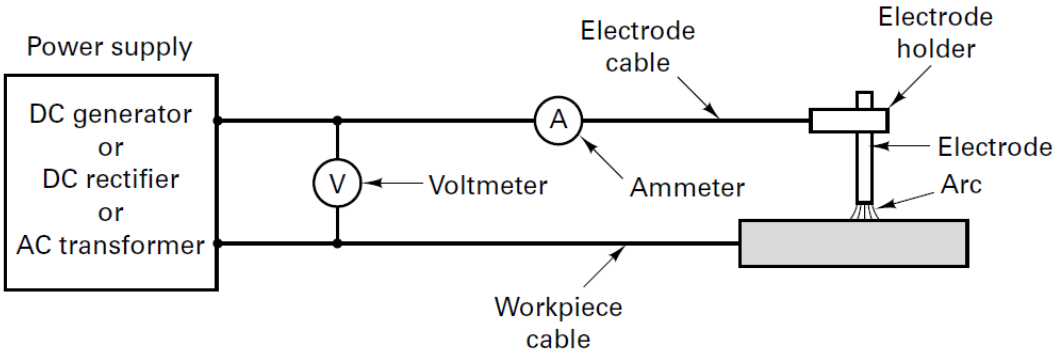

Figure 4 - Power supply scheme.

Source: (DEGARMO et al. 2010).

For most welds in TIG process, a DC power supply is used. In this configuration, the direction of the current flow (or polarity) is essential. The welding circuit can be associated as either electrode negative (straight polarity) or electrode positive (reverse polarity). The different types of configuration of a DC power supply depend on elements such as the width of the weld, the HAZ, the depth of the weld, the metals to be worked on and the type of electrode (KALPAKJIAN, 2013). And it has influence over weld penetration, heat input, cleaning action, bead profile (BOHNART, 2017).

In straight polarity – or direct-current electrode-negative (DCEN) – the work is connected to the positive terminal (cathode) and the electrode to the negative terminal (anode). That means the electrons flow from the electrode to the work. Figure 5(a) demonstrates that as the electrons are attracted to the work piece, the gas ions from the arc column flow in the direction of the negative electrode. The temperature of the arc is more intense at the electrode, since the ions are more massive than the electrons (DEGARMO et al. 2010; KALPAKJIAN, 2013; BOHNART, 2017).

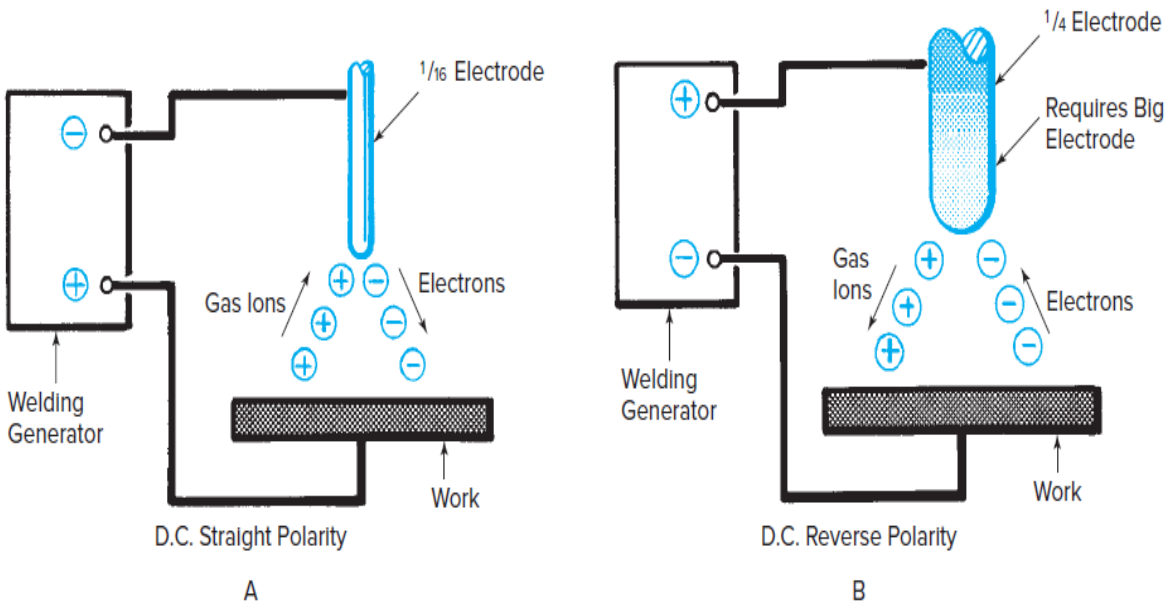

Figure 5 – Straight polarity and reverse polarity current flow.

Source: (BOHNART, 2017).

In reverse polarity – direct-current electrode-positive (DCEP) – the positive terminal is connected to the electrode and the negative is connected to the work piece. Therefore, in this configuration, the electrons flow from the work piece to the electrode and the gas ions now flow to the work piece as Figure 5 (b) illustrates. As the electrons flow to the electrode, it receives extra heat which can burn the tip of the electrode. Thus, DCEP requires a larger size electrode than DCEN (DEGARMO et al., 2010; KALPAKJIAN, 2013; BOHNART, 2017).

Because of its characteristics, DCEN presents higher metal deposition rates, deeper penetration, form narrower beads and give the possibility of welding at higher speed. In DCEP, on the other hand, as the positive ions bombard the work piece, it removes the oxide films cleaning the weld surface. Characteristic specially desired for metals such as aluminium and magnesium (KOU, 2003; CIRINO & DUTRA, 2010; PAN et al., 2016; BOHNART, 2017). As it can be seen in Figure 6, the heavy ions act on the oxide film atoms on the surface of the work piece and knock them off the surface.

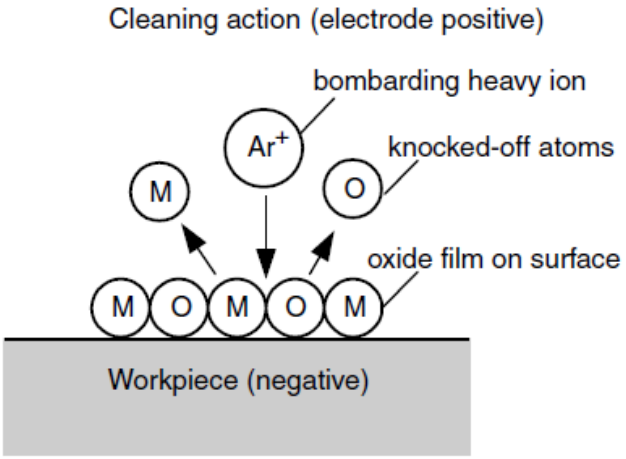

Figure 6 – DCEP cleaning action in TIG process.

Source: (KOU, 2003).

Bohnart (2017) points out that DCEP is not usually recommended for TIG process due to the excess heat the electrode receives. However, alternate current (AC) can be used instead. AC is a combination of DCEN and DCEP. Therefore, the welding characteristics vary between negative and positive conditions (CIRINO & DUTRA, 2010; PAN et al., 2016). The AC offers the oxide cleaning action and reasonably good penetration (KUMAR et al., 2018).

2.1.1.4 Electrode

In TIG process, the non-consumable electrode supplies the required heat for the welding, functioning as one of the electrical terminals of the arc. Tungsten electrode becomes thermionic when it approaches its melting point by resistance heating (3410 ºC). At this point, the electrons stem out of the electrode tip causing a cooling effect, making the cooling tip cooler than its immediate surrounding area (ASM INTERNATIONAL, 1993; AWS, 2009).

Electrodes are normally composed of pure tungsten or tungsten alloys. Thorium and zirconia are the most common alloys used. However, there are other elements used and their chemical composition is what classifies the electrodes, as shown in Table 1.

Table 1 - Electrode's classification.

AWS Classification	Color	Alloying Element	Alloying Oxide	Alloying Oxide %
EWP	Green	-	-	-
EWCe-2	Orange	Cerium	CeO_2	2
EWLa-1	Black	Lanthanum	LaO_3	1
EWLa-1.5	Gold	Lanthanum	LaO_3	1.5
EWLa-2	Blue	Lanthanum	LaO_3	2
EWTh-1	Yellow	Thorium	ThO_2	1
EWTh-2	Red	Thorium	ThO_2	2
EWZr-1	Brown	Zirconium	ZrO_2	0.25
EWG	Gray	Manufacturer must identify	-	-

Source: (Adapted from AWS, 2009).

ASM international (1993), AWS (2009) and Bohnart (2017) observe that each classification has its features:

a) Pure electrode tungsten (EWP) as the name implies, does not contain any intended alloying element. It should have at least 99.5% of tungsten in its composition. EWP are low-cost electrodes usually used for aluminium or magnesium alloys, since it provides good arc stability when used in AC;
b) EWTh electrodes have thorium in their composition. They have 20% higher current carrying capacity. They last longer and have better resistance to impurity from the weld. These electrodes also deliver a process with a more stable arc than EWP. EWTh electrodes were designed for DCEN applications, since they maintain a sharpened tip during the welding process. However, such qualities come with a price; thorium electrodes are radioactive and health and safety precautions should be taken for its use (COSTA, 2014);
c) EWCe electrodes have cerium in their composition. These electrodes came to the market as an alternative to the EWTh electrodes, which have a low-level of radioactivity and therefore require special requirement made by safety or environmental regulations. EWCe provide good results with either AC or DC. Compared to EWP it has a better performance in arc starting, reduced rate of burn off and it has better arc stability;
d) EWLa electrodes with lanthanide in their composition have similar operating characteristics and benefits as EWCe electrodes. They were also developed as an alternative to EWTh. In general, these electrodes boost arc starting and stability and reduce the tip erosion;

e) EWZr are electrodes composed of zirconium. These electrodes combine characteristics from both EWP electrodes (arc stability and rounded tip) and EWTh electrodes (current capacity and arc starting);
f) EWG electrodes are composed with alloys not available in Table 1. The manufacturer has to specify, however, the composition (specific addition and quantity) of the alloy.

2.1.2 TIG welding process variables

Understanding and establishing the values of the variables of any process is one of the most important steps to get appropriate results. When these parameters are out of range or improperly arranged, unexpected and undesirable outcome might be obtained or even lead to equipment technical issues and damage the material being used. The main variables of the TIG process are welding current, arc voltage, travel speed, wire-feeding speed and shielding gas (AWS, 2004). The relation between these variables is so strong that it is impossible to analyse them as if they are independent from each other.

2.1.2.1 Welding current

The welding current directly affects the welding penetration. That means that the higher the current the deeper the penetration is. However, too high currents can cause splatter and damage the work piece. Too little current is also an issue; it can lead to a much wider HAZ, as heat is applied for longer periods to deposit the required to produce the weld. It gets even worse if there is a filler material (AWS, 2004).

TIG can be used with AC or DC and the choice will depend on the material being welded. When using DC current, DCEN provides a deeper penetration and faster Welding travel speed– especially when helium is used. For AC the applications, the weld has cleaning action which removes the refractory oxides from the surface of the metal (BOHNART, 2017; KUMAR et al., 2018).

2.1.2.2 Arc voltage

Arc voltage is proportional to the distance between the tungsten electrode and the work piece (arc length). Therefore, the longer the arc length the higher the voltage at the same amount of current given. However, it does not make the process more efficient. That is, even though there is more heat being generated, it is not added to the work piece. This happens because all this extra energy is lost through radiation to the surrounding environment of the weld (ASM INTERNATIONAL, 1993).

At a fixed arc length, voltage is directly proportional to the current. Other factors such as the type of shielding gas, the air pressure where the welding is taking place and the shape of the electrode tip are also directly proportional to the arc voltage (BOHNART, 2017).

Other variables should also be carefully noted such as shielding gas contaminants, electrode tip damaged or eroded, electrode temperature changes and even problems with the filler wire system. All of them have influence over the arc voltage and if significant changes happen the system should be rearranged in order to maintain the desired voltage (BOHNART, 2017).

2.1.2.3 Welding travel speed

Penetration and weld with are both affected by the speed of the weld. When thinking of productivity this is a desirable parameter (PHILLIPS, 2016). However, one cannot simply increase the Welding travel speed. Defects such as humping weld and undercut are easily formed at high speeds (NGUYEN et al., 2006).

The speed of the welding is directly correlated to the welding current. Thus, the faster the welding the higher the amount of current required to control the welding. However, high currents are difficult to be kept under control. In this sense, an alternative to work with low current is to reduce the Welding travel speed (PRITCHARD, 2001).

2.1.2.4 Arc length

For manual processes, the arc length is a factor that is very likely to vary. This variation can be reduced by the use of a grip. In mechanized processes, it is less likely to become an issue since the torch is generally held by a torch holder (MUNCASTER, 1991).

Variances for both long and short arcs can cause problems. Short arcs can make the electrode touch the welding pool and contaminate the electrode. Long arcs spread the arc heating (PHILLIPS, 2016).

To avoid undercutting, excessive width of the weld bead and have control of the weld penetration a reasonably short arc should be maintained. The arc length should be similar to the diameter of the electrode (BOHNART, 2017).

2.2 MIG/MAG welding process

The MIG/MAG (Metal Inert Gas / Metal Active Gas) welding process also known as GMAW (Gas Metal Arc Welding) is a welding process that uses an arc to heat a continuously fed electrode wire into a molten pool. Shielding protection for both the molten weld metal and the arc are supplied by an external gas source (ASM INTERNATIONAL, 1993; KOU; 2003; AWS; 2004). Figure 7 illustrates the process.

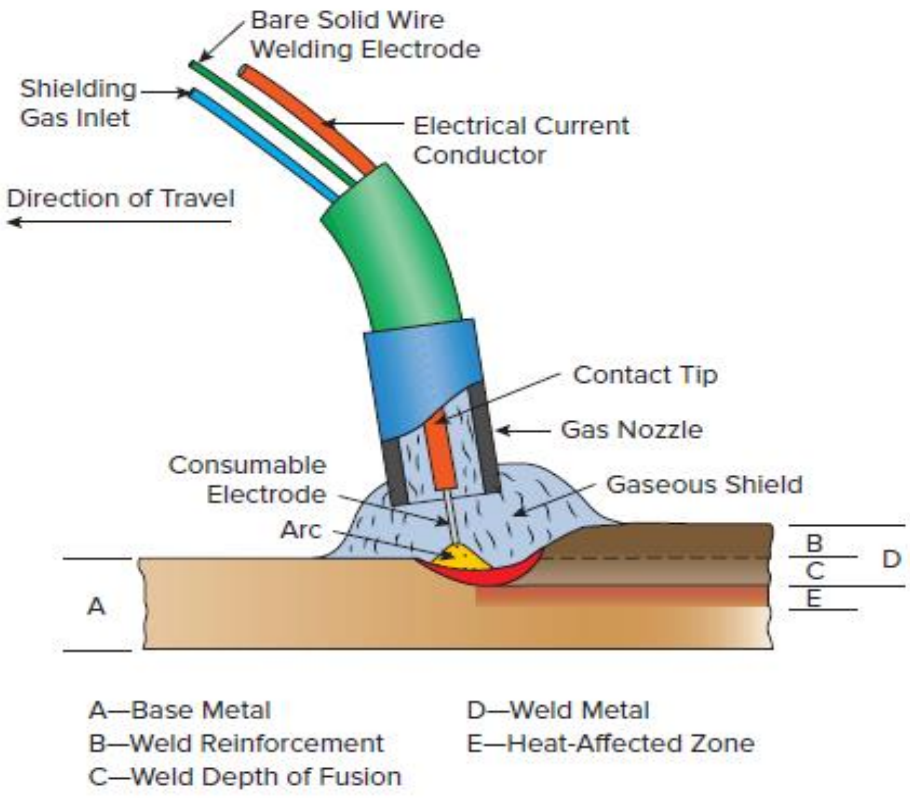

Figure 7 - MIG/MAG process.

Source: (AWS, 2004).

Shielding is obtained by using inert gases such as helium or argon. Thus, the process also receives the name of metal inert gas (MIG). When gases such as carbon dioxide and oxygen are added to the inert gases, the process receives the name of metal active gas (MAG). Inert gases are commonly used for aluminium alloys and stainless steels, while active gases are normally used for welding low and medium carbon steels. (GROOVER, ,2010; BOHNART, 2017).

The MIG/MAG process eliminates the need of cleaning the weld once it has cooled down. That is, it eliminates the slag-forming agents because of the shielding gas. Therefore, it allows multiple welding passes to be made at the same joint (DEGARMO, 2012).

GMAW is extremely flexible and can be used in virtually all metals. It provides fast Welding travel speed and high deposition rates. But what stands out is the relatively low cost and its adaptability to automated systems (PHILLIPS, 2016).

2.2.1 GMAW Equipment setup

Figure 8 shows the MIG/MAG equipment setup. It is composed of shielding gas supply, welding gun and cable assembly, power supply and an electrode supply unit. Water supply can also be added for high duty cycles and high current in order to cool the system (PHILLIPS, 2016).

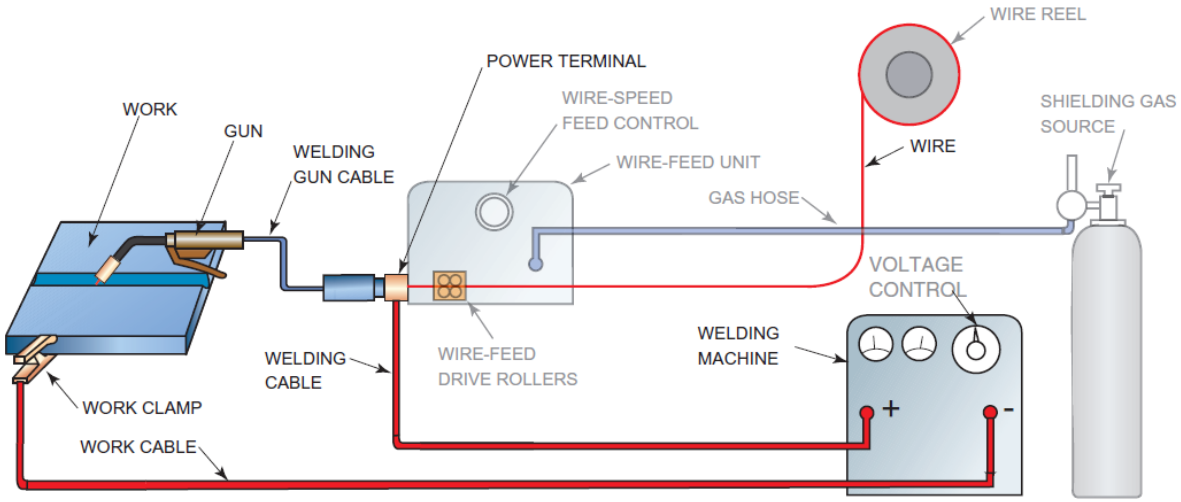

Figure 8 - MIG/MAG equipment setup.

Source: (JEFFUS, 2012)

GMAW is “self-correcting”, that means that the system is capable of changing its parameters to maintain the same arc length throughout the welding process. In this sense, for instance, when the arc voltage is set and the machine senses a change in the arc length. It automatically make changes to the current, which will affect the electrode melting rate and, therefore, will adjust the arc length up to the point the machine senses the initial set point voltage (PHILLIPS, 2016).

2.2.2 Filler metal transfer mode

The filler metal transfer mode is the mechanism by which the molten metal is transferred to the weld pool. There are four methods: short-circuiting, globular transfer, spray transfer and pulsed-arc transfer. It is possible to change from one method to another by simply change the parameters of the machine or for some cases changing the shielding gas (DEGARMO, 2012; JEFFUS, 2012).

The type of transfer depends upon the shielding gas, arc voltage, welding current, electrode diameter, composition and extent (AWS, 2004), type and thickness of the material (JEFFUS, 2012).

2.2.2.1 Short-circuiting transfer

Short-circuiting transfer is the most common process in GMAW (JEFFUS, 2012). It takes place at low currents and low voltages and with the use of CO2. Degarmo (2012) and Jeffus (2012) explain the process in a simple and straightforward way, as shown in Figure 9.

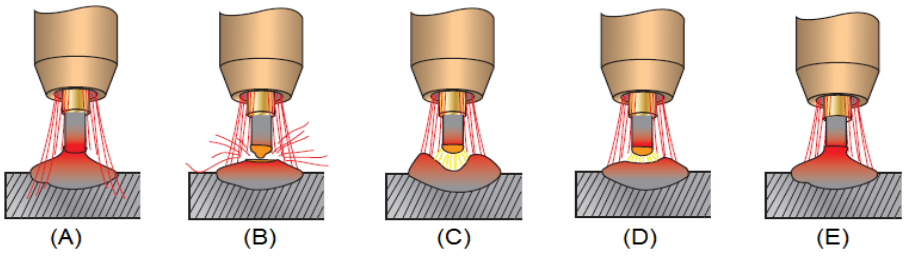

Figure 9 - Short-circuiting metal transfer in GMAW.

Source: (JEFFUS, 2012).

The electrode tip touches (short-circuit) the weld pool (Figure 9-A), eliminating the arc and its resistance. As there is no resistance anymore, the current value rises and it flows from the tip of the electrode to the molten weld pool. At this point, both electrode tip and molten metal are at very high temperature.

A combination of high current flows and high resistance heats the electrode tip up to a point that a small explosion happens (Figure 9-B), establishing the arc. A droplet comes out from the electrode tip to the work piece forming a gap between the work piece and the electrode (Figure 9-C). As the arc is re-established, the system has now resistance, therefore, the voltage surges and the current drops.

As now the current is low, the heat is not enough to consume the electrode tip as fast as it being fed by the wire-filler. As a result, the electrode tip moves forward shortening the arc length (Figure 9-D) and the electrode touches the molten pool again (Figure 9-E), restating the cycle.

2.2.2.2 Globular transfer

The difference between short-circuiting transfer and globular transfer lays on the increase of voltage and current values. The main characteristic of the globular metal transfer is the size of the drop, which is larger than the electrode tip diameter (Figure 10). Gravity plays an important role in the droplet transfer, making it highly unstable. As there is little control over the droplet, this process has generally limited applications. The arc is usually loud and erratic. There is also a great deal of spatter (DEGARMO, 2012; BOHNART, 2017).

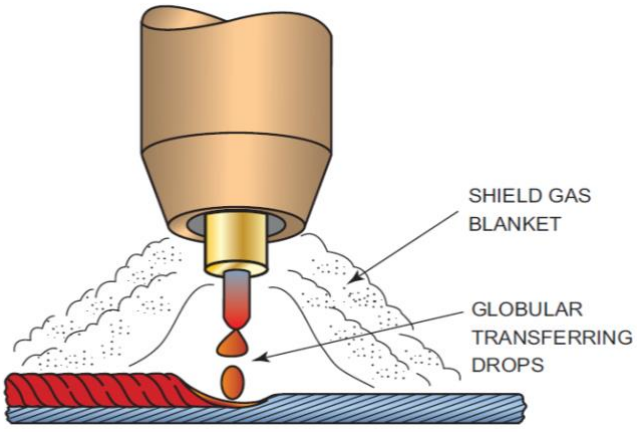

Figure 10 - Globular metal transfer in MIG/MAG.

Source: (JEFFUS, 2012).

2.2.2.3 Spray transfer

In spray metal transfer, very thin droplets of metal are transferred from the electrode to the molten weld pool that do not create short circuits in the arc, which results in a desirable condition: less spatters. This process happens at high currents and voltages (higher than short-circuit and globular modes) used with inert gases and usually DCEP (DEGARMO, 2012; PHILLIPS, 2016; BOHNART, 2017).

This process provides deep penetration, high deposition rate and high arc stability. Furthermore, as the droplets are so small, the electromagnetic effects have greater effect than gravity, allowing the droplets to be directed across the arc in any direction. These characteristics allow aluminium and magnesium allows welding at vertical or overhead positions (BOHNART, 2017).

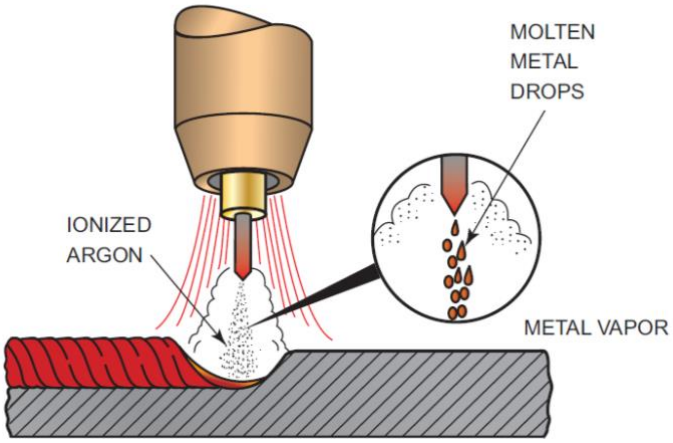

Figure 11 - Spray metal transfer in MIG/MAG.

Source: (JEFFUS, 2012).

2.2.2.4 Pulsed-arc transfer

Pulsed-arc transfer came up as solution to the limitations of the spray metal transfer mode. As spray transfer offers deep penetration, it may cut through thin metals. In addition, its high deposition rates generate large weld pool, which might not be held by the superficial

tension when the weld takes place in vertical or overhead positions (AWS, 2004; JEFFUS, 2012).

Pulsed-arc transfer is accomplished by precisely controlled waveforms and frequencies that “pulse” the current and voltage. It is a dual pulsed amperage. One pulse refers to the high current, which offers the spray transfer mode. The other pulse is at low current and there is no droplet transfer (AWS, 2004; JEFFUS, 2012).

2.2.3 GMAW welding process variables

Degarmos (2012) states that the MIG/MAG process variables are type of current, shielding gas, electrode diameter, composition and extension, Welding travel speed, arc length and welding voltage.

2.2.3.1 Shielding gas

In order to have an efficient gas shield, the gas should flow through the nozzle and have a laminar flow instead of a turbulent flow. Turbulence in the gas flow can cause contamination of the weld due to the arc not being fully covered. Figure 12 illustrates both laminar and turbulent gas flow (BOHNART, 2017).

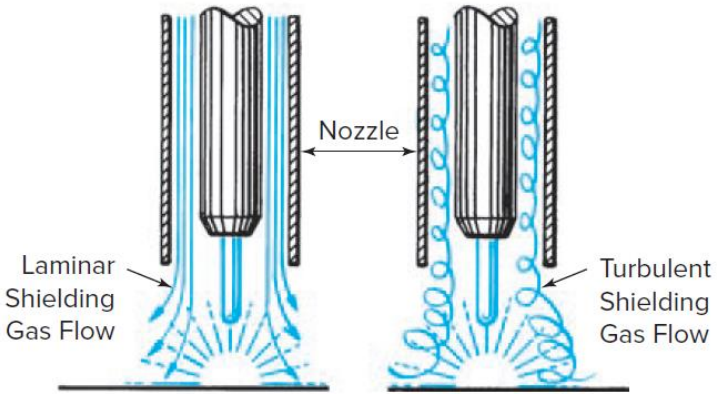

Figure 12 - Shielding gas flow in MIG/MAG welding process.

Source: (BOHNART, 2017).

Selecting shielding gases for MIG/MAG process is not an easy task. Factors such as arc surrounding atmosphere, arc stability, bead shape, porosity-free, Welding travel speed and depth of penetration should be considered to weigh the gas choice. Bohnart (2017) states that the three main gases for MIG/MAG process are argon, helium and carbon dioxide. Phillips (2016) reinforces that the choice of the shielding gas greatly affects the weld profile, as Figure 13 illustrates.

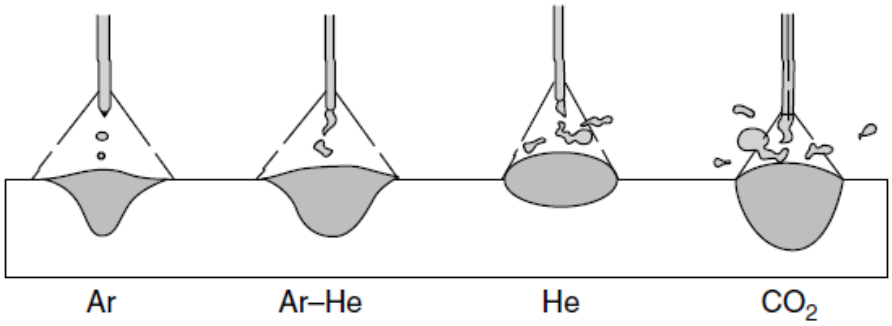

Figure 13 - Shielding gas effect on weld profile.

Source: (PHILLIPS, 2016).

On one hand, argon provides a more stable and quieter arc and consequently less spatter. It gives the welding deeper penetration and narrow weld bead. Helium, on the other hand offers a wider weld with less penetration than argon. Mixture of both argon and helium are used in an attempt to get beneficial characteristics from both products. Finally, yet importantly, is the carbon dioxide. It provides wide weld pattern and deep penetration, making it easier to avoid incomplete fusion. Besides, there is no tendency to undercutting and the bead contour is reasonably good. However, the arc tends to be unstable and cause spatter (BOHNART, 2017).

Several studies are conducted in an attempt to find the best combination of the shield gas components, their concentration and their flow rate. Li et al. (2018) studied GMAW process for 10Ni5CrMoV steel, which is a low carbon micro-alloyed HSLA steel, welded using Cr-Ni austenitic wire. They found out that the arc stiffness can be improved and the incomplete fusion of the sidewall can be lessened by adding CO_2 into the inert shielding gas.

Cai et al. (2017) did a study with a ternary (Ar-CO_2-He) shielding gas in narrow gap applications with GMAW. They explained in their study the effects of shielding gas composition on weld bead profile, wire meting characteristics and arc properties.

2.2.3.2 Welding current

Phillips (2016) defines current as a major player in arc heating and it is the primary variable governing the amount of melting. In MIG/MAG process, DCEP is the most common type of current used because it delivers the maximum heat input. It allows deep penetration, stable arc, smooth metal transfer and small amount of spatter. Conversely, DCEN and AC provide erratic metal transfer (KOU, 2003; DEGARMO, 2012; BOHNART, 2017).

Sumesh et al. (2018) state that defects such as cracks and tears are not usually reflected by the arc. Nonetheless, the instability these defects generate due to burn through and porosity are sensed in the welding current and voltage signatures. In their study a decision tree algorithm was proposed to establish a correlation between welding current and arc voltage signatures with the weld quality.

2.2.3.3 Arc voltage

Arc voltage is related to arc length. They are not the same thing, though. The arc length has influence over the arc voltage. In MIG/MAG process, a constant voltage welding machine is used. That is, the fixed voltage value is set in the machine and it grants the self-adjustment of the arc length to meet the previously configured welding voltage (BOHNART, 2017).

The process of self-adjusting is straightforward. If there is any nuisance to the system, for instance, the arc length is shortened. It will cause the decrease in the arc voltage, increasing the current. The higher current will consume the electrode faster; stabilizing the arc length up to the point where the desirable voltage is restored (JEFFUS, 2012).

Bohnart (2017) certifies that there is a matching voltage value for any given current established. When these parameters match, the best weld profile can be achieved with the best bead provide. Nonetheless, the author reinforces that either low or high voltages cause problems. High voltages cause flat weld bead with increased width, spatters, porosity and undercut. Low voltages cause narrow and high weld bead and the electrode might stub on the place in extremely low voltages.

2.2.3.4 Electrode and extension

The electrode extension is the length between the contact tip and the electrode tip. Figure 14 illustrates the area related to the electrode extension along with some other important areas located in between the nozzle and the work piece. Electrode extension has influence over penetration and weld bead dimensions. The longer the electrode extension, the greater the resistance in the electrode. This resistance to the current flowing through the wire causes it to heat up. If the electrode extension is reduced, the current drops (BOHNART, 2017).

The increase in the current does not improve the depth penetration as one might think. It happens because all this extra current is directed to the electrode tip and not the weld metal. Phillips (2016) augments that understanding not only the effect of the electrode extent, but also variables as standoff distance, voltage, current, travel speed, wire speed (and their interactions), is vital in order to have a reasonable good weld profile using GMAW.

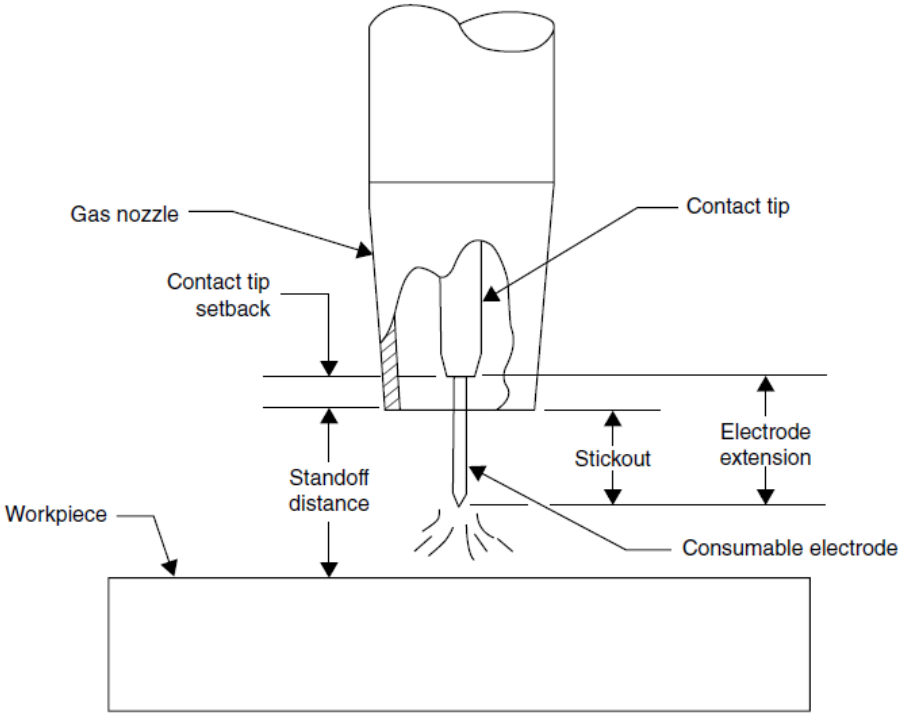

Figure 14 - MIG/MAG terminology (area between the nozzle and work piece).

Source: (AWS, 2004).

2.2.3.5 Welding travel speed

The Welding travel speed or travel speed is the linear rate the arc moves along the weld joint (AWS, 2004). It directly affects the weld penetration. Jeffus (2012) complements that the Welding travel speed cannot exceed the ability of the arc to melt the base metal. The author refers to the fact that if the Welding travel speed is too fast, less thermal energy per unit of length of weld is supplied to the base metal. Therefore, the weld is prone to have undercutting defects. Wang et al. (2016) comment that if the speed of welding reaches a certain value, it can cause humping and geometric weld defects. Nguyen et al. (2006) add that humping and undercuts negatively influence the progress in welding productivity.

On the other hand, if the Welding travel speed is too slow, the weld pool size increases as the welding arc acts on the welding pool instead of the base metal. As the arc is not focused on the base metal, the penetration is less effective (JEFFUS, 2012).

2.2.3.6 Welding gun angle

The angle of the electrode affects the penetration way more than factors such as arc voltage or travel speed (AWS, 2004). The position of the gun is defined in two ways: the work angle and the travel angle. The relation between the electrode axis and the direction of the travel defines the travel angle. The relation between the electrode axis and the work surface is the work angle. Figure 15 illustrates both the work angle and the travel angle in welding.

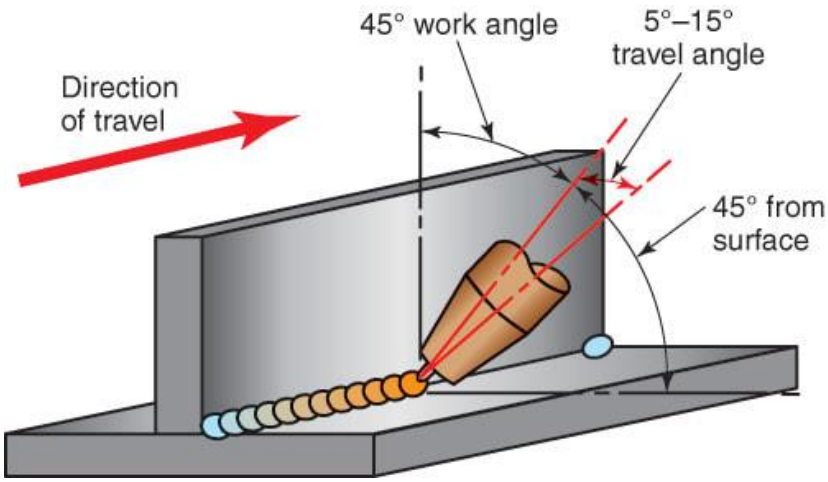

Figure 15 - Work angle and travel angle.

Source: (ALTHOUSE et al., 2020).

In relation to travel angle, there are three technics used to hold the gun known as backhand, perpendicular and forehand techniques. These terms describe the angle at which the gun is held in relation to the weld bead as Figure 16 shows.

Backhand welding (also often referred as drag angle as the electrode tip points to the opposite direction to the travel) provides the best penetration out of the three techniques. It also provides narrower and more convex surface configuration than the forehand technique. Both Pillips (2016) and Althouse et al. (2020) agree that the drag angle at 25º offers the deepest penetration. Jeffus (2012) adds that weld bead visibility and a uniform weld can be achieved by this method. However, the author states that through this method, the weld bead might be more convex and have a rounded shape.

Perpendicular welding is done with the gun held at a 90º angle to the work piece. In terms of penetration and weld reinforcement, the perpendicular method is a balance between the results obtained with forehand and the backhand techniques. As the arc is directly pointed to the weld, more spatters might be produced by the perpendicular technique (JEFFUS, 2012).

When the electrode points to the same direction to the travel, it is called forehand technique (also referred as push angle). This technique provides better visualization of the joint being welded, and less penetration depth, which is an advantage for thin metals. This method also works well with out-of-position welds (JEFFUS, 2012). Althouse et al. (2020) point out that guns at angles ranging from 15º to 25º, for both drag and push angles, deliver better control over the welding pool and the best shielding.

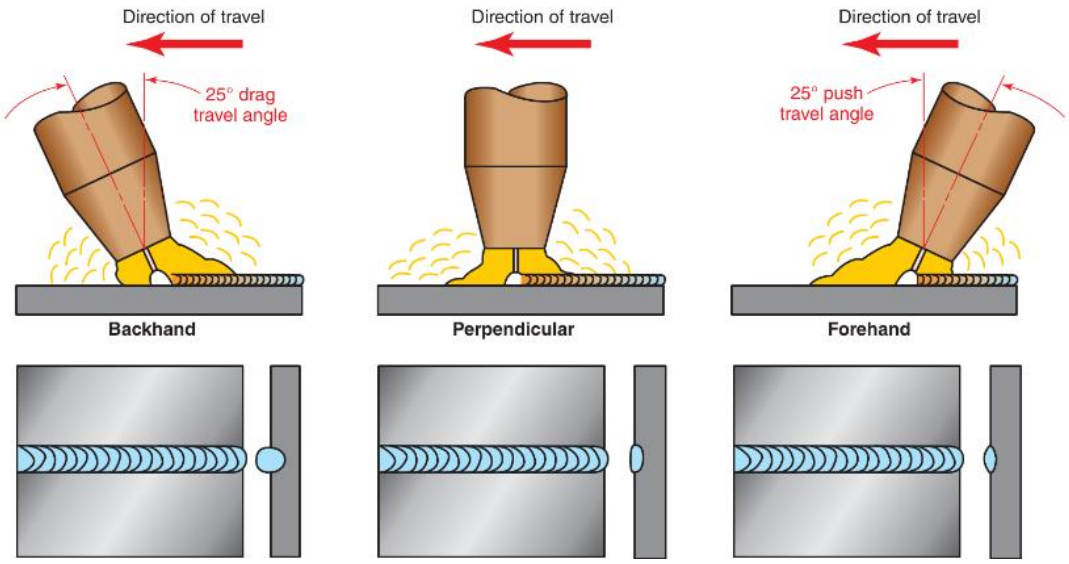

Figure 16 - Backhand (A), perpendicular (B) and forehand (C) welding technics.

Source: (ALTHOUSE, 2020).

2.3 TIG-MIG/MAG welding process

Before diving into the concepts of TIG-MIG/MAG welding process, an overview of the evolution of some of the hybrid process developed is given.

2.3.1 Hybrid welding

A combination of two or more traditional processes should result in a new one. This new process should overcome limitations that none of the traditional processes separately applied would (MESSLER, 2004; SAHASRABUDHE & RAUT, 2019). Messler (2004) established a timeline of the hybrid process developed throughout the years, which can be seen in Figure 17.

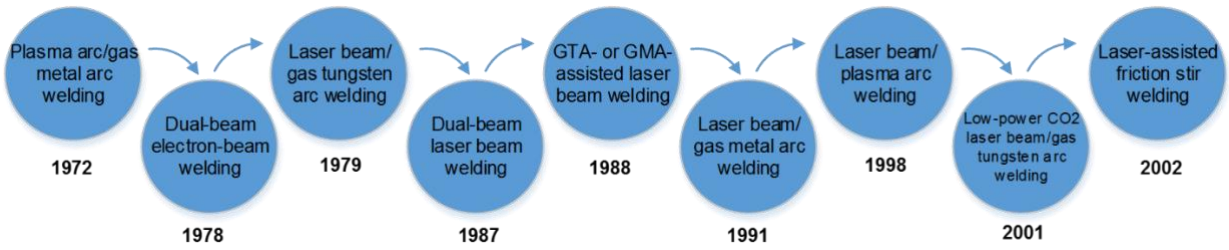

Figure 17 - Hybrid processes development chronology.

Source: (adapted MESSLER, 2004).

Plasma arc/gas metal arc welding (or Plasma-GMAW) was developed in 1972. This process combines the deep penetration and high energy density of plasma arc and high deposition rate, wide processing parameter range of GMAW (RESENTE et al. 2009).

Dual-beam electron-beam welding (or Dual-beam EBW) is the combination of two beams that can emanate from the same source, be in tandem or side by side. Messler (2004) states that Dual-beam EBW is questionably a hybrid process, because both parent processes might come from the same source and they are the same type. The benefits are mitigation of porosity (HAROONI et al. 2014), decreasing hardness and irregularity (XIE et al. 2002).

Laser beam/gas tungsten arc welding (or Laser-GTA) in this process a laser beam and a GTAW torch work simultaneously. This type of process great advantages on joint fit-up tolerance, adjustable heat source state depending on the welding needs and improved gap tolerance, which is specially desired for keyhole applications (LEE et al. 2016; WANG et al. 2017).

Dual beam laser beam welding (or Dual beam LBW) can significantly improve the quality of the weld (XIE et al. 2002). This process also offers prolonged weld metal solidification time (CAO et al. 2006). Dual beam LBW presented to be 23% more productive than single beam LBW in the study conducted by Liu et al. (1997).

GTA- or GMA- assisted laser beam welding combines the heat source of laser and arc. Laser-GTA comprises of a TIG torch and a laser beam being operated simultaneously. Whereas Laser-GMA consists of the combination of a laser and a torch of gas metal arc. Each of these processes bring advantages such as manufacturing stability, which allows the process to be performed at high speeds, reduced energy consumption when compared to the single process executed manually. It also provides good quality and efficiency (GUMENYUK and RETHMEIER, 2013).

Laser beam/plasma arc welding, also known as the Plasma-MIG, associates the plasma welding and MIG welding. In Plasma-MIG, the plasma arc involves both the welding wire and the MIG arc. This process promotes good bead formation and weld penetration (MAMAT et al., 2017).

Low-power CO2 laser beam/gas tungsten arc welding is capable of producing better results in terms of welding performance and arc stability in comparison to the plasma arc process alone (MAHRLE, 2013).

Finally, yet importantly, laser-assisted friction stir welding. Friction stir welding is a process that generates heat by the friction between the work piece and a highly wear resistant rotating tool. The tool mechanically mixes the softened material from both joints. In order to this process to work heavy duty clamps to the weld joints are required and large pressure is imposed to the tool, which can break it (ZHAN et al., 2019). To lessen these downsides, and extend the uses of this process to be used in materials with higher melting points, came the laser beam. The laser beam is used to preheat the welding, and therefore, facilitating the way to the rotating tool. It dramatically drops the tool wear and the likelihood if it being broken, less clamping force is required and less force is required to move the tool (MESSLER, 2004).

The next sections provide a better understanding of TIG-MIG/MAG hybrid process.

2.3.1 TIG-MIG/MAG welding setup

Figure 18 shows the equipment set up for TIG-MIG/MAG hybrid process. It shows the GTAW torch leading and the GMAW trailing. This type of process is often referred as TIG-MIG/MAG, whereas the reverse is referred as MIG-TIG (ZONG et al., 2019). Both torches are supplied by a gas source and each of them is connected to a power supply. The GMAW torch also has a wire feeder. This process is automated. Therefore, torch holders at a pre-determined angle hold both torches and they move at the same speed throughout the entire welding process.

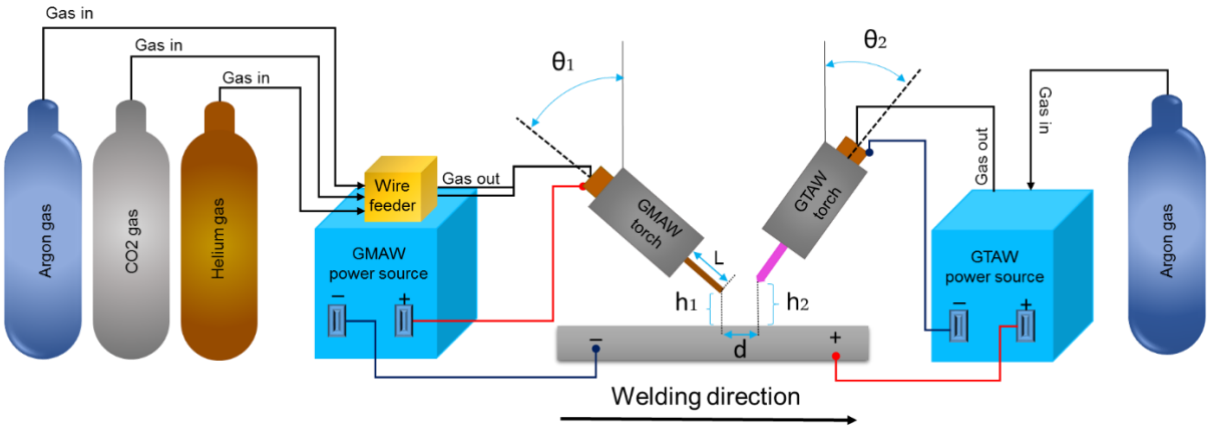

Figure 18 - TIG-MIG/MAG hybrid process setup

Source: Adapted from Schneider et al. (2017).

Parameters such as the distance between the electrodes (d), MIG/MAG contact tip to work distance (L), the height of each electrode (h1 and h2) and their angles in relation to the work piece (θ1 and θ2) are part of the set up and they significantly affect the droplet transfer (SHEN et al. 2017).

2.3.2 TIG-MIG/MAG advantages and limitations

The TIG-MIG/MAG hybrid process came to light in an attempt to overcome the setbacks of either GTAW or GMAW process being applied individually. The most common

limitations seen for these two processes when applied unaccompanied are relatively wide HAZ, arc instability, lack of preheating of the joint and defects in the metal transfer (SAHASRABUDHE; RAUT, 2018). With the hybrid process, many accomplishments could be achieved throughout the years.

Chen et al. (2013) studied the use of pure argon in TIG-MIG/MAG hybrid welding. Their study revealed that pure argon shielding gas could be used in this new hybrid process to achieve better weld metal hardness. At this same condition, the higher the TIG current, the deeper the weld penetration. They noted, however, that the TIG current must be higher than the MIG current to stable the MIG arc. This is a remarkable finding since MAG arcs became unstable when pure argon is used as shielding gas. In their study they could find that the welding time could have a reduction of 17~44% as compared to conventional TIG process. Numerical simulation and experiments were run to analyse parameters such as penetration depth, stability of the arc, repulsion between arcs.

Soon after, Chen et al. (2018) analysed the effects of square AC waveform parameters and the GTAW and GMAW electrode positions on the arc and droplet behavior. Their study revealed that when GMAW electrode was on the stage of cathode the arc had a curved cylinder shape. At this stage, the droplet would swing towards the tungsten side. However, when the polarity of the wire changed to anode, the droplet would swing towards the wire side and the arc had a triangular shape.

Mishima et al. (2013) stretched a little more on understanding the mechanisms involving the arc phenomena. A three-dimensional numerical model was used to calculate the plasma property in TIG-MIG/MAG hybrid welding. The torch angle was the variable input parameter in the model. The results showed a direct positive effect between the torch angle and the electrode temperature and the current between the electrodes. They also found out that by adjusting the torch angles, both plasma property and heat property could be optimized. Another finding was related to the heat flux, which could be improved if proper balance was found between arc repulsion and the stiffness of both TIG and MIG arcs.

Zhang et al. (2014) proposed TIG-MIG/MAG process to join aluminium alloy and stainless steel. They concluded that the additional heat brought by the TIG torch improved the wettability, which made the motel metal spread more effectively on the upper surface. The study also found out that the tensile strength obtained with the new process was 51% higher than a joint made with the conventional MIG process.

Ding et al. (2015) studied TIG-MIG/MAG hybrid process of stainless steel and magnesium alloys with Cu interlayer of different thickness. The authors discovered that the joint mechanism changes as the Cu interlayer lengthens. Their study revealed through analysis of microstructure and properties, that the joint and strengthen mechanisms are directly proportional to the thickness of the interlayer.

Sahasrabudhe & Raut (2018a) proposed an analytic framework to rank the most influential controlling parameters for TIG-MIG/MAG hybrid welding performed on mild steels. They ranked up to 13 parameters and they concluded that 5 of them were responsible for 62% of the parameters interactions that need to be optimized. These 5 parameters are the distance between TIG and MIG arcs, TIG arc current, welding traverse, MAG wire feed and MAG arc voltage.

Meng et al. (2014) focused on productivity in their study. A high speed TIG-MIG/MAG process was proposed in their paper. Orthogonal experiment was used to analyse the welding parameters on Welding travel speed and welding appearance. Mechanical and microstructure properties were tested and compared to the conventional MAG process. With the hybrid process, they could achieve a speed of 3.5 m/min and 4.5 m/min for bead-on-plate welding and butt welding, respectively. The mechanical properties of the weld performed by the hybrid process was not lower than the conventional process. They also concluded that the auxiliary TIG made the MAG current and MAG arc more stable at high-speed welding. For the authors, the stabilization of the welding could be achieved by the balance between the TIG and MAG current and the distance between the electrodes. I their study, the optimum parameters values found were TIG current at 315 A, the distance between electrodes of 12 mm, TIG torch angle at 10º, MAG torch angle at 20º and the distance between the work piece and the TIG electrode of 3 mm.

Kanemaru et al. (2015) experimentally evidenced the existence of direct current between the TIG and MIG arcs in TIG-MIG/MAG hybrid welding. They were able to see in their experiments that, at certain conditions of which the TIG current is lower than the MIG current, the arc shape can be seen even when the power supply of the TIG torch is cut. It causes instability of the MIG arc. Through these finding they confirm that the stability and heat input of the MIG arc are highly influenced by the TIG arc. They were also able to confirm that the heat efficiency for hybrid welding is 10% lower than TIG process alone.

Chen et al. (2016) also compared the TIG-MIG/MAG hybrid welding with the MIG conventional process. In this paper, arc shape, weld pool behavior, droplet transfer and were analysed to understand the influence of low auxiliary TIG current arc on weld microstructure and weld formation. They analysed the hybrid process in two configurations: TIG trailing and TIG leading. The arc stabilized only when TIG was leading. Heedlessly of the TIG position, there was a reduction in the impingement of the droplet. Undercut defect was mitigated due to a slower backward fluid flow, which prevented filler metal at high temperatures at the tail of the weld, allowing more time to the metal to fill the weld toe. An interesting finding in this study was that although the heat input was higher, the surface temperature of the weld was lower in comparison to the conventional process.

Liang at al. (2016) proposed a new hybrid method using cold metal transfer (CMT), which is a metal inert gas welding performed at lower temperatures than regular GMAW. They compared TIG-CMT to TIG-MIG/MAG process. The main feature of the TIG-CMT process is that the two arcs do not interact. They concluded that the TIG current had great influence over the contact changing angle and the weld bead dilution. They found in their study that the partially melted zone has a positive relation to the addition of heat input and its microhardness decreases because the grains in the HAZ are coarser.

Later on, Liang et al. (2018) specifically analysed the effects of TIG current on microstructural and mechanical properties of 6061-T6 aluminium alloys joints while using TIG-CMT process. Their reached up the conclusion that the added TIG increased the weld penetration and provided better weld formation. They also found out that there was as soft zone in the HAZ, which made it wider and causing a decrease in the mechanical properties. However, the TIG current could be chosen to increase the mechanical properties. Additionally, the heat input increase caused the grains to coarse, which decreased the hardness in the partially melted zone broadening it.

Shen et al. (2017) examined the effects of welding parameters of TIG-MIG/MAG hybrid welding process for AZ31B magnesium alloy. They examined the bypass current, wire extension, and the distance from the TIG electrode to the weld material. These parameters were examined on the spheres of welding forming, microstructure effects and welding microhardness. The hybrid process in their study proved to be a highly efficient method to weld magnesium alloys with good weld forming and high-quality weld bead. However, they noted that with the increase of the bypass current up to a certain range could decrease the penetration and increase width and reinforcement. With this fact, they concluded that the bypass current is a key point to control the weld formation.

Samir Khan et al. (2018) used full factorial design to examine the mechanical properties of 10 mm thick 304 Stainless steel plates. The effects of voltage, current and gas flow rates on hardness and weld bead were studied. The authors found that, at some extent, there is a direct negative relation between the gas flow rate and the bead width. The relation between gas flow rate and hardness of the weld bead is proportionally negative. Another conclusion made in this study was related to the amount of gas added to the system. They experimentally found that too much gas causes turbulences and decreases the quality of the weld.

Zong et al. (2019) compared both TIG-MIG/MAG and MIG-TIG to the conventional MIG process in terms of the arc and droplet behavior and the weld pool. They reached the conclusion that regardless of the position of the TIG and MIG torches, the hybrid process could reach a Welding travel speed to a minimum of 1.5 m/min.

Huang et al. (2019) examined the swing TIG-MIG/MAG process in narrow gap applications in an attempt to solve the lack of sidewalls penetration. The authors compared three processes conventional MIG, TIG-MIG/MAG hybrid and swing TIG-MIG/MAG hybrid. The arc voltage and arc shapes were examined. Results from the study showed that the swing TIG-MIG/MAG process provided good sidewall penetration and the MIG welding voltage was stabilized, which improved the weld quality. In addition, the weld spread was improved due to the welding molten metal spreading from the MIG wire to the TIG weld molten pool.

Costa and Resende (2020) pioneered on the analysis of the effects of both electrodes in direct polarity on the TIG-MIG/MAG process against the weld bead geometry parameters. In their study they compared conventional MIG/MAG process to the results obtained in the TIG-MIG/MAG process. Their results show that the change in the polarity has influence over the weld bead geometry. They also confirmed that addition of the TIG to the conventional MIG/MAG process caused more wettability, greater penetration, more melted area, wider weld width and smaller reinforcement.

Azevedo and Resende (2021) studied the effects of TIG current, the distance between the electrodes and the TIG and MIG/MAG torches angles over the TIG-MIG/MAG welding process. They concluded that larger penetration area and penetration depth can be achieved with the combination of the increase in the TIG current, TIG torch angle and MIG/MAG torch angle and the decrease in the wire-electrode distance. To achieve larger weld width the combination of minimum values of TIG current and MIG/MAG angles and the maximum of wire-electrode distance and TIG torch angle must be set. The highest reinforcement height is obtained with the combination of maximum of MIG/MAG torch angle, TIG current, TIG torch angle and a minimum of wire-electrode distance.

Table 2 shows the data gathered from studies that analysed the TIG-MIG/MAG hybrid welding process.

Table 2 – Parameters from recent research (continue).

Authors		Azevedo & Resende (2021)	Costa & Resende (2020)	Zong et al. (2019)	Huang et al. (2019)	Chen et al. (2018)	Zuo et al. (2018)	Tang et al. (2018)	Schneider et al. (2017)	SHEN et al. (2017)	Kanemaru et al. (2015)	Zhang et al. (2014)	Meng et al. (2014)	Kanemaru et al. (2013)	Mishima et al. (2013)
Current (A)	MIG-MAG	-	250	250	160	250	180	-	-	230	-	135	70 / 140 / 210 / 280 / 350	270	270
	TIG	40 / 140	0 / 50 / 150	50 / 80/ 100 / 120 / 180 / 250	180	50	-	100	150 / 175 / 200	125 / 140 / 155 / 170	370	0 / 60	255 / 275 / 295 / 315	150 ~500	300
Voltage (V)	MIG/ MAG	31	30 / 32	30	21.4	30	16	26.4	25 / 27.5 / 30	21	-	23	-	-	-
	TIG	-	-	-	-	0	-	-		-	-	-	-	-	-
Torch Angle (°)	MIG/ MAG	15 / 30	30	0	0	90	50	0 / 40	45	0	0 / 45	0	5 / 10 / 15 / 20	30	30 / 45 / 60
	TIG	30 / 0	0	30	30	60	20	0	0	43	0 / 45	0	5 / 10 / 15 / 20	30	0 / 30
Polarity	MIG/ MAG	DCEP	DCEP/ DCEN	DCEP	DCEP	DCEP	-	DCEP	DCEP	DCEP	DCEP	-	DCEP	DCEP	DCEP
	TIG	DCEN	DCEN	DCEN	DCEN	DCEN	-	DCEN	DCEN	DCEN	DCEN	-	DCEN	DCEN	DCEN
Leading process		TIG	TIG	TIG / MIG	TIG	TIG	MIG	TIG	TIG	TIG	TIG	TIG	TIG	TIG	TIG
Distance between electrodes (mm)		30 / 50	12	5	6	5	3	6	4	2	4	35	10 / 12 / 14 / 16	4	4
MIG/MAG wire extension		20	20	18	22	20	-	22	10	20	25	-	-	25	25
Distance between the tip of the TIG electrode and the workpiece (mm)		2	5	5	4	5	6	6	3	3 / 4 / 5 / 6	6	-	2 / 4 / 6 / 8	5	5

Table 2 – Parameters from recent research (end).

TIG electrode tip angle	Electrode material		Electrode diameter (mm)		Base material	Gas feeding rate (l/min)		Shielding gas		Welding travel speed (cm/min)	Feed wire speed (m/min)
	TIG	MIG/MAG	TIG	MIG/MAG		TIG	MIG/MAG	TIG	MIG/MAG		
60	SEWTh-	ER70S-6	2.4	1.2	Steel SAE 1020	10	12	Argon	Argon + 8% CO_2	38	6
30	SEWTh-	ER70S-6	2.4	1.2	Steel SAE 1020	10	15	Argon	Argon + 8% CO_2	110 / 80	11 / 8
-	-	(Fe-0.11C-0.65Si-1.80Mn-0.020P-	-	1.2	Mild Steel (Fe-0.17C-0.15Si-0.30Mn-0.015P-	10	20	Argon	Argon	100	7.8
-	-	ER50-6	-	1.2	Q235 (10 mm thick)	10	10	Argon	Argon	8	4
-	-	ER50-6	2.4	1.2	Mild steel (2.5 mm thick)	20	20	Argon	Argon	100 / 150	-
-	-	5356 aluminium Alloy	-	1.2	5356 aluminium Alloy	-	15	Argon	Argon	30	-
-	WC 20	Stainless steel type 304	3.2	1.2	Stainless steel type 304 (4 mm thick)	6	15	Argon	Argon	30	4
60	SEWTh-	ER70S-6	2.4	1	AISI 1045 steel (8 mm thick)	10 / 12.5 /15	-	Argon	Argon / 79%Ar–21%CO2/ CO2	10 / 12.5 /15	7 / 8 / 9
-	-	AZ31B magnesium alloy	-	1.2	AZ31B magnesium alloy	-	-	-	-	290	-
30	2% La2 O3	Stainless steel type 308	4	1.2	Stainless steel type 304 (12 mm thick)	-	-	Argon	Ar-2% O2	30	0~18
-	-	Aluminum	-	1.2	aluminium alloy and stainless steel	-	-	-	-	40	-
-	-	ER50-6	-	1.2	Mild steel (2 mm thick)	9.5	19	Argon	87%Ar–13%CO2	80 / 160 / 240 / 320 / 400	-
30	La2 O3	308 stainless steel	4	1.2	Stainless steel 304 (12 mm thick)	-	-	Argon	Argon	30	10
30	-	-	1	1.2	Carbon steel (10 mm thick)	25	25	Argon	Argon	30	8

Source: (Author).

2.4 Weld overlay

2.4.1 Concept

The deposition of a layer of metal with specific characteristics onto the surface of a base metal with the purpose of improving desirable properties that are not intrinsic to the base metal is the definition of the term weld overlay or weld cladding. It is traditionally used by the industry to give longer lasting life for parts that to no meet the required properties for specific uses, to bring worn or corroded pieces back to use, and also, for the creation surfaces with special characteristics.

Industrial components are often subjected to hostile environment conditions such as hight heat, corrosive atmosphere, corrosive liquids, high pressure, and friction. Such scenery requires special characteristics from the materials that are going to be used. These materials need to be corrosion resistant, wear resistant, high heat resistant, have improved hardness or even have properties that provide good dimensional control.

The maintenance of industrial components is a high-cost activity, therefore extending these components lives can lessen the company's costs. This is the reason why weld overlay is commonly used, and its advantages are mainly:

a) Protection for the parts;
b) Improved surface properties where it is needed;
c) Cost effective use of highly costly alloy elements;
d) Faster method for use of materials with high hardness and wear resistant properties;
e) Less maintenance due to the recovery of worn parts, the use of less expensive materials as base metal, longer lasting parts, and others.

2.4.2 Operational principles

The weld overlay process is done by layering the weld beads side by side on to the base metal. These weld beads also need to have a certain level of overlap. This level will depend on the application and the materials used in the process. The process is finally completed when all the surface is covered (Figure 19).

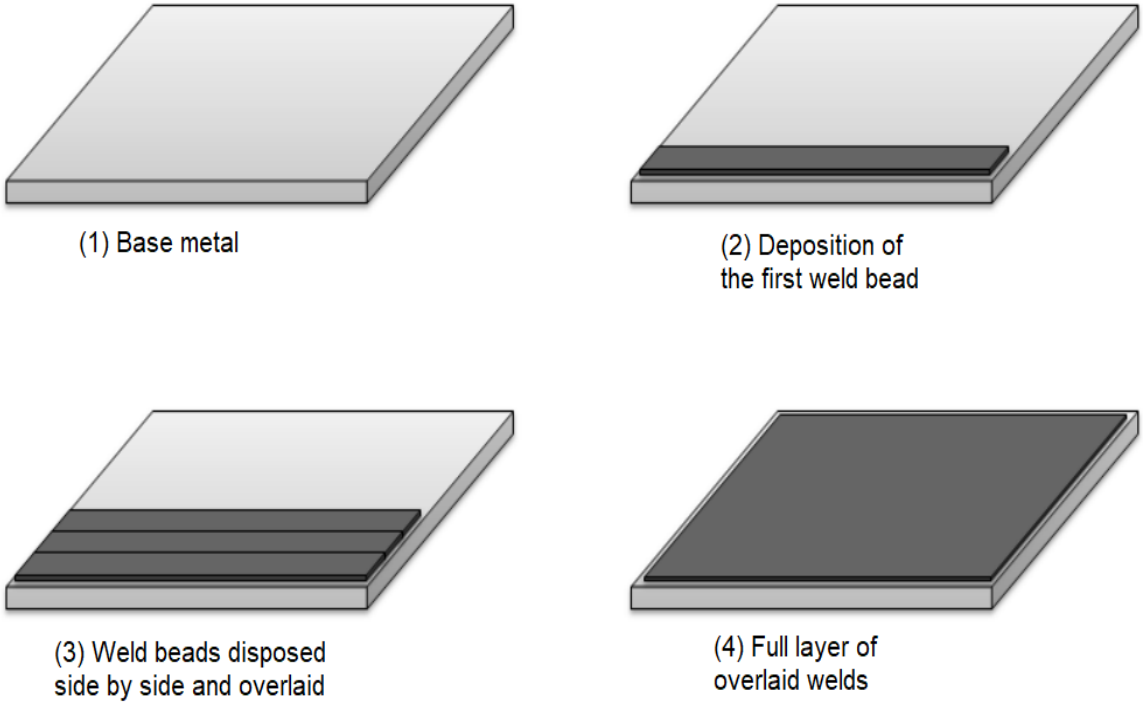

Figure 19 – Weld overlay operational principles.

Source: (adapted from GOMES, 2010).

2.4.3 Process characteristics

Covering as much area as possible with the least number of weld beads can result in savings for both time and materials. Consequently, this is one of the challenges of the weld overlay process. Kannan and Murugan (2006) point some of the following geometry parameters objectives to achieve the desirable weld bead geometry profile: larger weld bead width (W), high reinforcement height (R), lower penetration depth (P), small toe angle (Θ) and a minimum of dilution rate (D), which is obtained by the relation between the penetration area (PA) and the reinforcement area (RA).

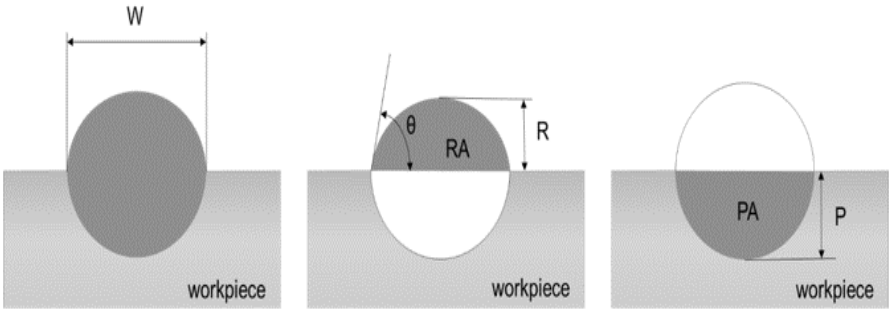

$$D = PA/(RA + PA)$$

Figure 20 - Weld bead geometry parameters.

Source: (Author).

2.5 Design of Experiments (DOE)

To understand the relationship between variables of a process, a researcher needs to change the input variables of the system and analyse what output these changes produce. The process of making these adjustments to the system is known as experiment. Through experiments, theories and assumptions made about how the system would behave at certain conditions can be sustained or rejected (MONTGOMERY, 2013).

2.5.1 The 2k factorial designs

Factorial designs are used when the effects of several factors are under investigation in an experiment. It is widely used for screening experiments, which are experiments conducted in the early stages of a study and many factors taken into consideration have little or no effect on the response. In the 2^k factorial design, each *k* factor (or control variable) has two levels. These levels can be qualitative or quantitative. The replicate of this design considers all possible combinations existing between each level of each variable. These combinations receive the name of treatments (MONTGOMERY, 2013).

Montgomery (2013) proposes a sequence of steps as the general approach to statistically analyse the 2^k design:

a) Step 1: define the problem to be solved;
b) Step 2: select the response variables;

c) Step 3: choice of factors;
d) Step 4: choice of experimental design;
e) Step 5: run the experiment;
f) Step 6: perform the statistical analysis;
g) Step 7: interpret results.

As an example, Equation (1) denotes the linear polynomial first order model that represents the observations of a two-factor factorial design (MONTGOMERY, 2013).

$$y = \beta_0 + \beta_1 x_1 + \beta_2 x_2 + \cdots + \beta_k x_k + \varepsilon$$

Equation (1)

Where:
y – Response variable
x_i – Independent variables
β_i – Coefficients to be estimated
k – Number of independent variables
ε – Experimental error

For more complex systems, such as the ones that present curvature. A higher degree equation should be used, such as presented in Equation (2).

$$y = \sum_{i=1}^{k} \beta_i x_i + \sum_{i<j} \sum_{i=1}^{k} \beta_{ii} x_i^2 + \sum_{i<j} \sum \beta_{ij} x_i x_j + \varepsilon$$

Equation (2)

Nearly all response surface problems are solved using Equations (1-2)

2.5.2 Response surface methodology (RSM)

The response surface methodology (RSM) is a set of mathematical and statistical tools used to model, analyse, and optimize complex systems, which the response variable is

influenced by multiple factors (MONTGOMEY, 2013). The RSM uses polynomial functions as shown in the Equation (1) to describe the relation between the variables.

The Ordinary Least Square (OLS) method is commonly used to define de coefficients for the model equations. As a result, the approximate function which relates the response variables to the process variables is obtained. Once the model is created, its significance has to be verified through the analysis of variance (ANOVA). The ANOVA is not only used to test if the model is statistically significant.

The ANOVA also allows the experimenter to check which terms of the model are significant and which are not and, therefore, can be removed from the model. The percentage of the response that can be explained by the model is represented by the coefficient of determination coefficient (R^2). Associated to R^2 is the adjusted R^2, it is a modified version of the R^2 that is adjusted according to the number of factors in the model. The adjusted R^2 has its value increased if a new predictor added improves the model. The opposite is also true.

ANOVA and other important analysis such as the residual and the lack-of-fit analysis are discussed in the following sections.

The main objective of RSM is to optimize (maximize or minimize) the response of interest of a function. Two graphical features are used to help interpret the behavior of the response variables. Response surface plots and contour plots. The latter is used to help visualize the shape of the response surface, as represented in Figure 21 (OEHLERT, 2013).

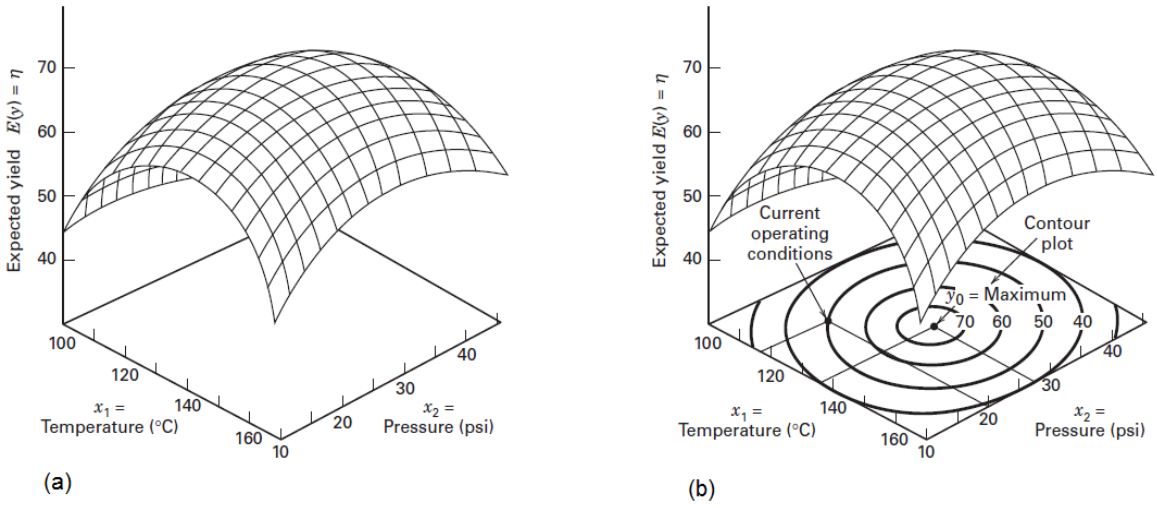

Figure 21 – (a) Response surface of expected yield in relation to pressure and temperature and (b) contour plot of a response surface.

Source: (MONTGOMEY, 2013).

2.5.2.1 Central Composite Design (CCD)

The Central Composite Design (CCD) is one of the standard designs used in the response surface methodology. The CCD usually derives from a 2k factorial design and it is commonly used when k > 2. It is composed of three elements (OEHLERT, 2010):

a) Factorial points, which are those derived from a 2^k factorial design;
b) Center points, that are the *n* observations taken from the 2^k factorial design with all variables set as 0. The center points are used for two purposes: Firstly, to test the lack of fit of the model, since the difference between the mean of the factorial points and the mean of the center points. Secondly, to give an estimate of pure error given by the discrepancy of the response at the center point;
c) Axial points (or star points). There are 2^k axial points at $\pm \alpha$ from the axis and all the remaining variables set at 0.

Figure 22 represents the CCD for a three-factor experiment.

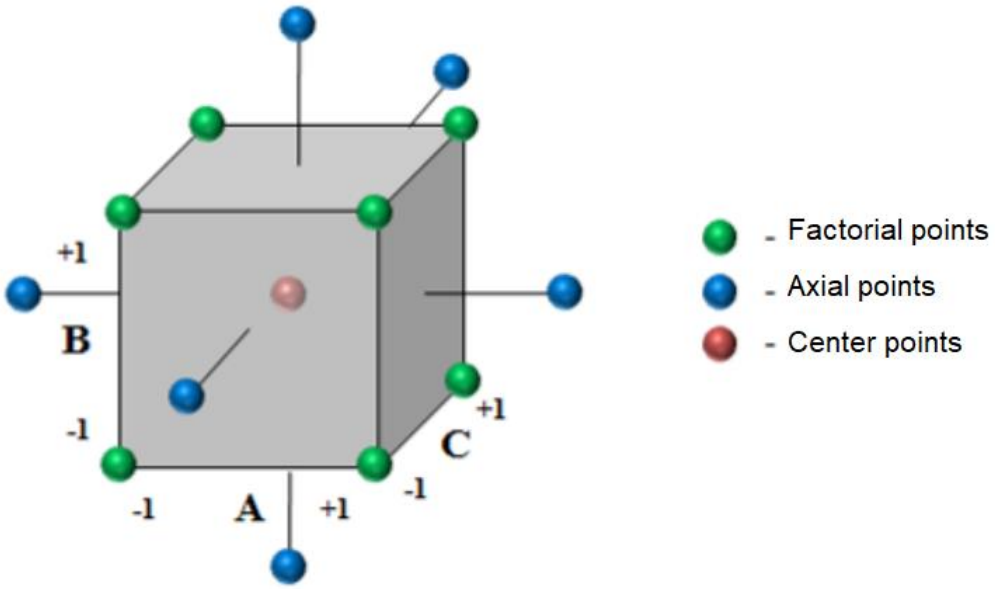

Figure 22 - CCD for three factors.

Source: (GOMES, 2010).

Both the α of the axial points and the number of center points can be chosen. Box et al. (2005) suggest that a CCD should be rotatable and orthogonal, which means that there would be no variance between the measured distance of any points of the design to its

center point (rotatable) and each parameter can be estimate independent from all other parameters of the model (orthogonal).

Montgomery (2013) states that for a rotatable design $\alpha = \sqrt{k}$ and recommends 3 to 5 center runs. Box et al. (2005) proposed Table 3 as a reference for design parameters for CCD. Where n_F corresponds to the number of factorial points, n_A consists of the number of axial points, n_{CA} represents the number of center points and N is the total number of observations.

Another important concept is blocking. Montgomery (2013) describes blocks as groups with similar characteristics. They are specially used for control of variance. Box et al. (2005) reinforce that by using blocks one can isolate the source of variability in between blocks. Therefore, there is no interfaces when comparing treatments.

Table 3 - Design parameters for CCD with rotatable blocking.

k	2	3	4	5	5 $\frac{1}{2}$ Rep.	6	6 $\frac{1}{2}$ Rep.	7	7 $\frac{1}{2}$ Rep.
Factorial Block(s)									
n_F	4	8	16	32	16	64	32	128	64
Number of blocks	1	2	2	4	1	8	2	16	8
Number of points in each block	4	4	8	8	16	8	16	8	8
Number of center points in each block	3	2	2	2	6	1	4	1	1
Total number of points in each block	7	6	10	10	22	9	20	9	9
Axial Block									
n_A	4	6	8	10	10	12	12	14	14
n_{CA}	3	2	2	4	1	6	2	11	4
Total number of points in the axial block	7	8	10	14	11	18	14	25	18
Total number of points N in the design	14	20	30	54	33	90	54	169	80
Values of α									
Orthogonal blocking	1.4142	1.6330	2.0000	2.3664	2.0000	2.8284	2.3664	3.3333	2.8284
Rotatability	1.4142	1.6818	2.0000	2.3784	2.0000	2.8284	2.3784	3.3636	2.8284

Source: (MONTGOMERY, 2013).

2.5.3 Analysis of variance (ANOVA)

The significance of the main effects and interaction are tested by the analysis of variance (ANOVA). The effects τ_i, β_j and $(\tau\beta)_{ij}$ are seen as deviations from the mean. With ANOVA the main point is to test the hypothesis that these effects are equal to zero $(\tau_{i_{1,\dots,a}} = 0,\ \beta_{j_{1,\dots,b}} = 0,\ (\tau\beta)_{ij_{1,\dots,ab}} = 0)$. That is, there is no main effect of any of the factors and there is no interaction between them. Table 4 shows an example of the ANOVA for a two-factor factorial design.

Table 4 – ANOVA for a two-factor factorial design.

Source of Variation	Sum of Squares	Degrees of Freedom	Mean Square	F_0
A treatments	SS_A	$a-1$	$MS_A = \frac{SS_A}{a-1}$	$F_0 = \frac{MS_A}{MS_E}$
B treatments	SS_B	$b-1$	$MS_B = \frac{SS_B}{b-1}$	$F_0 = \frac{MS_B}{MS_E}$
Interaction	SS_{AB}	$(a-1)(b-1)$	$MS_{AB} = \frac{SS_{AB}}{(a-1)(b-1)}$	$F_0 = \frac{MS_{AB}}{MS_E}$
Error	SS_E	$ab(n-1)$	$MS_E = \frac{SS_E}{ab(n-1)}$	
Total	SS_T	$abn-1$		

Source: (MONTGOMERY, 2003).

The a, b and n values from Table (2) are the same ones of the Equation (1). The F_0 value is the statistical test. In the displayed example, each ratio is testing one hypothesis: $F_0 = \frac{MS_A}{MS_E}$ and $F_0 = \frac{MS_B}{MS_E}$. That is, it is testing the hypothesis of no main effects existing for the factors A and B, respectively. $F_0 = \frac{MS_{AB}}{MS_E}$ tests the hypothesis of no interactions between factors. This value has an F-distribution, the hypothesis of non-effects or non-existing interaction is rejected if the P-value of the F-distribution is greater than the α value chosen (MONTGOMERY, 2003).

The Equation (3) gives the equivalence to the sum of squares represented in the ANOVA (MONTGOMERY, 2003).

$$\sum_{i=1}^{a}\sum_{j=1}^{b}\sum_{k=1}^{n}(y_{ijk}-\bar{y}...)^2 = bn\sum_{i=1}^{a}(\bar{y}i..-\ \bar{y}...)^2 + an\sum_{j=1}^{b}(\bar{y}.j.-\ \bar{y}...)^2 + n\sum_{i=1}^{a}\sum_{j=1}^{b}(\bar{y}ij.-\bar{y}i..-\bar{y}.j.+\ \bar{y}...)^2 + \sum_{i=1}^{a}\sum_{j=1}^{b}\sum_{k=1}^{n}(y_{ijk}-\bar{y}ij.)^2$$

Equation (3)

Where $\bar{y}i..$ is the average of the total number of observations taken at the i[th] level of the factor A, $\bar{y}.j.$ is the average of the total number of observations taken at the i[th] level of the factor B, $\bar{y}ij.$ Is the total average of observations taken at the ij[th] level. Finally, $\bar{y}...$ is the total average taken in all levels of all factors.

Equation (2) is the symbolic representation of Equation (4) and it is the one used in the ANOVA table.

$$SS_T = SS_A + SS_B + SS_{AB} + SS_E$$

Equation (4)

Before running any experiment, properly designing is an essential step. Misled conclusions can be drawn by a not well-designed experiment. Oehlert (2000) points out that an experiment should be designed in accordance with the following characteristics:

a) Avoid systematic error. It avoids biases in the responses of the system. That is, when conducting an experiment and the material used come from two different production lots, the researcher is unable to know whether the effects are due to some difference between the two lots or in fact due to any purposeful changes made by the researcher;
b) Be precise. This characteristic depends on the size of the error. The smaller the random error between the responses, the less variability the experiment has;

c) Allow estimation of error. Experiments must be designed in a way that it is possible to estimate the error so statistical inference can be made.
d) Have broad validity. This means that the researcher should know well the population so he or she would not neglect some important input variables. However, if too many input variables are taken into consideration, the precision of the response variables would decrease.

2.5.4 Main effects and interaction effects

The main effect and interaction are two important concepts in DOE. The variation in the response caused by a change in the level of a factor is called main effect. Box et al. (2005) describe the main effect as the difference between averages. They propose the Equation (4) to explain it for a two level factorial experiment. Where $\bar{y}_+$ corresponds to the average response of the plus level of the factor and the $\bar{y}_-$ relates to the average response of the minus level.

$$Main\ effect = \bar{y}_+ - \bar{y}_- \quad \text{Equation (5)}$$

The interaction is the relationship existing between two factors, Figure 23 illustrates the interaction phenomena happening for a 2^3 full factorial design, of which there are three factors A, B and C. The experiment has 8 runs.

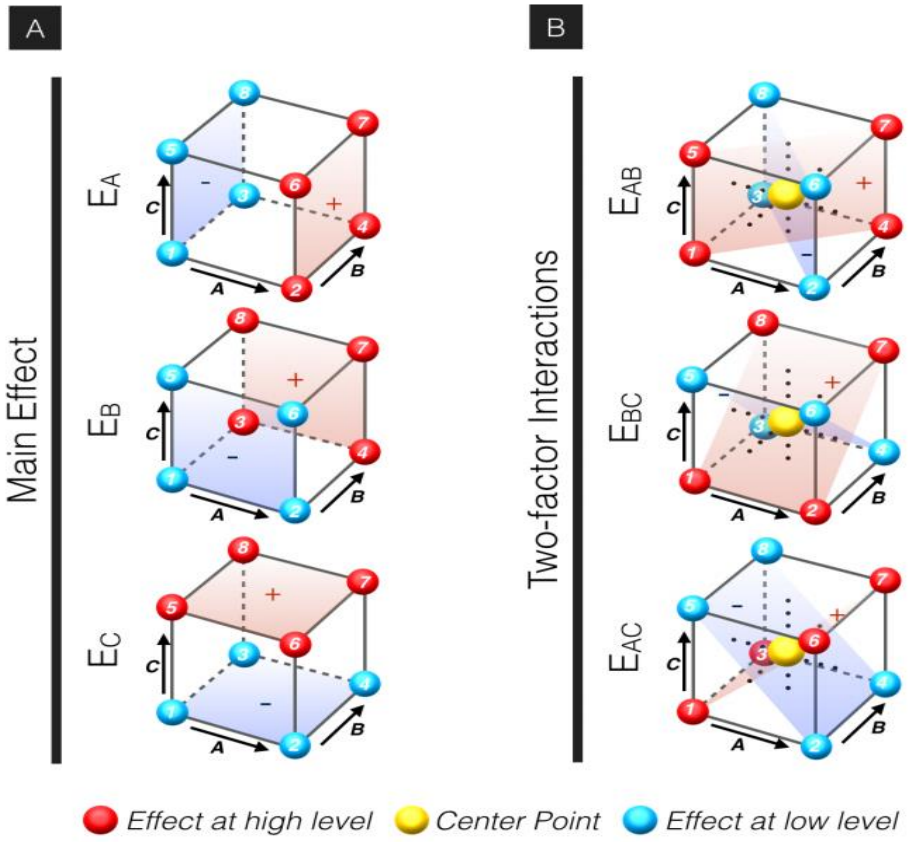

Figure 23 - Factorial experiment for a 2^3 design: (A) Main effect (B) Two-factor interactions.

Legend: E_A (Main effect of factor A), E_B (Main effect of factor B), E_C (Main effect of factor C), E_{AC} (Interaction between factors A and C), E_{BC} (Interaction between factors B and C), E_{AB} (Interaction between factors A and B).

Source: (MEI et al., 2015).

2.6 Optimization

2.6.1 Weighted global criterion method (weighted GCM)

A multi-objective optimization problem is a mathematical problem with more than one objective function to be optimized and sometimes, these object functions conflict. The weighted global criterion method (weighted GCM) can be used for multi-objective optimization problems. This approach takes into consideration the extent of the variation of each response variable. It is called global optimization problem due to this transformation of multiple objective functions into one global function (GOMES et al., 2018). Similarly, Arora

(2004) defines it as a scalarization method since it combines all the objective functions into one and then minimizes it.

Ardakani and Wulff (2013) propose the Equation (6) for the scalarized function.

$$Minimize: F(x) = \sum_{i=1}^{q} w_i \overline{f_i}(x)$$

$$Subjected\ to: g_j(x) \leq 0$$

Equation (6)

Where $F(x)$ is the global criterion, w_i is the relative importance given to each objective function $f_i(x)$. The constraints of the multi-objective functions are denoted by $g_j(x)$. Ardakani and Wulff (2013) comment that it is advisable to normalize the objective functions to avoid issues such as measuring objectives with different units. Therefore, the objective function will vary from 0 to 1. That is $f[0,1]$. As the objective of the function is the minimization, the smaller the better.

The normalized function for problems of minimization and maximization are displayed in Equations (7-8):

$$To\ minimize: \overline{f_i}(x) = \frac{f_i(x) - f_i^U}{f_i^N - f_i^U}$$

Equation (7)

$$To\ maximize: \overline{f_i}(x) = \frac{f_i^U - f_i(x)}{f_i^U - f_i^N}$$

Equation (8)

f_i^U is commonly called utopia point or ideal point. It is comprised by the best points out of the pay-off table, while f_i^N is often called nadir point or worst point retrieved from the pay-off table (MAKOWSKI, 1994).

The optimization algorithm chosen for this work is the generalized reduced gradient (GRG) algorithm. It is broadly used in nonlinear mathematical programming and it is a very robust algorithm (CARLYLE & MONTGOMERY, 2000; KROS & MASTRANGELLO, 2004).

This algorithm uses several random starting points, then at each interaction it provides the reduced gradient, then it tries to move towards the solution based on the values of the reduced gradient. It is called reduced gradient because it groups the variables into two sets for each interaction. The first set is called basic variables and the second are the independent variables (MONTGOMERY & CASTILLO, 1993). The version of GRG algorithm available in the Excel®-Solver software package is used in this work.

CHAPTER III

EXPERIMENTAL METHODOLOGY AND EQUIPMENT

This section shows the workbench configuration and the equipment used to perform the experiments. It also presents the methodology for the samples treatment.

3.1 Workbench and equipment

The workbench is equipped with an inverter power source for the TIG process and a multi-process power source to the MIG/MAG process. To stabilize the welding travel speed and to provide a consistent pace in the welding a mechanized mover which moves in a rail is used.

A two-torch holder gadget is attached to the automated mover to allow both process to happen at the same time. The automated mover is manufactured by SPS, model TARTÍLOPE V2F. The torch holder allows several angle configurations, spacing between torches and different heights for either torches.

3.1.1 Welding work bench set up

The workbench set up and the equipment used are depicted in Figure 24. They are identified as follows: (1) steel workbench; (2) automated mover TATÍLOPE V2F with the (3) two-torch holder gadget; (4) TIG torch; (5) MIG/MAG torch; (6) TIG power source supply manufactured by ESAB, model LHN 220i Plus; (7) MIG/MAG power source supply manufactured by IMC, model DIGIPlus A7 AC; (8) gas used for the TIG process; (9) gases

used for the MIG/MAG process; (10) automated mover control panel, (11) cooling system manufactured by IMC, model UPR 7500 and (12) MIG/MAG wire feeder system.

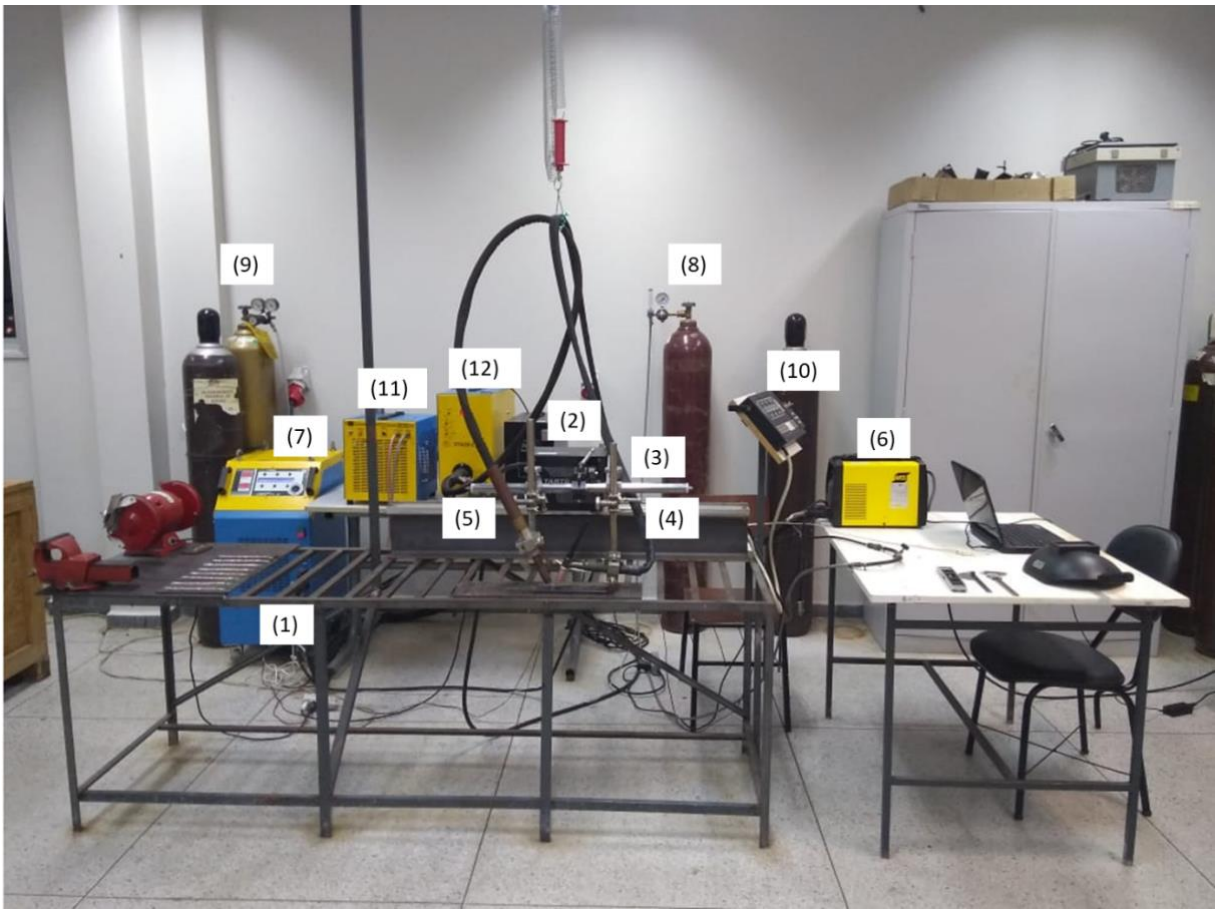

Figure 24 – Workbench set up.

Source: (Author).

3.1.2 Torches, torch holder gadget

Figure 25 illustrates the TIG and MIG/MAG torches attached to the two-torch holder gadget. The device allows both torches to have several angle configurations. It also gives a wide range of spacing options between torches along with varies possibilities of torch height configuration.

Figure 25 – TIG and MIG/MAG torches and the two-torch holder.

Source: (Author).

It is important to note that this study used common torch equipment with no special changes made to it. It implies that some restrictions may apply such as the grip the torch holder has to the TIG torch, some adaptions made to the MIG/MAG torch to provide a better grip, the sizes of the nozzles and even some dimension restrictions regarding the distances and angles each equipment handles. That is discussed later in this study.

3.2 Consumables

The consumables used in the study were:

- Steel plates (SAE 1020) on the sizes 200 mm x 50,8 mm x 6,35 mm.
- Pure Argon for the TIG torch process at a flow rate of 10 L/min;
- Argon plus 8% CO_2 for the MIG/MAG process at a flow rate of 12 L/min;
- 2.4 mm Tungsten electrode (class AWS EWTh-2 with 2% of Thorium);

- 1.2 mm wire electrode (ER70S-6);
- Sheets of sandpaper with grits of 80, 210, 360, 600, 1200 and 1500.

3.3 Welding procedure

3.3.1 Equipment set up

The first parameters that needed to be set were the electrical parameters. The MIG/MAG voltage was set through the equipment screen. The TIG current was set through its power source manual knot and checked the real current through the data acquisition equipment.

The gas composition for the TIG was pure Argon and for MIG/MAG was Argon + 8%CO_2. The flow rate set for both air lines were 10 L/min and 12mL/min, respectively. To start the process, the gas from the TIG torch was released to the metal some seconds before the TIG arc was opened. The TIG arc was opened with the aid of another electrode to make the physical contact between the part and the TIG electrode. Then, the automated mover was activated, and the MIG/MAG arc was also opened through a switch. The MIG/MAG gas source was released to the metal and the wire feeder was automatically activated by the same switch. To finish the welding process the following steps were followed: Close the TIG arc, close the MIG/MAG arc, which also included closing its gas source and wire feed, only then close the TIG gas source and finally stop the mover.

The steps of opening the TIG gas source before any torch was opened and only closing it after the welding process was finished are taken to provide extra protection to the weld bead.

3.3.2 Positioning set up

Due to the characteristics of the equipment, the positioning for each experiment had to made exactly at the same order:

1. Define TIG angle;
2. Define MIG/MAG angle;

3. Define MIG/MAG contact tip to work distance (from the welding plate to the entire wire extension at the nozzle tip);
4. With both MIG/MAG wire and TIG electrode at the same height (both touching the welding plate bare surface), define the distance between the electrodes;
5. Define the TIG height.

3.4 Samples treatment for further analysis

To be able to analyse the samples, a series of steps were taken. A horizontal bandsaw machine, model SFH-12 manufactured by Ferrari, was used to section the pieces. The samples were 30 mm wide. The cuts were made in the marks of 30 mm from the end of the weld bead as presented in Figure 26.

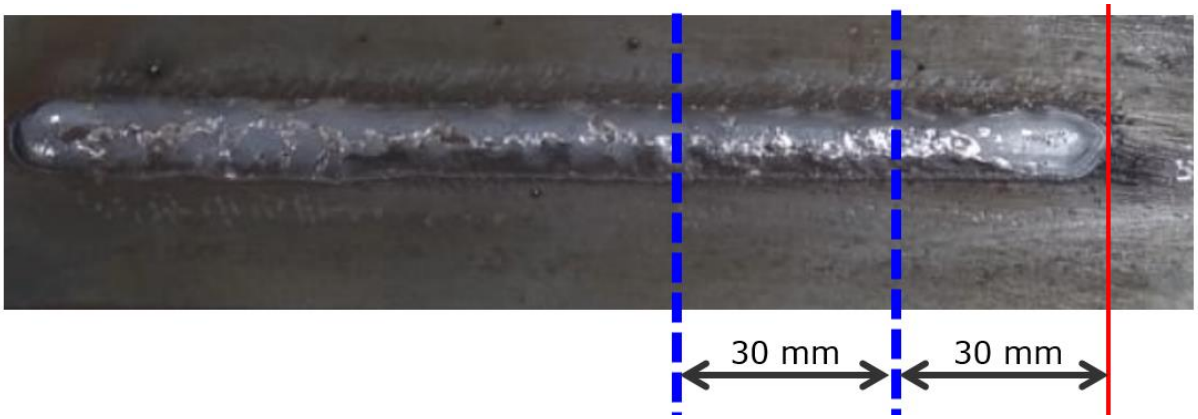

Figure 26 – Location of the weld bead cuts.

Source: (Author).

The samples were then embedded in a resin manufactured by Zanatta. To clean and polish the surface, sheets of sandpaper with granulometry of 80, 210, 360, 600, 1200 and 1500 were used in a sand polisher (model PVV manufactured by TECLAGO). A solution of Nital at 5% was used to chemically activate the weld bead section and reveal its macrography.

Photographs were taken from a digital microscopy, model S02 manufactured by HOT. The ImageJ software was used to measure the geometry of the weld bead and the Minitab software was used to treat and analyse the data.

3.5 Experimental Method

Defining the research methodology is extremely important so we can treat and solve the problems in a systematic way. As a result, clear information and real contribution to other scientific studies can be seen. Following this thinking, this chapter will strategically highlight the research problem and the experimental method of this work.

3.5.1 Research problem

As presented in the first chapter, this works aims to assess the influential variables of the welding process performed by a TIG and a MIG/MAG torch working simultaneously on steel plates (SAE 1020). The parameters studied are MIG/MAG contact tip to work distance (L), distance between the electrodes (d), TIG angle (θ2), MIG/MAG angle (θ1), TIG current (TC) and TIG height (h2).

The main objective is to find an optimal combination which allows the operator to maximize the weld bead geometric characteristic. The specific process that is under evaluation is the welding overlay. As mentioned in section 2.4, the desirable conditions for welding overlay are: larger weld bead width (W), high reinforcement height (R), lower penetration depth (P), small toe angle (Θ) and a minimum of dilution rate (D).

Based on the desired characteristics for the welding overlay, the generalized reduced gradient algorithm is used to solve the model constructed with the weighted global criterion method. The optimization of the multi-objective function aims to:

- Maximize the weld width;
- Maximize the reinforcement height;
- Minimize the penetration depth;
- Minimize the toe angle;
- Minimize the dilution.

3.5.2 Experimental Method

This object of study requires the optimization of multiple response variables which can be affected by several parameters of the process analysed (Figure 27). Therefore, the solution for the object of this study is complex. In this sense, a scientific approach is important for this type of problem so the correct tools can be defined so the findings of the study are coherent and relevant for the scientific community.

Figure 27 – schematics of the study.

Source: (Author).

The general step-step concept for the methodology that is going to be followed in this work is displayed in Figure 28.

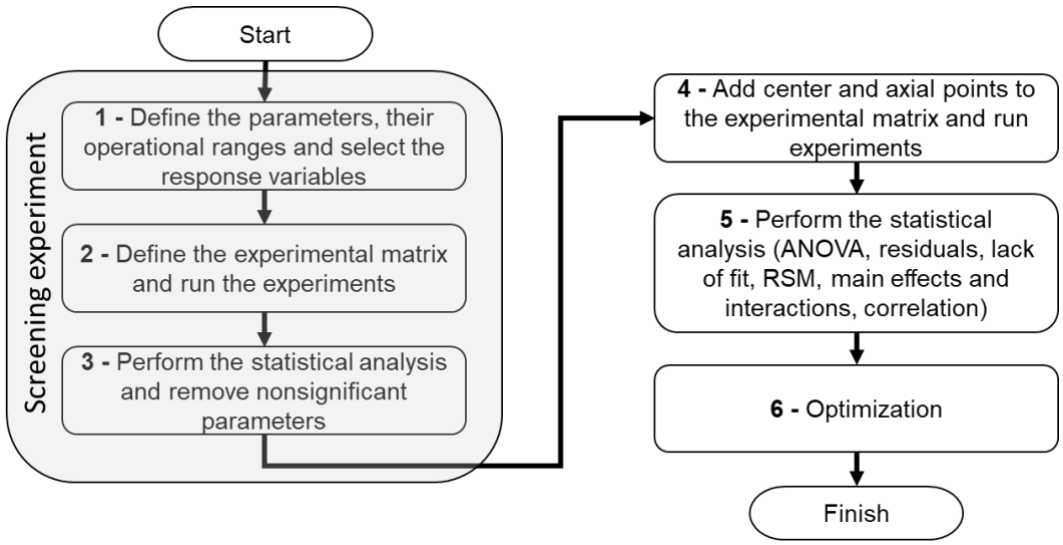

Figure 28 – General workflow for the RSM and optimization of this study.

Source: (adapted from MONTGOMEY, 2013).

The first step comprises the definition of the parameters and their ranges. To evaluate the proper ranges a series of test experiments might be undertaken in order to evaluate which ranges to choose and which response variables are going to be evaluated. Step number 2 corresponds to run of the experiments built on the definition of the experimental matrix based on the number of variables selected and their ranges. The statistical analysis is then run in step number 3. Pareto charts can be used to filter out the variables that are proved not significant to the experiment. The result is a reduced number of variables to manage. In step 4, axial points and center points are added to the experiment matrix and new experiments are run. Step 5 comprises the statistical analysis, now with more in-depth analysis. The ANOVA is performed for the models obtained. The model's lack of fit is also studied. The residual analysis is examined. Subsequently, the response surface analysis, main effect analysis and the interaction between effect analysis are carried over. The correlation is also appraised in this step. Finally, step 6 is where it is proposed an optimization model for the objective function.

CHAPTER IV

EXPERIMENTAL METHOD APPLICATION

4.1 Premises

This chapter focuses on the application of the experimental method defined in the section 3.5.2 to optimize the geometric characteristics of the weld overlay produced through TIG-MIG/MAG hybrid process. All the steps of the experimental methodology are presented in this section along with the results and the discussion.

On this study we wanted to simulate a process with spray metal transfer mode characteristics. Therefore, the combination of the below parameter values was chosen to provide a MIG/MAG current of about 230 A, with the data from the oscillogramme for the MIG/MAG current and voltage presenting spray metal transfer mode characteristics. It is important to mention that several trial experiments were run before these results were found. The initial values were taken according to what was available from previous studies to serve as a base line for the needs of this study. From there the values of each variable was changed to achieve the best results possible in terms of arc stability and weld bead visual aspect.

4.2 Response surface methodology

4.2.1 Define the parameters and their initial ranges

For the initial experiments the parameters displayed in Table 5 were constant throughout the process.

Table 5 – Fixed parameters for the first run of experiments.

Parameter	**Value**
MIG/MAG voltage	31 V
Wire feed rate	7.2 m/min
Welding travel speed	38 cm/min
TIG electrode tip angle	60 º

Source: (Author).

Before starting any experimental study, we needed to raise some hypothesis test. For our specific case, we needed to evaluate which variables that, by having two torches working at the same time, are affecting the geometry of the welding bead. Therefore, this chapter focuses on identifying the influential variables of the TIG-MIG/MAG hybrid process which are the TIG height (h2), MIG/MAG contact tip to work distance (L), Distance between the electrodes (d), TIG angle (θ2), MIG/MAG angle (θ1), TIG current (TC). These variables were chosen based on the experiments seen in the current literature, as sown in Table 2 previously.

Two Levels were chosen for each controlling variable, presented in Table 6.

Table 6 - Variables and their levels.

Factors/Levels	-1	1
TIG height (h2)	4.0 mm	6.0 mm
MIG/MAG contact tip to work distance (L)	20 mm	25 mm
distance between the electrodes (d)	12 mm	16 mm
TIG angle (θ2)	15 º	25 º
MIG/MAG angle (θ1)	25 º	35 º
TIG current (TC)	50 A	120 A

Source: (Author).

4.2.2 Select the response variables

The parameters to be used as response variables for the welding geometry analysis are:

a) W – Weld width;
b) Θ – Toe angle;

c) R – Reinforcement height;
d) P – Penetration depth.
e) D - Dilution, which is based an equation involving the reinforcement area (RA) and the penetration area (RA).

4.2.3 Define de experimental matrix

The 2k factorial design, with k = 6 was the design choice for these initial experiments, making a total of 16 experiments. Nevertheless, we added 4 center points to this initial block to give strength to the model. Hence, 20 experiments were conducted. Table 7 illustrates the design of experiments with each variable and their levels.

Table 7 – Design of experiments, variables, and their uncoded levels where h2 is TIG height, L is MIG/MAG wire extension, d is distance between the electrodes, θ2 is TIG angle, θ1 is MIG/MAG angle and TC is TIG current.

Run order	Point type	Blocks	h2 (mm)	L (mm)	d (mm)	θ2 (º)	θ1 (º)	TC (A)
1	1	1	-1	-1	-1	-1	-1	-1
2	1	1	1	1	-1	1	-1	-1
3	1	1	-1	1	1	-1	-1	-1
4	1	1	1	-1	1	1	-1	-1
5	1	1	-1	1	-1	1	1	-1
6	1	1	1	-1	-1	-1	1	-1
7	1	1	-1	-1	1	1	1	-1
8	1	1	1	1	1	-1	1	-1
9	1	1	-1	-1	-1	1	-1	1
10	1	1	1	1	-1	-1	-1	1
11	1	1	-1	1	1	1	-1	1
12	1	1	1	-1	1	-1	-1	1
13	1	1	-1	1	-1	-1	1	1
14	1	1	1	-1	-1	1	1	1
15	1	1	-1	-1	1	-1	1	1
16	1	1	1	1	1	1	1	1
17	0	0	0	0	0	0	0	0
18	0	0	0	0	0	0	0	0
19	0	0	0	0	0	0	0	0
20	0	0	0	0	0	0	0	0

Source: (Author).

Table 8 represents the design of experiments with their uncoded values.

Table 8 – Design of experiments with uncoded values where h2 is TIG height, L is MIG/MAG wire extension, d is distance between the electrodes, θ2 is TIG angle, θ1 is MIG/MAG angle and TC is TIG current.

Run order	Point type	Blocks	h2 (mm)	L (mm)	d (mm)	θ2 (º)	θ1 (º)	TC (A)
1	1	1	4	20	12	15	25	50
2	1	1	6	25	12	25	25	50
3	1	1	4	25	16	15	25	50
4	1	1	6	20	16	25	25	50
5	1	1	4	25	12	25	35	50
6	1	1	6	20	12	15	35	50
7	1	1	4	20	16	25	35	50
8	1	1	6	25	16	15	35	50
9	1	1	4	20	12	25	25	120
10	1	1	6	25	12	15	25	120
11	1	1	4	25	16	25	25	120
12	1	1	6	20	16	15	25	120
13	1	1	4	25	12	15	35	120
14	1	1	6	20	12	25	35	120
15	1	1	4	20	16	15	35	120
16	1	1	6	25	16	25	35	120
17	0	1	5	22.5	14	20	30	85
18	0	1	5	22.5	14	20	30	85
19	0	1	5	22.5	14	20	30	85
20	0	1	5	22.5	14	20	30	85

Source: (Author).

4.2.4 Run the experiment and register the results

The results of the response variables obtained for each experiment run is displayed in Table 9. Each response will be analysed individually in the following sections.

Table 9 – Response variables results for the initial analysis where W is weld width, R is reinforcement height, P is penetration depth, Ɵ is toe angle and D is dilution.

Run order	Point type	Blocks	W (mm)	R (mm)	P (mm)	Ɵ (º)	D (%)
1	1	1	11.15	2.61	1.94	36	41.97
2	1	1	10.23	2.84	1.88	42	34.81
3	1	1	10.93	2.69	2.05	39	40.31
4	1	1	12.10	2.68	2.22	42	44.4
5	1	1	11.14	2.76	1.69	34	36.68
6	1	1	10.87	2.54	1.92	36	37.67
7	1	1	10.02	2.73	1.77	41	36.82
8	1	1	10.65	2.78	2.04	40	38.15
9	1	1	9.47	2.87	2.25	45	37.58
10	1	1	10.66	2.82	2.32	37	40.68
11	1	1	11.90	2.46	2.43	36	40.72
12	1	1	13.49	2.65	2.61	32	45.65
13	1	1	9.45	2.89	1.95	48	33.57
14	1	1	10.45	2.76	2.29	52	39.34
15	1	1	11.53	2.68	2.34	35	44.6
16	1	1	12.14	2.43	2.54	33	46.76
17	0	1	10.26	2.66	2.18	36	36.96
18	0	1	10.75	2.74	2.22	39	40.18
19	0	1	10.87	2.53	2.01	34	41.74
20	0	1	10.80	2.64	2.03	38	41.4

Source: (Author).

4.2.5 Perform the statistical analysis

4.2.5.1 Pareto chart

Through the Pareto charts it is possible to classify the most influent variables on each response variable. The Pareto chart in Figure 29 shows that the most influent factor over all response variables is the distance between the electrodes (d). It is then followed by the interaction between the distance (d) and TIG height (h2). The TIG angle (Ɵ2) and the

MIG/MAG angle (Θ1) are not shown as significant, but they still present some influence over the process.

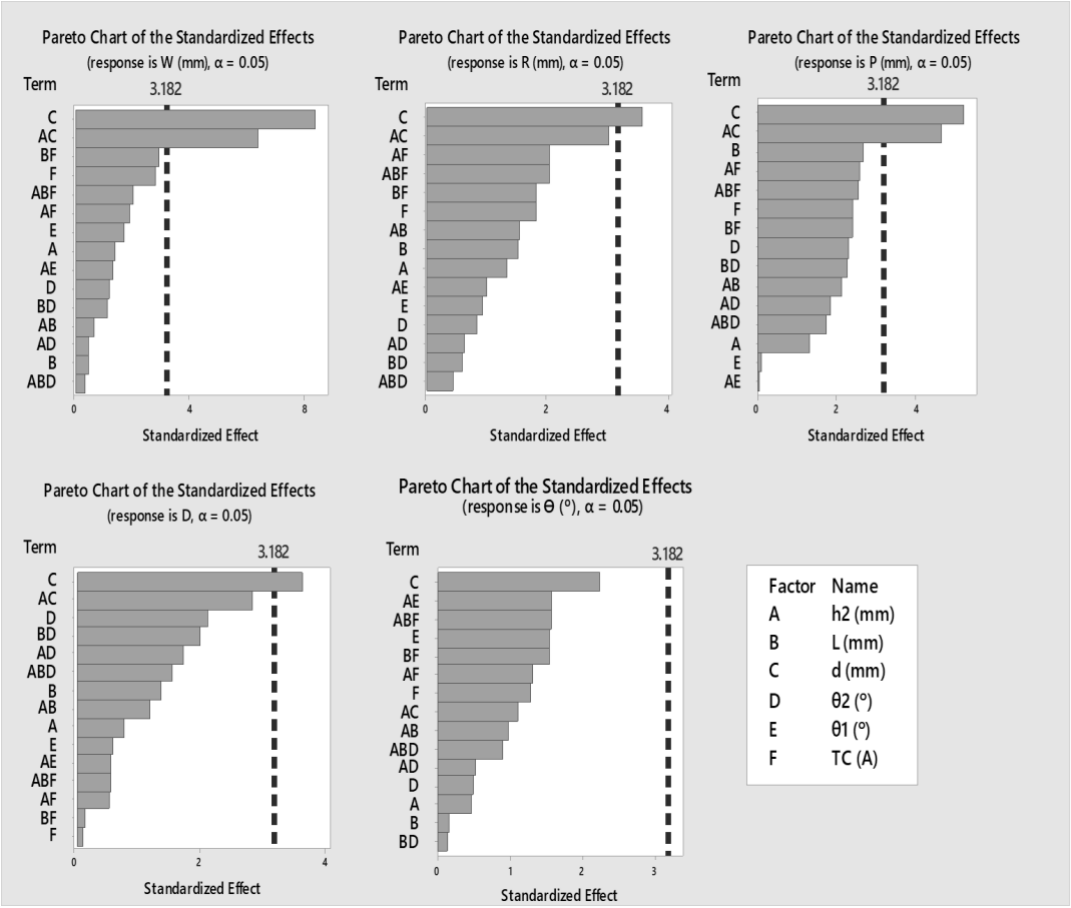

Figure 29 – Pareto Chart of the Standardized Effects for W, R, D, P and Θ.

Source: (Author).

The MIG/MAG contact tip to work distance is seen as influential in studies such as Azevedo (2019) Costa (2019). However, we believe this is not representative in this study due to the range chosen (from 20 mm to 25 mm). It brings us some possibilities. First, this range might be too short to show any important changes. Secondly, it might be already at the optimal solution for this variable and lastly, it could be the exact opposite. That is, this range could be very far from an optimal region. Nonetheless, as this range was chosen based on some studies from the literature using similar values, we strongly believe this result is close to its optimal region.

Based on the Pareto data, to complete this section of the analysis, four factors were chosen as the most representative from the screening experiment:

- distance between the electrodes (d);
- MIG/MAG angle (Ɵ1);
- TIG current (TC);
- TIG height (h2).

4.2.6 Add center and axial points to the experimental matrix

As per the current literature on axial points, this DOE could have axial points that could stretch even more the ranges of the variables. However, due to the equipment technical limitations, the furthest the axial points could go was + 1.41 or – 1.41. At this point it is important to reinforce that the experiments were run with conventional welding equipment for both TIG and MIG/MAG torches. Therefore, the minimum distances were challenging since the nozzle tips would not allow some distances and angle arrangements with the torches too close from each other. The minimum distance the torches would go for this equipment was 3.5 mm.

Also, here it is valid to mention the importance of understanding the equipment limitations before the execution any kind of DOE. If these limitations were not checked beforehand it could be a hindrance to this work.

For this second phase of the DOE, we run the experiments based on the same premises of the first run, but only varying the parameters that were selected from the Pareto chart. The excluded variables (MIG/MAG contact tip to work distance and TIG angle) were kept at their center point values. Table 10 shows the fixed values for this phase.

Table 10 – Fixed parameters for the second run of experiments.

Parameter	**Value**
MIG/MAG voltage	31 V
Wire feed rate	7.2 m/min
Welding travel speed	38 cm/min
TIG electrode tip angle	60 º
MIG/MAG contact tip to work distance (L)	22.5 mm
TIG angle (θ2)	20 º

Source: (Author).

Table 11 displays the coded design of experiments with 4 new center points and 8 axial points. So now, 12 more experiments were run, making a total of 32.

Table 11 – Coded design of experiments with 8 axial and 4 center points added. Where h2 is TIG height, d is distance between the electrodes, θ1 is MIG/MAG angle and TC is TIG current.

Run order	Point type	Blocks	h2 (mm)	d (mm)	θ1 (º)	TC (A)
1	1	1	1	-1	-1	-1
2	1	1	-1	1	1	1
3	1	1	-1	-1	1	1
4	1	1	-1	-1	-1	-1
5	1	1	1	-1	-1	1
6	1	1	1	-1	1	1
7	1	1	1	-1	1	-1
8	1	1	1	1	-1	1
9	1	1	-1	1	1	-1
10	1	1	1	1	1	-1
11	1	1	-1	1	-1	1
12	1	1	-1	1	-1	-1
13	1	1	-1	-1	1	-1
14	1	1	1	1	1	1
15	1	1	1	1	-1	-1
16	1	1	-1	-1	-1	1
17	0	0	0	0	0	0
18	0	0	0	0	0	0
19	0	0	0	0	0	0
20	0	0	0	0	0	0
21	-1	2	-1.41	0	0	0
22	-1	2	1.41	0	0	0
23	-1	2	0	-1.41	0	0
24	-1	2	0	1.41	0	0
25	-1	2	0	0	-1.41	0
26	-1	2	0	0	1.41	0
27	-1	2	0	0	0	-1.41
28	-1	2	0	0	0	1.41
29	0	2	0	0	0	0
30	0	2	0	0	0	0
31	0	2	0	0	0	0
32	0	2	0	0	0	0

Source: (Author).

Table 12 – Uncoded design of experiments with 8 axial and 4 center points added. Where h2 is TIG height, d is distance between the electrodes, θ1 is MIG/MAG angle and TC is TIG current.

Run order	Point type	Blocks	h2 (mm)	d (mm)	θ1 (º)	TC (A)
1	1	1	4	12	25	50
2	1	1	6	12	25	50
3	1	1	4	16	25	50
4	1	1	6	16	25	50
5	1	1	4	12	35	50
6	1	1	6	12	35	50
7	1	1	4	16	35	50
8	1	1	6	16	35	50
9	1	1	4	12	25	120
10	1	1	6	12	25	120
11	1	1	4	16	25	120
12	1	1	6	16	25	120
13	1	1	4	12	35	120
14	1	1	6	12	35	120
15	1	1	4	16	35	120
16	1	1	6	16	35	120
17	0	0	5	14	30	85
18	0	0	5	14	30	85
19	0	0	5	14	30	85
20	0	0	5	14	30	85
21	-1	2	3.59	14	30	85
22	-1	2	6.41	14	30	85
23	-1	2	5	11.18	30	85
24	-1	2	5	16.82	30	85
25	-1	2	5	14	22.95	85
26	-1	2	5	14	37.05	85
27	-1	2	5	14	30	35.65
28	-1	2	5	14	30	134.35
29	0	2	5	14	30	85
30	0	2	5	14	30	85
31	0	2	5	14	30	85
32	0	2	5	14	30	85

Source: (Author).

4.2.7 Run the experiment and register the results

The response variables' results obtained for each experiment run is displayed in Table 13. Each response will be examined individually in the following sections.

Table 13 – Response variables results for the initial analysis where W is weld width, R is reinforcement height, P is penetration depth, Ɵ is toe angle and D is dilution.

Run order	Point type	Blocks	W (mm)	R (mm)	P (mm)	Ɵ (º)	D (%)
1	1	1	11.15	2.61	1.94	36	41.98
2	1	1	10.23	2.84	1.88	42	34.81
3	1	1	10.93	2.69	2.05	39	40.32
4	1	1	12.10	2.68	2.22	42	*
5	1	1	11.14	2.76	1.69	34	36.69
6	1	1	10.87	2.54	1.92	36	37.68
7	1	1	10.02	2.73	1.77	41	36.82
8	1	1	10.65	2.78	2.04	40	38.16
9	1	1	9.47	2.87	2.25	45	37.58
10	1	1	10.66	2.82	2.32	37	40.68
11	1	1	11.90	2.46	2.43	*	40.73
12	1	1	13.49	*	2.61	32	45.65
13	1	1	9.45	2.89	1.95	48	33.57
14	1	1	10.45	2.76	2.29	52	39.34
15	1	1	11.53	2.68	2.34	35	44.60
16	1	1	12.14	2.43	2.54	33	46.76
17	0	1	10.26	2.66	2.18	36	36.97
18	0	1	10.75	2.74	2.22	39	40.19
19	0	1	10.87	2.53	2.01	34	41.74
20	0	1	10.80	2.64	2.03	38	41.40
21	-1	2	11.45	2.51	2.10	32	42.95
22	-1	2	11.27	2.45	2.38	32	42.19
23	-1	2	10.47	2.61	2.18	40	41.96
24	-1	2	12.05	2.34	2.03	30	45.07
25	-1	2	10.76	2.66	2.19	38	41.32
26	-1	2	10.19	2.75	2.04	43	37.16
27	-1	2	10.88	2.72	1.74	37	35.79
28	-1	2	10.77	2.58	2.70	33	46.20
29	0	2	10.65	2.66	2.12	36	39.93
30	0	2	10.84	2.54	2.13	34	40.63
31	0	2	10.44	2.51	2.14	31	41.16
32	0	2	10.97	2.60	2.11	35	38.91

Large residual terms that were removed from the analysis are displayed as *

Source: (Author).

Figure 30 shows the sections of each experiment run.

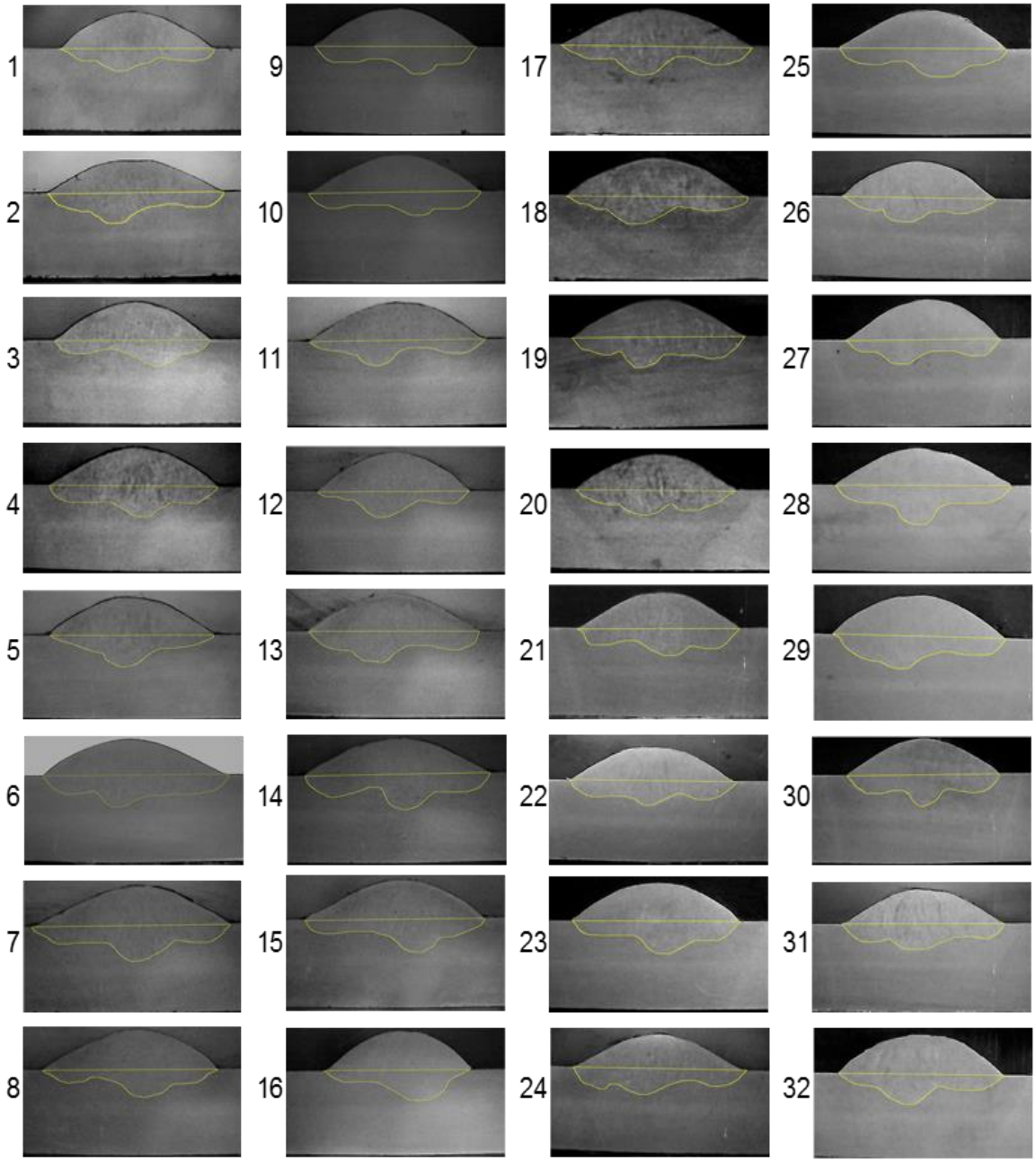

Figure 30 – Cross-section of each experiment of table 13. Plate thickness of 6.35 mm.

Source: (Author).

4.2.8 Perform the statistical analysis

4.2.8.1 Mathematical models and ANOVA

The software Minitab® was used to obtain the models and run the ANOVA. This is an interactive process where if pointed some inconsistencies the researcher must make some adjustments. In this specific work, some of the response variables are stated as * in the previous table as they were reported as large residuals in the ANOVA. These values were accounted for in the initial runs. However, they were removed to improve the model equations (9-13).

W = *24.15 - 4.09*H2- 1.635*D+ 0.807θ1- 0.1398* TC + 0.284H2*H2 + 0.0584D*D - 0.00646 θ1*θ1 + 0.000012 TC*TC + 0.0938H2*D - 0.0132H2*θ1 + 0.00675H2*TC - 0.02800D*θ1 + 0.00779D*TC - 0.000079 θ1*TC*

Equation (9)

R = *1.31 + 0.760*H2+ 0.284*D- 0.1911θ1+ 0.01453* TC - 0.0408*H2*H2 - 0.01084*D*D + 0.002893 θ1*θ1 + 0.000036* TC*TC - 0.00397*H2*D - 0.00791*H2*θ1 - 0.001012*H2*TC + 0.00379*D*θ1 - 0.001363*D*TC + 0.000088* θ1*TC*

Equation (10)

P = *2.281 - 0.165*H2+ 0.0388*D- 0.0562θ1+ 0.006541*TC + 0.00850*H2*θ1*

Equation (11)

Ɵ = *72.9 + 22.34*H2+ 1.15*D- 8.26θ1+ 0.694*TC - 1.060*H2*H2 + 0.103*D*D + 0.1281* θ1*θ1 + 0.000423*TC*TC - 0.368*H2*D - 0.197*H2*θ1 + 0.0046*H2*TC + 0.0750*D*θ1 - 0.07269*D*TC + 0.00775* θ1*TC*

Equation (12)

D = *141.1 - 13.95*H2- 8.93*D+ 0.64θ1- 0.461*TC + 0.551*H2*H2 + 0.257*D*D - 0.0448*θ1*θ1 - 0.000197*TC*TC - 0.294*H2*D + 0.306*H2*θ1 + 0.0366*H2*TC + 0.0425*D*θ1 + 0.03322*D*TC - 0.00264*θ1*TC*

Equation (13)

The ANOVA is displayed in Table 14. The null hypothesis tested is that the models are adequate. As the p-values are < 0.05, there is not enough evidence to reject the null hypothesis. Therefore, these results indicate that the models are adequate. The table shows that the models for the weld width (W), penetration (P) and toe angle (Ɵ) are substantial, since their adjusted R^2 are above 80%. The models for the reinforcement height (R) and the dilution rate (D) are satisfactory as they are above 70%. The table also shows that the models did not present lack of fit (> 0.05). The reduced model as used for the penetration (P) since it presented a model with better R^2 adjusted than the model given by the complete square method. This behavior was not evidenced for the remaining variables.

Table 14 – ANOVA table.

Coefficient	Degrees of freedom	Adjusted SS	Adjusted MS	F-value	P-value	Lack of fit *P-value*	adjusted R^2 (%)	RSM method
W	15	18.089	1.20593	9.64	0	0.141	80.69	Complete square method
P	5	1.45149	0.2903	27.57	0	0.178	81.08	Reduced model
R	15	0.475787	0.031719	6.09	0.001	0.64	71.79	Complete square method
Ɵ	15	705.866	47.058	11	0	0.622	83.80	Complete square method
D	15	286.082	19.072	5.86	0.001	0.402	71.55	Complete square method

Source: (Author).

The levels of significance of the coefficients of each model are displayed in Table 15. It is possible to see some interactions between factors are significant. It means that the joined effect of these parameters has impact on the process results. The analysis of these interactions is presented in section 4.2.9.

Table 15 – P-values of the coefficients of each model.

Coefficient	W	R	P	Ɵ	D
h2	**0.008**	0.130	**0.001**	0.064	0.595
d	**0.000**	**0.000**	**0.002**	**0.000**	**0.001**
θ1	**0.012**	0.320	**0.006**	0.177	0.125
TC	0.260	0.134	**0.000**	0.790	**0.000**
h2 *h2	**0.029**	0.111	**-**	0.148	0.377
d *d	0.065	0.092	**-**	0.560	0.111
θ1*θ1	0.190	**0.009**	**-**	**0.000**	0.084
TC *TC	0.903	0.084	**-**	0.466	0.696
h2 *d	0.050	0.690	**-**	0.231	0.293
h2 *θ1	0.465	0.061	0.110	0.132	**0.013**
h2 *TC	**0.017**	0.090	**-**	0.799	**0.025**
d *θ1	**0.006**	0.071	**-**	0.243	0.420
d *TC	**0.000**	**0.000**	**-**	**0.000**	**0.001**
θ1*TC	0.878	0.442	**-**	**0.037**	0.403

Source: (Author).

4.2.8.2 Residual analysis

The residuals of a model are characterized by the difference between the values predicted in a model and the observed values obtained during the experiment. The residual analysis is an important step to make sure that the models developed are truly representative of the response variables. Table 16 shows the Anderson-Darling normality test conducted to the standard residuals. The table shows small A-squared values and large p-values (>0.05) indicating that the residuals are normally distributed.

Table 16 – Anderson-Darling normality test applied to the standard residuals.

Normality test	W	R	P	Ɵ	D
A-squared	0.211	0.175	0.109	0.195	0.140
p-value	0.844	0.918	0.993	0.884	0.970

Source: (Author).

4.2.9 Main effects analysis and response surface analysis

Minitab® was the tool used to build the main effect analysis. Surface plots were obtained through the software Statistica®, they are used to aid on the visualization of the effects between interactions which were evidenced on Table 15.

Once final models are obtained it is possible to understand the behavior of the dependent variables based on changes made on the independent variables. More specifically, the independent variable subjected to the analysis can be changed while the others are kept constant. In this sense, the effects that this specific variable has on the response variables can be known.

Figures (32 – 45) display how the weld width (W), reinforcement height (R), penetration depth (P), toe angle (Ɵ) and dilution rate (D) are influenced by distance between the electrodes (d), MIG/MAG angle (Ɵ1), TIG current (TC) and TIG height (h2).

To analyse the main effects, it is important to keep in mind what are the objectives wanted for each variable:

- **Maximize**: weld width and reinforcement height;
- **Minimize**: penetration depth, toe angle and dilution.

4.2.9.1 Weld width (W)

Figure (31) presents the results for the weld width (W). The distance between the electrodes is directly proportional to the increase in the weld width. At larger distances the hybridization is generated and therefore the arc is more stable providing more heating area along with the course of the welding.

The TIG height is also a parameter that is positively affecting the weld width. Previous studies (MENDEZ & EAGAR, 2003; MENG et al., 2014; LIANG et al., 2017) showed equivalent results. The authors also advocate that the premature solidification of the weld pool was prevented by the larger heating area formed at these conditions. Azevedo and Resende (2021) in a more recent study advocate that as the leading TIG arc is pre-heating the base metal, it helps on the weld pool formation in the TIG-MIG/MAG process. As the TIG electrode distance is increased from the base metal, its bell-shaped arc covers a larger area, and therefore, it pre-heats more base material and as a consequence the weld pool area is greater.

The MIG/MAG angle is not affecting the weld width as much as the TIG height or the electrodes distance but is causing some effect on it. As the MIG/MAG angle increases the weld width decreases. The MIG/MAG angle interaction with the wire-electrode distance is representative to the model. Figure (32) illustrates the results of the joined behavior of these two variables. The combination of longer wire-electrode distances with smaller MIG/MAG angle provide wider welds. Corresponding results were observed by Azevedo and Resende (2021).

The TIG current is slightly positively significant to the weld width, that is from the minimum and maximum values applied for the TIG current it was not observed great changes in the weld width. Schneider et al. (2017) found similar results in their work. However, the authors mention that this factor might interact with other variables and cause greater changes to this parameter. Some interaction is indeed found with the TIG current, which is observed in Figure (33) which shows that as the TIG current and the wire-electrode distance are mutually increased, the weld bead width becomes larger.

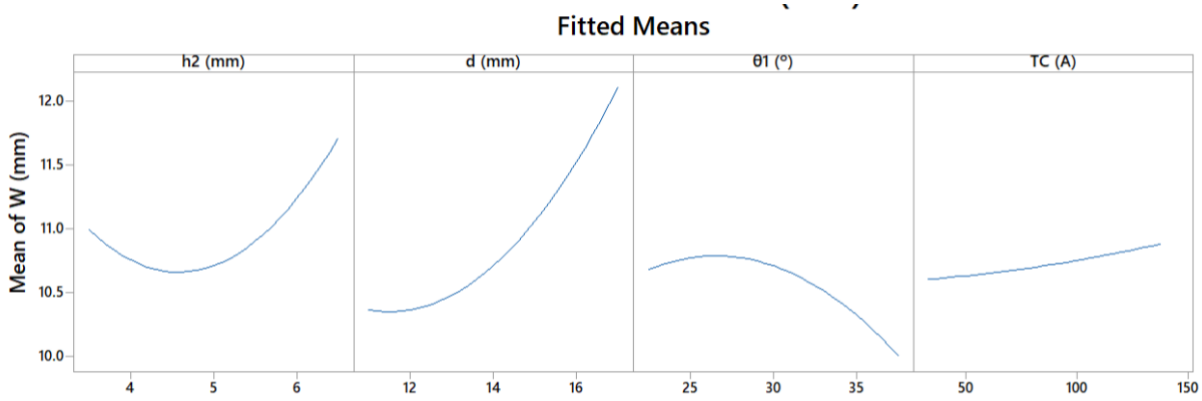

Figure 31 – Main effects plot for weld width (W).

Source: (Author).

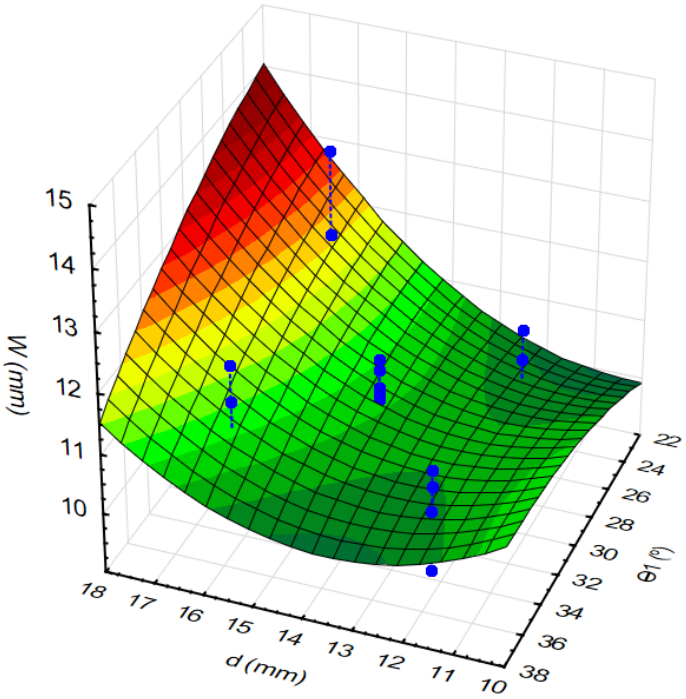

Figure 32 – Effect of the interaction between Θ1 (º) and d (mm) for weld width (W).

Source: (Author).

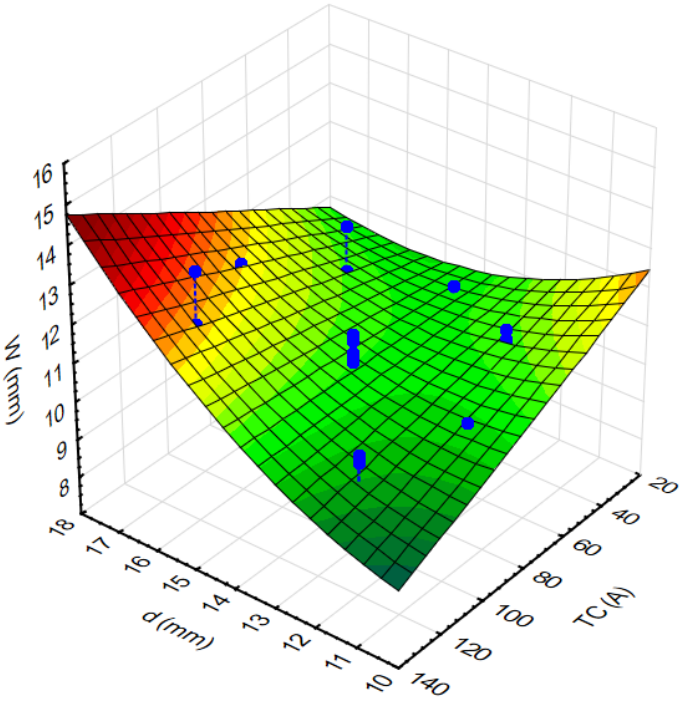

Figure 33 – Effect of the interaction between TC (A) and d (mm) for weld width (W).

Source: (Author).

4.2.9.2 Reinforcement height (R)

Figure (34) shows a negative relationship between the reinforcement height and the distance between the electrodes. In the studies of Adak et al. (2015), Liang et al. (2014) and Resende and Scotti (2017) it is possible to see that the welding parameters cause inverse relationship between the reinforcement height and the weld width. As the weld volume is the same, the larger the weld bead width, the smaller the reinforcement height.

Figure (35) contains the interaction between the wire-electrode distance and the TIG current shows two scenarios where the reinforcement is higher. First is at longer wire-electrode distance and lower TIG current. It happens because at longer distances the heat influx coming from both torches are not, at the same time, acting on a specific location on the weld pool. Therefore, there is less molten metal when the material from the MIG/MAG wire is placed on the weld pool, making the reinforcement higher. On the other hand, one thing to notice is the increased reinforcement at lower TIG currents. Azevedo and Resende (2021) pointed in their study that the arc is less stable at lower current values such as 40 A. It is one possible explanation for the behavior seen in Figures (34-35), where it is indicating that at lower currents the reinforcement is increased. Another possible explanation is that the arcs are interacting with each other and are causing this behavior. There is also an extra possible explanation for this behavior is due to how the remaining variables of the experiments were set in the software used for the interactions effect. There is the likelihood that they were not set at their center point or that the points chosen were not the best ones to represent the experiment behavior for these two variables.

The second scenario is showing that at shorter wire-electrode distance and higher TIG current there is an increase in the reinforcement. Even though there is more current coming from the TIG arc, both torches are very close to each other. As there is not enough time for the heat influx to spread and go to the sides of the plate, it stays focused on the center of the plate. This behavior hinders the expansion of the weld pool and favours the reinforcement height. Similar behavior was noticed by Azevedo and Resende (2021).

Figure (36) illustrates the interaction between the MIG/MAG angle and the distance between the electrodes. It shows the inverse relation between the variables, of which, to achieve higher reinforcements it is needed to enlarger the distance and reduce the MIG/MAG angle. Similar result is obtained if MIG/MAG angle is increased while the distance is decreased.

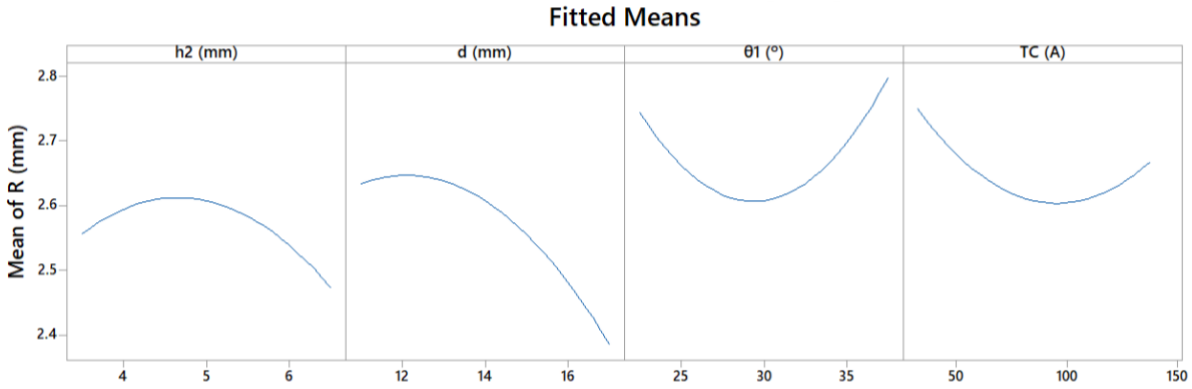

Figure 34 – Main effects plot for reinforcement height (R).

Source: (Author).

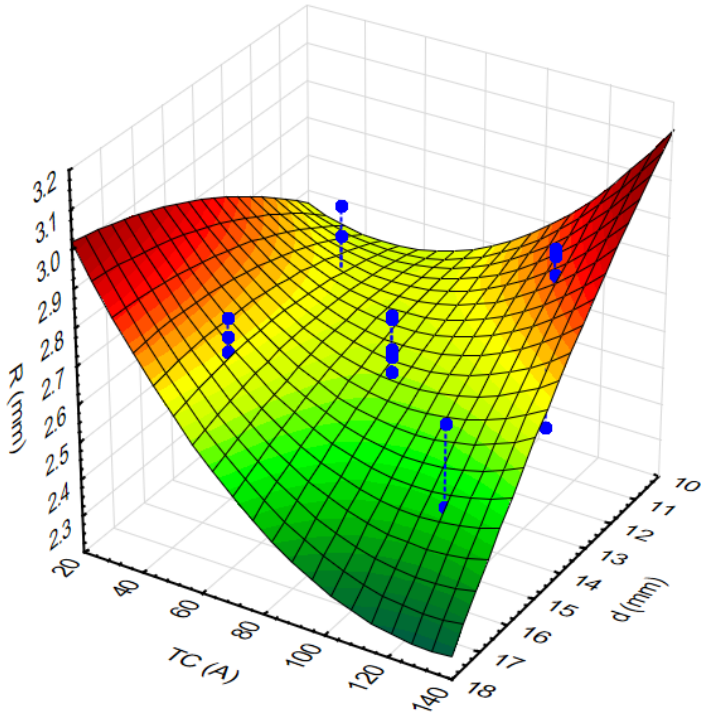

Figure 35 – Effect of the interaction between TC (A) and d (mm) for reinforcement height (R).

Source: (Author).

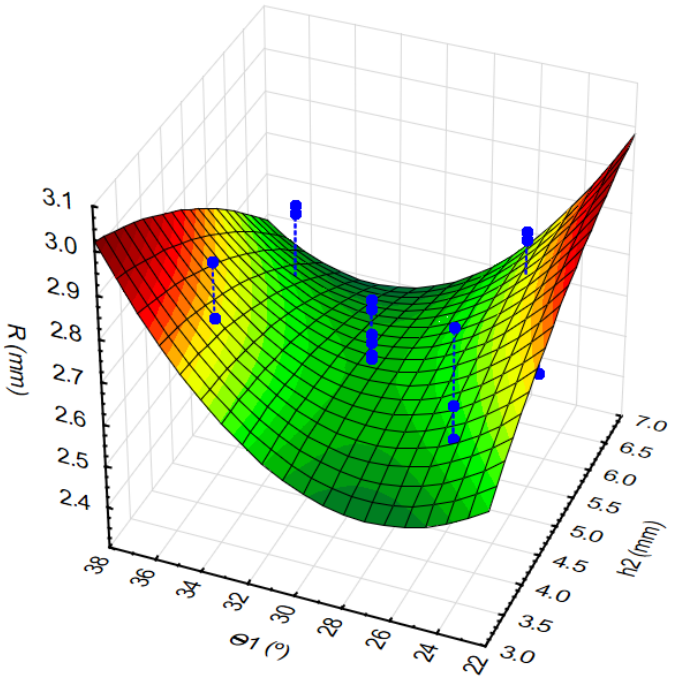

Figure 36 – Effect of the interaction between Θ1 (º) and h2 (mm) for reinforcement height (R).

Source: (Author).

4.2.9.3 Penetration depth (P)

Figure (37) indicates strong positive effect between the penetration depth and the value of the TIG current. As the current is increased, the heat input on the weld pool also increases, resulting in deeper welds. The same result was found in a similar study made by Liang et al. (2016) involving 6061 aluminium alloy.

Kanemaru et al. (2015) and Liang et al. (2016) also observed in their studies that the higher the TIG current they applied in their experiments, the deepest was the weld depth. This phenomenon can be explained by with higher currents, the radius of the TIG arc also increases improving the volume of molten material. Once this molten metal solidifies the penetration of the weld is deeper.

Figure (38) displays the joined effect of the TIG current along with the distance between the electrodes. It turns out that by increasing both parameters, the penetration depth also increases.

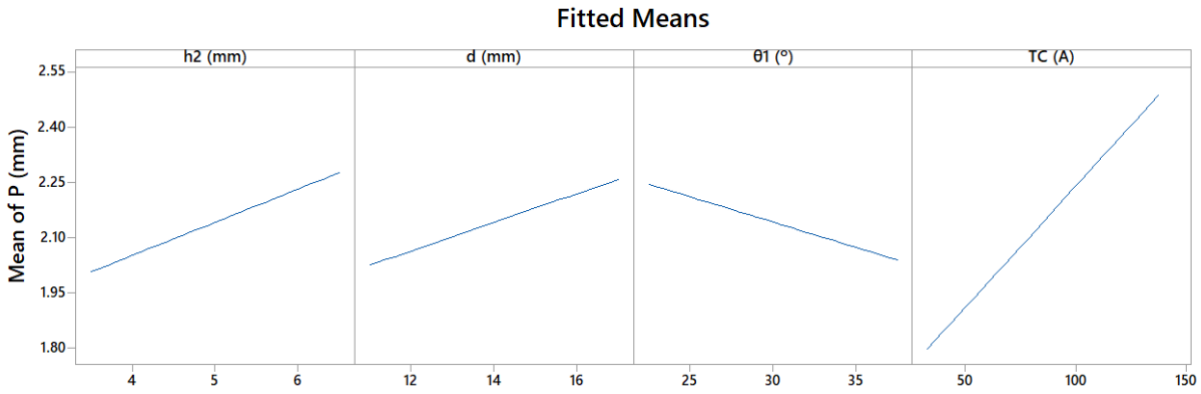

Figure 37 – Main effects plot for penetration depth (P).

Source: (Author).

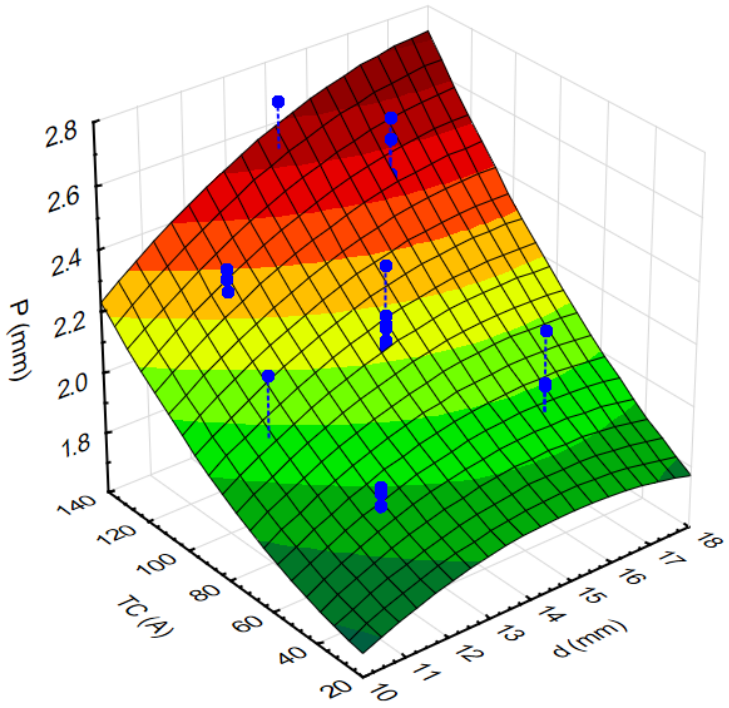

Figure 38 – Effect of the interaction between TC (A) and d (mm) for penetration depth (P).

Source: (Author).

4.2.9.4 Toe angle (Ɵ)

The toe angle values were obtained by measuring the tangent line of the weld bead surface against the tangent line that faces the steel please surface. A measurement was taken from each side of the weld bead surface and then the average of this value as calculated to form the data that is being used.

Figure (39) indicates an inverse relationship between the wire-electrode distance and the toe angle. At short distances both torches are close from each other there is more heat input onto the same area on the weld pool. The toe angle is directly linked to the weld pool temperature. Therefore, as the heat input is increased the smaller the toe angle is. This behavior is also seen in the research conducted by Zhang et al. (2014), Adak et al. (2015) and Liang et al. (2016). The combination of higher TIG current and smaller distance between the electrodes can grant this specification as displayed in the interaction plot from Figure (40).

Figure (41) displays the relationship between the TIG current and the MIG/MAG angle. It illustrates an inverse relation between these two variables. To decrease the toe angle, the TIG current must be increased as the MIG/MAG angle decreases.

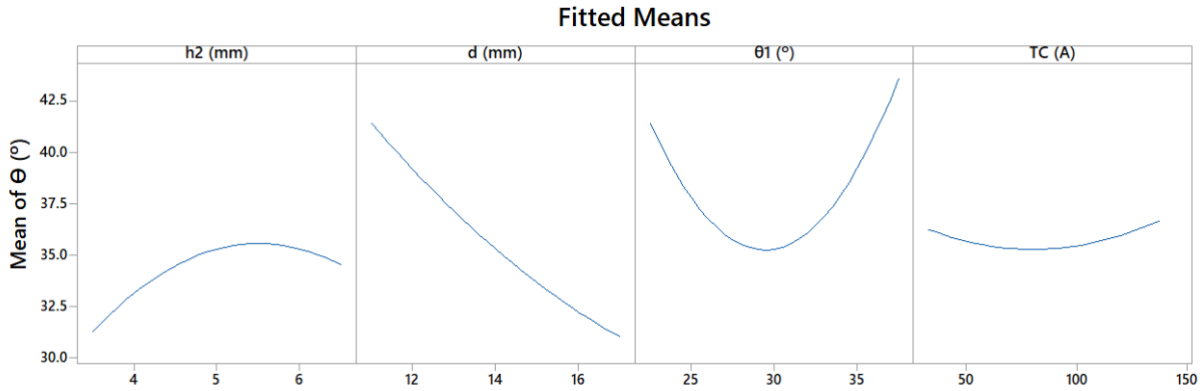

Figure 39 – Main effects plot for toe angle (Ɵ)

Source: (Author).

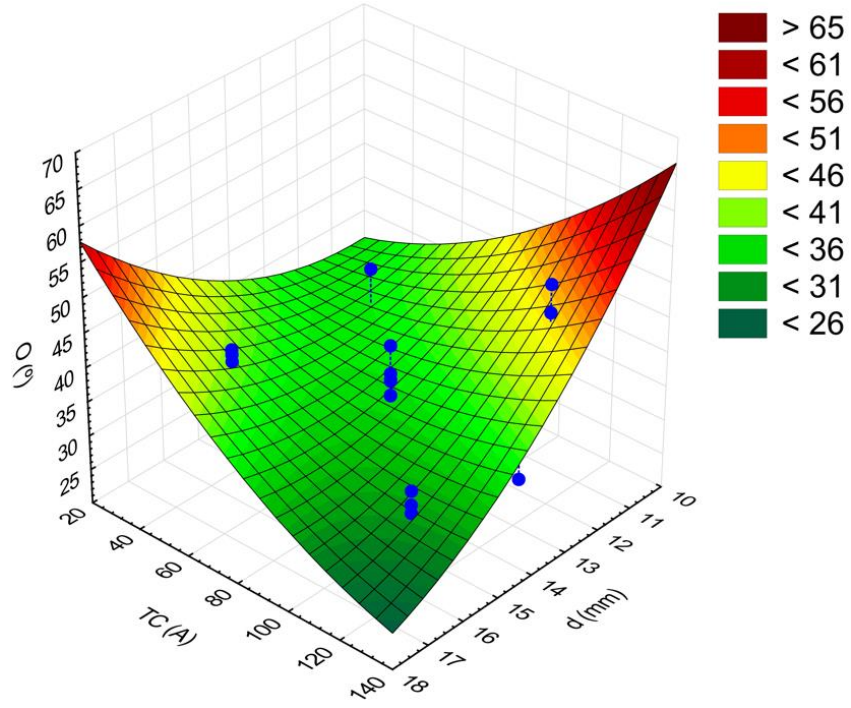

Figure 40 – Effect of the interaction between TC (A) and d (mm) for toe angle (Θ).

Source: (Author).

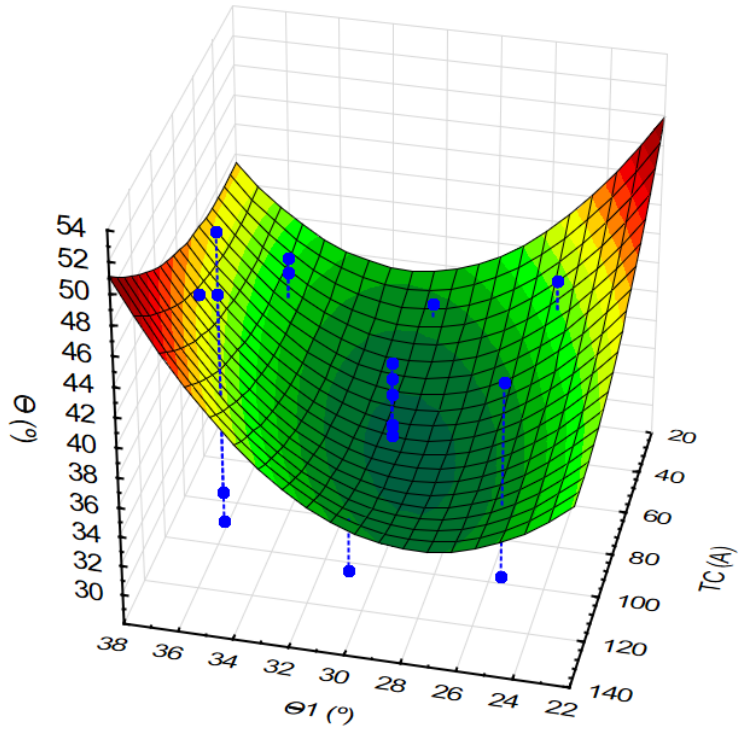

Figure 41 – Effect of the interaction between Θ1 (º) and TC (A) for toe angle (Θ)

Source: (Author).

4.2.9.5 Dilution rate (D)

Figure (42) presents the main effects results for the dilution rate (D). The distance between the electrodes is positively affecting the dilution. Shen et al. (2017) in their study with magnesium alloy were able to reach the similar results. As the distance is increased, the arc radius is also increased lessening the thermal power. Therefore, the penetration area is reduced. As the wire feed rate is the same throughout the process, the reinforcement increases.

The TIG current is also presenting a positive effect on the dilution rate. Even though the penetration tends to be deeper with the increase in the heat source from the TIG arc on the weld pool, it also improves the ability of the weld fluid to spread more easily on the course of the weld bead as the molten metal takes longer to cool down the reinforcement area is lower. This same characteristic is mentioned in the work of Resende and Scotti (2017).

The interaction effect between TIG current and TIG height is exhibited in Figure (43). The decrease of both variables causes a drop in the dilution rate. The same behavior, just a little less intense, is seen in Figure (44) which shows the interaction between the distance and the TIG current. Lian at al. (2016) present the same outcomes and the authors state that for weld overlay process low dilution rate is the desired.

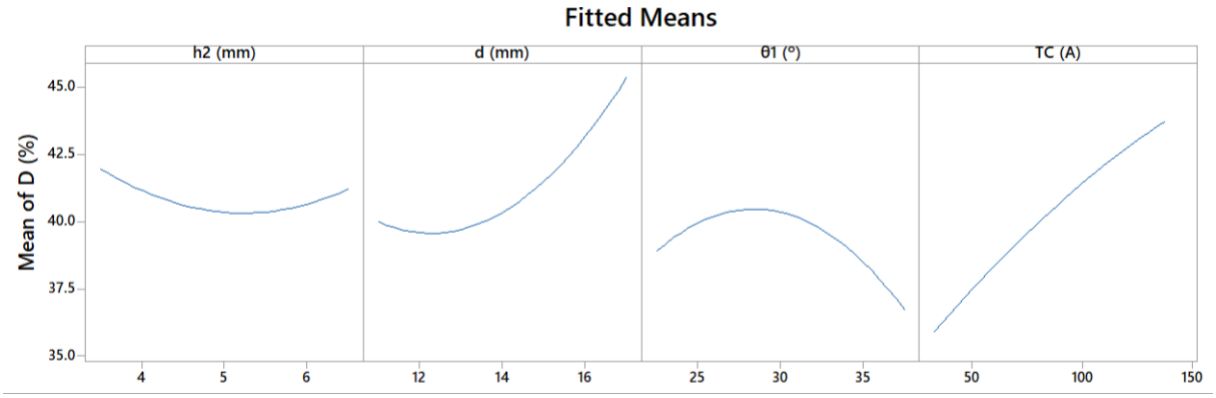

Figure 42 – Main effects plot for dilution rate (D)

Source: (Author).

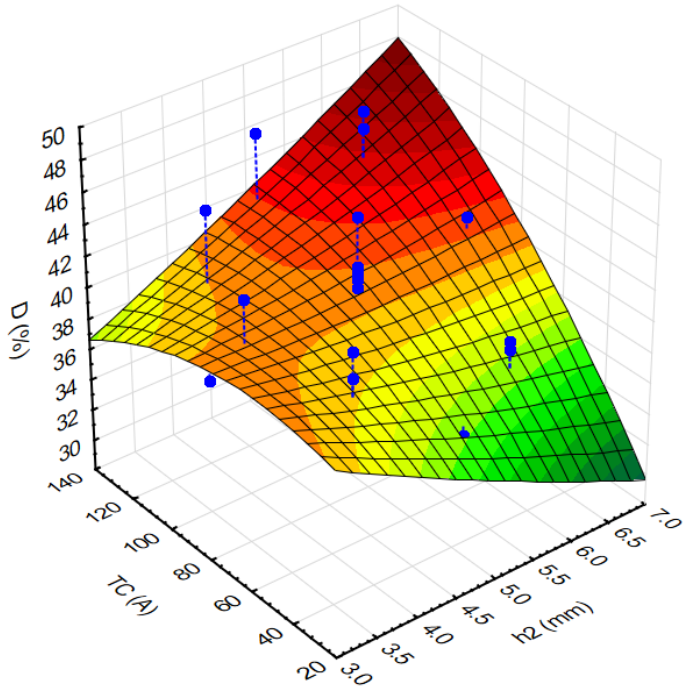

Figure 43 – Effect of the interaction between h2 (mm) and TC (A) for dilution (D)

Source: (Author).

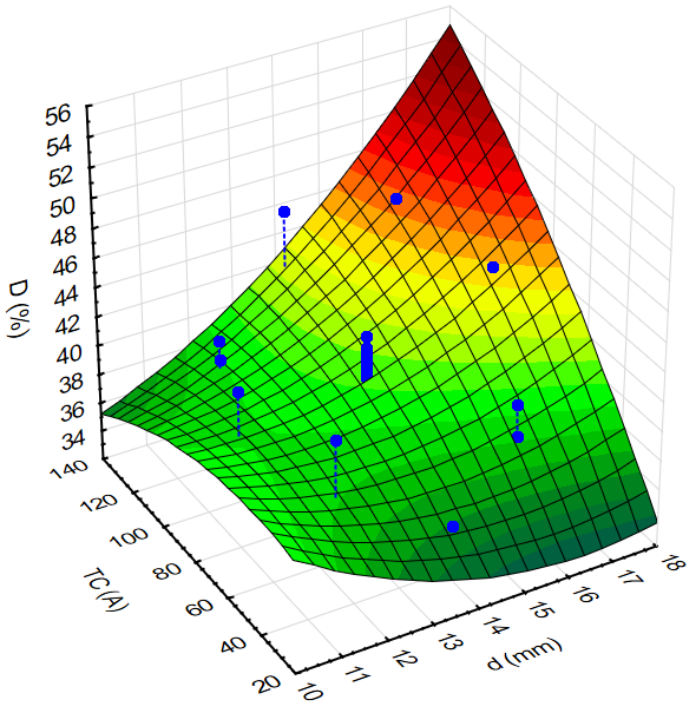

Figure 44 – Effect of the interaction between d (mm) and TC (A) for dilution (D)

Source: (Author).

CHAPTER V

OPTIMIZATION

The work developed on the previous chapter is already of great relevance for the process studied. From the models and analysis obtained, it was possible to acknowledge the variables that have impact over the process results and their significance, which is vital to achieve better control of the process parameters.

To achieve the proposed objectives of this work, the optimization is the next step to be taken. Therefore, the weighted global criterion method (weighted GCM) is used to optimize the parameters for the TIG-MIG/MAG hybrid welding applied on weld overlay on steel plates (SAE 1020). The GRG is applied to the weld width, reinforcement height, penetration depth, toe angle and the dilution rate. The following sections consist of the application of the GRG method.

Let us recap the optimization objectives before moving to the analysis:

- **Maximize**: weld width and reinforcement height;
- **Minimize**: penetration depth, toe angle and dilution.

5.1 Correlation between the response variables

The correlation table was obtained from Minitab® and it is important what is the relationship between the response variables of the models obtained. From Figure (45) displays the results of the correlation between these variables. It is possible to see that nearly all correlations presented are significant (p-value < 0.05).

This information helps us to understand the trade-offs we might have in the models. For example. Both weld width and the reinforcement have maximization objectives, but the correlation table shows they have a negative relationship. This means that we have conflicting variables, since they cannot be maximized up to their ideal level. There is the need to find an intermediate level for them. Except for the toe angle, the same type of trade-off happens for all the remaining variables that present any correlation to the variable W. It

means that maximizing the weld width variable is challenging since its objective is not going in favor of the other variable's objectives.

For the reinforcement variable the correlation with the toe angle is positive, but they have different optimization objectives. In addition, the ire a negative relationship with the dilution, which is good because while the reinforcement needs to be maximized the dilution needs to be minimized.

The only correlation for penetration is with the dilution variable and this relationship is positive and since both have the same optimization objectives, it is promising for the optimization model. The toe angle presents a negative correlation with the dilution, which is also good for the optimization since they have oppositive objectives.

	W (mm)	R (mm)	P (mm)	Θ (°)
R (mm)	-0.693 0.000			
P (mm)	0.425 0.015	-0.311 0.089		
Θ (°)	-0.584 0.001	0.798 0.000	-0.214 0.257	
D	0.724 0.000	-0.717 0.000	0.714 0.000	-0.623 0.000

Cell Contents
Pearson correlation
P-Value

Figure 45 – Correlation between the response variables

Source: (Author).

5.2 Modelling

Equation (14) is an adaptation of the Equation (5), and it is used for the solution of the problem. This adaptation was made so the values for the optimization would be maximized and the objective would be to get them as close as possible to 1. This would then avoid any misunderstanding in the table values.

$$Maximize: F(x)_{mod} = \sum_{i=1}^{5} w_i * d_{mod}(\boldsymbol{x})$$

$$Subjected\ to: g_j(x) \leq \alpha^2$$

Equation (14)

Where:

$$d_{mod}(\boldsymbol{x}) = 1 - \overline{f_i}(x)$$

$$\alpha = 1.141$$

$$f(x) = \text{W, R, P, Θ, D.}$$

It is important to keep in mind the α chosen was due to the physical limitations of the equipment. In a different scenario it could be higher considering the number of variables. The schematic built in the spreadsheet from Microsoft Excel® to solve the formulation is presented in the Appendix, Figure A.1.

Different weights were adopted to the variables for the purposing of proving the efficiency of what is proposed by the weighted GCM. Therefore, the scenario is built under the circumstance that the penetration depth minimization received a weight of 0.8 while the remaining variables were set to the same weight of 0.05. More eight was applied to the penetration depth minimization since it is considered a common objective in weld overlay. These weight conditions can be applied in studies and even in the industry based on specific needs. Therefore, the results shown here can and will change depending on the weights the researcher chooses.

The optimized values show that it was possible to improve the values of P to 100%. Meaning that between the Nadir and Utopia points from the payoff matrix it was the best result possible. That is, the solution touched the Utopia point for the responsible variable P. The other variables presented lower values. W was optimized to 4%, R to 82%, θ to 44% and D to 80%. From this specific configuration of weights, the target for each variable is: w = 10.76 mm, R = 2.68 mm, P = 1.76 mm, θ = 34.34º and D = 37.72 %. Another output of this optimization is Table 17, which contains the parameters configuration to reach these response variables targets.

Table 17 – Parameter's configuration to obtain the optimum configuration under the conditions set.

h2 (mm)	d (mm)	θ1 (º)	TC (A)
4.5	13.2	32.2	44.0

Source: (Author).

5.3 Results validation

Confirming experiments were made to check the viability of the optimization. The purpose is to compare the experimental results with the modelled results. Therefore, the optimum combination of parameters from Table 18 was used in 3 weldments. The values of MIG/MAG contact tip to work distance (L) and TIG angle (θ2) were kept on their center points to keep the same standard as the last blocks of experiments (see Table 10).

Table 18 – Confirmation experiments parameters.

h2 (mm)	L (mm)	d (mm)	θ2 (º)	θ1 (º)	TC (A)
4.5	22.5	13.2	20.0	32.2	44.0

Source: (Author).

Table 19 displays the results obtained for the confirming experiments.

Table 19 – Confirmation experiments results.

Experiment	W (mm)	R (mm)	P (mm)	Θ (º)	D (%)
1	11.22	2.69	1.75	36.29	38.84
2	10.92	2.50	1.73	35.99	40.39
3	11.56	2.51	1.53	35.52	38.00
Average	11.23	2.57	1.67	35.93	39.08
Target	10.76	2.68	1.76	34.34	37.72
Error	4.38%	-4.17%	-4.87%	4.66%	3.59%

Source: (Author).

The results obtained from the confirmation experiments are satisfactory since the disparity between what was foreseen by the model and the experimental values was below 5%. It is a strong indication that the model build in this study is valid and can be used for

further analysis of the of the parameters for the TIG-MIG/MAG hybrid welding applied on weld overlay on steel plates (SAE 1020).

Figures (46-47) display the visual and geometric parameters for the optimized weldment based on the optimization.

Figure 46 – Visual aspect of the optimized parameters.

Source: (Author).

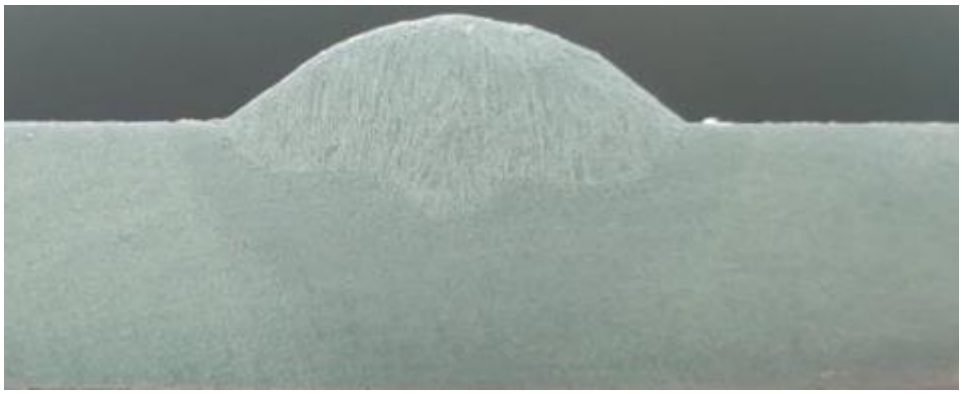

Figure 47 – Geometry aspect of the optimized parameters.

Source: (Author).

CHAPTER VI

CONCLUSIONS

6.1 General conclusions

From the results and the thoroughly analysis performed in chapter 4 and 5, this work has the following conclusions:

1. The models obtained from the response surface analysis are highly reliable, since for most of the coefficients the results were above 80%. The only exceptions are the reinforcement height and the dilution, yet these models presented an adjusted R^2 of above 70%, which is a satisfactory result.
2. The parameters TIG height (h2), MIG/MAG contact tip to work distance (L), distance between the electrodes (d), TIG angle (θ2), MIG/MAG angle (θ1), TIG current (TC)) are significant to the TIG-MIG/MAG hybrid welding applied on weld overlay on steel plates (SAE 1020).
3. Considering the effect of the process parameters, the following conclusions can be made:
    - To increase the distance between the electrodes and increase the TIG electrode height will enlarge the weld width.
    - Higher reinforcement is obtained by shortening the distance between the electrodes and lessening the TIG current and also setting the TIG height at about 4.5 mm and the MIG/MAG angle at about 35º.
    - Shallower penetration depth is obtained by lessening the TIG current, the TIG electrode height and the distance between the electrodes. And increasing the MIG/MAG angle.
    - To decrease the toe angle, the distance between the electrodes needs to be increased along with the TIG height and the MIG/MAG to angle set to about 30º.

- To minimize the dilution the distance between the electrodes must be shortened along with the TIG current. The MIG/MAG angle also impacts, it presents a curvature, and the value that best minimizes the dilution is set to about 35º.

4. The correlation analysis showed that most of the variables were correlated and some trade-offs of the process were already at sight. At this stage it was possible to identify that the weld with presented great trade-offs with all other variables of the process, and therefore, it would be very challenging to reach its optimum point in the model since its success would mean the hindrance for the other variables of the process.
5. The application of the weighted global criterion method to obtain the optimization results proved to be successful, since the results could be experimentally confirmed.
6. The results of this work proved to be useful to the academic community and to the industry. The models obtained through the optimization could be reproduced experimentally with acceptable error values (below 5%). Therefore, these models can surely be used to achieve better control over the TIG-MIG/MAG hybrid welding applied on weld overlay on steel plates (SAE 1020).

6.1.1 Contributions of this work

This study's contributions are:

1. Better understanding of the effects of the TIG-MIG/MAG hybrid welding process parameters and their interactions.
2. Provide a systematic procedure to the TIG-MIG/MAG hybrid welding applied on weld overlay on steel plates with efficient results and made with common equipment which is easily found on the market and used by companies around the globe.
3. Production of reliable mathematical model which allow better control of the process parameters over the response variables.
4. The production of an optimization model that can provide an optimum solution based on the values set to the parameters and the degree of importance given to each parameter.

6.2 Future work suggestions

The suggestions for future works are:

1. Use mixture methodology in the weights of the optimization variables values. As an interactive process, it is believed that an even better result could be achieved.
2. Analyse the process with variables related to the quality of the process such as the superficial aspect of the welding, the formation of humps and spatters
3. Evaluate variables related to the productivity of the process such as weld travel speed and deposition rate.
4. Examine the properties of the welded zone such as the hardness, the heated affected zone, the microstructure to evaluate the TIG effect on the process.

REFERENCES

ADAK, D.; MUKHERJEE, M.; PAL, T. Development of a Direct Correlation of Bead Geometry, Grain Size and HAZ Width with the GMAW Process Parameters on Bead-on-plate Welds of Mild Steel. **Transactions of the Indian Institute of Metals**, v. 68, n. 5, p. 839-849, 2015.

ALTHOUSE, A. D.; TURNQUIST, C. H.; BOWDITCH, W. A.; BOWDITCH, K. E.; BOWDITCH, M. A. **Modern welding**. 12. Edition. Goodheart-Willcox, 2020.

AMERICAN WELDING SOCIETY (AWS), **Welding Handbook, Volume 2 - Welding Processes, Part 1**. 9th Edition. Miami: American Welding Society (AWS), 2004.

ARDAKANI, M. AND WULFF, S. An overview of optimization formulations for multiresponse surface problems. **Quality and Reliability Engineering International**, Vol. 29, No. 1, pp.3–16, 2013

ARORA, J., **Introduction to optimum design**. 2nd ed. San Diego, Calif.: Elsevier Academic Press, pp.673-674, 2004.

ASM INTERNATIONAL, **ASM handbook: Welding, brazing, and soldering**.10th Edition. Materials Park, OH: ASM International, 1993.

AZEVEDO, S. C. **Avaliação de Aspectos Operacionais do Processo de Soldagem GTAW-GMAW**.109p. Dissertação de Mestrado, Universidade Federal de Goiás, Catalão, GO. 2019.

AZEVEDO, S.C.; DE RESENDE, A. Effect of angle, distance between electrodes and TIG current on the weld bead geometry in TIG-MIG/MAG welding process. **The International Journal of Advanced Manufacturing Technology**, v. 114, n. 5-6, p. 1505-1515, 2021.

BOHNART, E.R. **Welding: Principles and Practices**. 6TH Edition. New York. McGraw-Hill Education, 2017.

BOX, G.; HUNTER, J.; HUNTER, W. **Statistics for Experimenters: Design, Innovation,**

and Discovery. 2nd ed. New Jersey: JOHN WILEY & SONS INC., 2005.

CAI, X.; FAN, C.; LIN, S.; JI, X.; YANG, C.; GUO, W. Effects of shielding gas composition on arc properties and wire melting characteristics in narrow gap MAG welding. **Journal of Materials Processing Technology**, v. 244, p. 225-230, 2017. Accessed on: 01/26/2020.

CAO, X.; JAHAZI, M.; IMMARIGEON, J.; WALLACE, W. A review of laser welding techniques for magnesium alloys. **Journal of Materials Processing Technology**, v. 171, n. 2, p. 188-204, 2006.

CARLYLE W, MONTGOMERY D, RUNGER K. Optimization problems and methods in quality control and improvement. **J. Qual. Technol.** 2000; 32: 1–17.

CASTILLO, E., D.; MONTGOMERY, D. **A Nonlinear Programming Solution to the Dual Response Problem.** Journal of Quality Technology, v. 25, n. 3, p. 199-204, 1993.

CHEN, J.; ZONG, R.; WU, C.; PADHY, G.; HU, Q. Influence of low current auxiliary TIG arc on high speed TIG-MIG/MAG hybrid welding. **Journal of Materials Processing Technology**, v. 243, p. 131-142, 2017.

CIRINO, L.; DUTRA, J. The influence of positive polarity time on GTAW AC of aluminium. **Welding International**, vol. 24, p.825-833, 2010.

COSTA, G. C. S. **Avaliação de potencialidades do processo de soldagem tig-mig/mag com variação de polaridade no eletrodo MIG/MAG.** 118 p. Master Dissertation, Federal University of Goiás, Catalão, GO. 2019.

COSTA, G. S.; DE RESENDE, A. Evaluation of the TIG–MIG/MAG welding process in direct polarity. **SN Applied Sciences**, v. 2, n. 2, 2020.

COSTA, L. Welding with non-consumable thoriated tungsten electrodes. **Welding in the World**, v. 59, n. 1, p. 145-150, 2014.

DAI, H.; SHEN, X.; WANG, H. Study on the arc pressure of GTAW welding under the condition of Ar-Ar and Ar-He supply alternately. **Results in Physics**. vol 10, p. 917-922. doi:10.1016/j.rinp.2018.08.015, 2018.

DEGARMO, E.; BLACK, J.; & KOHSER, R. **DeGarmo's materials and processes in manufacturing**. 11th Edition. Wiley & Sons, 2012.

DING, M., LIU, S., ZHENG, Y., WANG, Y., LI, H., XING, W., YU, X. AND DONG, P. TIG–MIG hybrid welding of ferritic stainless steels and magnesium alloys with Cu interlayer of different thickness, **Materials and Design**, v. 88, pg. 375–383, 2015.

GOMES J. H. F. **Análise e otimização da soldagem de revestimento de chapas de aço ABNT 1020 com utilização de arame tubular inoxidável austenítico**; Universidade Federal de Itajubá, 2010.

GOMES, J. H. F.; SALGADO JÚNIOR, A. R. ;DE PAIVA, A. P. ;FERREIRA, J. R. ;COSTA, S. C. ;BALESTRASSI, P. P. . **Global Criterion Method Based on Principal Components to the Optimization of Manufacturing Processes with Multiple Responses.** Strojniški vestnik - Journal of Mechanical Engineering, [S.l.], v. 58, n.5, p. 345-353, june 2018. ISSN 0039-2480.

GROOVER, M. P. **Fundamentals of Modern Manufacturing : Materials, Processes, and Systems.** 4th Edition. J. Wiley & Sons, 2010.

GUMENYUK, A.; RETHMEIER, M. Developments in hybrid laser-arc welding technology. **Handbook of Laser Welding Technologies**, p. 505-521, 2013.

HAROONI, M.; CARLSON, B.; KOVACEVIC, R. Dual-beam laser welding of AZ31B magnesium alloy in zero-gap lap joint configuration. **Optics & Laser Technology**, v. 56, p. 247-255, 2014.

JEFFUS, L. **Welding principles and applications**. Clifton Park, N.Y.: Delmar Cengage Learning, 2012.

KALPAKJIAN, S., SCHMID, S., SEKAR, K. **Manufacturing Engineering And Technology**. 7th Edition. Prentice Hall; 2013.

KANEMARU, S.; SASAKI, T.; SATO, T.; ERA, T.; TANAKA, M. Study for the mechanism of TIG-MIG/MAG hybrid welding process. **Welding in the World**, v. 59, n. 2, p. 261-268, 2015.

KANEMARU, S., SASAKI, T., SATO, T., MISHIMA, H., TASHIRO, S. AND TANAKA, M. Study for TIG–MIG hybrid welding process. **Welding in the World**, v. 58, n. 1, p. 11-18, 2013.

KANNAN, T. e MURUGAN, N. **Effect of flux cored arc welding process parameters on duplex stainless steel clad quality.** Journal of Materials Processing Technology, v. 176, n. 1- 3, p. 230-239, 2006.

KOU, S. **Welding Metallurg**. 2nd Edition. New Jersey: John Wiley & Sons Incorporated; 2003.

KROS J, MASTRANGELLO C. **Comparing multi-response design methods with mixed responses**. Qual. Reliab. Eng. Int. 2004; 20: 527–539

KUMAR, K.; MOHAN, P.; MASANTA, M. Influence of welding current on the mechanical property of 3 mm thick commercial 1050 aluminium butt joint weld by AC-GTAW welding method. **Materials Today: Proceedings**, vol 5, n. 11, p. 24141-24146. doi:10.1016/j.matpr.2018.10.208, 2018.

LEE, C.; WOO, W.; BAEK, J.; KIM, E. Laser and arc manufacturing processes: A review. **International Journal of Precision Engineering and Manufacturing**, v. 17, n. 7, p. 973-985, 2016.

LI, D.; YANG, D.; LUO, X.; ZHANG, G. Effects of shielding gas on GMAW of 10Ni5CrMoV HSLA steel using high Cr-Ni austenitic wire. **Journal of Materials Processing Technology**, v. 259, p. 116-125, 2018.

LIANG, Y.; SHEN, J.; HU, S.; WANG, H.; PANG, J. Effect of TIG current on microstructural and mechanical properties of 6061-T6 aluminium alloy joints by TIG–CMT hybrid welding. **Journal of Materials Processing Technology**, v. 255, p. 161-174, 2018.

LIANG, Y.; HU, S.; SHEN, J.; ZHANG, H.; WANG, P. Geometrical and microstructural characteristics of the TIG-CMT hybrid welding in 6061 aluminium alloy cladding. **Journal of Materials Processing Technology**, v. 239, pg. 18–30, 2016.

LIU, Y.N.; KANNATEY-ASIBU E., Experimental study of dual-beam laser welding of AISI 4140 steel, **Weld**. J. 9,342–348, 1997.

MAHRLE, A.; ROSE, S.; SCHNICK, M.; BEYER, E.; FÜSSEL, U. Laser-assisted plasma arc welding of stainless steel. **Journal of Laser Applications**, v. 25, n. 3, p. 032006, 2013.

MAKOWSKI, M. **Methodology and a Modular Tool for Multiple Criteria Analysis of LP Models**. IIASA Working Paper. IIASA, Laxenburg, Austria: WP-94-102, 1994.

MAMAT, S.; TASHIRO, S.; TANAKA, M. Observation of Metal Transfer in Plasma MIG Welding Process. **QUARTERLY JOURNAL OF THE JAPAN WELDING SOCIETY**, v. 35, n. 2, p. 33s-37s, 2017.

MARINELLI, G.; MARTINA, F.; GANGULY, S.; WILLIAMS, S. Effect of shielding gas composition and Welding travel speed on autogenous welds of unalloyed tungsten plates. **International Journal of Refractory Metals and Hard Materials**, vol. 85, p. 105043. doi: 10.1016/j.ijrmhm.2019.105043, 2019.

MEI, K., GUO, Y., BAI, J., COSTA, P. M., KAFA, H., PROTTI, A., HIDER, R. C. AND AL-JAMAL, K. T. Organic Solvent-Free, One-Step Engineering of Graphene-Based Magnetic-Responsive Hybrids Using Design of Experiment-Driven Mechanochemistry. **ACS Applied Materials & Interfaces**, v. 7, n. 26, p. 14176-14181, 2015.

MENDEZ, P.F., EAGAR, T.W., **Penetration and defect formation in high-current arc welding**. Welding Journal 82, 296-306, 2003.

MENG, X.; QIN, G.; ZHANG, Y.; FU, B.; ZOU, Z. High speed TIG–MAG hybrid arc welding of mild steel plate. **Journal of Materials Processing Technology**, v. 214, n. 11, p. 2417-2424, 2014.

MESSLER, Robert W. What's next for hybrid welding? **Welding Journal**, v. 83, n. 3, p. 30-34, 2004.

MISHIMA, H.; TASHIRO, S.; KANEMARU, S.; TANAKA, M. Numerical simulation on plasma property in TIG-MIG/MAG hybrid welding process. **Quarterly Journal of the Japan**

Welding Society, v. 31, n. 4, p. 22s-25s, 2013.

MONTGOMERY, D. **Design and analysis of experiments**. New York. J. Wiley & Sons, 2013.

MUNCASTER, P. **Practical TIG (GTA) welding**. Cambridge: Abington, 1991.

MYERS, R.; MONTGOMERY, D.; ANDERSON-COOK, C. **Response surface methodology**. Hoboken, N.J.: Wiley, 2009.

NGUYEN, T. C.; WECKMAN, D. C.; JOHNSON, D. A.; KERR, H. W. High speed fusion weld bead defects. **Science and Technology of Welding and Joining**, v. 11, n. 6, p. 618-633, 2006.

OEHLERT, G. **A first course in design and analysis of experiments**. New York: Freeman, 2000.

PAN, J., HU, S.; YANG, L.; LI, H. Simulation and analysis of heat transfer and fluid flow characteristics of variable polarity GTAW process based on a tungsten–arc-specimen coupled model. **International Journal of Heat and Mass Transfer**, vol. 96, p.346-352, 2016.

PHILLIPS, D. **Welding engineering. Traducao** . Chichester: John Wiley & Sons, Ltd., 2016.

PRITCHARD, D. **Soldering, Brazing and Welding**. 1st Edition. Ramsbury: The Crowood Press Ltd, 2001.

RESENDE, A. A.; FERRARESI, V.; SCOTTI, A.; DUTRA, J. Influência das correntes de soldagem do processo Plasma-MIG sobre a geometria do cordão de solda e taxa de fusão do arame. **Soldagem & Inspeção**, v. 14, n. 4, p. 320-328, 2009.

RESENDE, A. A.; FERRARESI, V.; SCOTTI, A.; DUTRA, J. Influence of welding current in plasma–MIG weld process on the bead weld geometry and wire fusion rate, **Welding International**, 25:12, 910-916, 2011.

RESENDE, A. A.; SCOTTI, A. Influence of current levels, the tilt angle of the torch and the

distance between the torch and the part on the geometry of the weld bead using ‘Plasma-MIG’ with concentric arcs. **Welding International**, v. 31, n. 10, p. 747-757, 2017.

RYBERG A. B, DOMEIJ B. R, NILSSON L. **Metamodel-Based Multidisciplinary Design Optimization for Automotive Applications**. Linköping: Linköping University Electronic Press; 2012.

SAHASRABUDHE, O.; RAUT, D. Benchmarking of Hybrid TIG-MAG Arc Welding for Mild Steel. **Transactions of the Indian Institute of Metals**, v. 72, n. 3, p. 801-810, 2019.

SAHASRABUDHE, O.; RAUT, D. Analytic framework on parameter ranking for hybrid TIG MAG arc welding of mild steel. **Journal of Advanced Research**, v. 12, p. 27-37, 2018a.

SAHASRABUDHE, O.; RAUT, D. Effect of Heat Source Positioning on Hybrid TIG-MAG Arc Welding Process. **Materials Today: Proceedings**, v. 5, n. 9, p. 18518-18526, 2018b.

SAMIR KHAN, M.; KUMAR, V.; MANDAL, P.; CHANDRA MONDAL, S. Experimental Investigation of Combined TIG-MIG/MAG Welding for 304 Stainless Steel Plates. **IOP Conference Series: Materials Science and Engineering**, v. 377, p. 012067, 2018.

SCHNEIDER, C.; LISBOA, C.; SILVA, R.; LERMEN, R. Optimizing the Parameters of GTAW-GMAW Hybrid Welding on the Geometry of Bead Welding Using the Taguchi Method. **Journal of Manufacturing and Materials Processing**, v. 1, n. 2, p. 14, 2017.

SHEN, X.; MA, G.; CHEN, P. Effect of welding process parameters on hybrid GMAW-GTAW welding process of AZ31B magnesium alloy. **The International Journal of Advanced Manufacturing Technology**, v. 94, n. 5-8, p. 2811-2819, 2017.

SPS – **Sistemas e Processos de Soldagem**. (2012) Available: http://www.sps-soldagem.com.br/tartilope_v2.php. Accessed on: 07/21/2020

SUMESH, A.; NAIR, B. B.; RAMESHKUMAR, K.; SANTHAKUMARI, A.; RAJA, A.; MOHANDAS, K. Decision tree based weld defect classification using current and voltage signatures in GMAW process. **Materials Today: Proceedings**, v. 5, n. 2, p. 8354-8363, 2018.

TAGUCHI, G.; CHOWDHURY, S.; WU, Y.; TAGUCHI, S.; YANO, H. **Taguchi's quality**

engineering handbook. Hoboken, N.J.: John Wiley & Sons, 2005.

TANG, Y.; ZHU, Z.; YANG, Z.; FU, P.; YU, Y. TIG arc-induced non-contact MIG arc ignition. **Journal of Materials Processing Technology**, v. 257, p. 45-53, 2018.

TAZETDINOV, R.; NOVIKOV, O.; PERSIDSKII, A.; KHASYANOV, B.; IVANOV, E.; PLAKSINA, L. Arc welding in shielding gases with alternate pulsed supply of dissimilar gases. **Welding International**, vol 27, p.311-314. doi:10.1080/09507116.2012.715912, 2013.

WANG, L.; CHEN, J.; WU, C.; GAO, J. Backward flowing molten metal in weld pool and its influence on humping bead in high-speed GMAW. **Journal of Materials Processing Technology**, v. 237, p. 342-350, 2016.

WANG, L.; LI, X.; GAO, M.; ZENG, X. Stabilization mechanism and weld morphological features of fiber laser-arc hybrid welding of pure copper. **Journal of Manufacturing Processes**, v. 27, p. 207-213, 2017.

WANG, W.; CHENG, Y.; TAN, G. Design Optimization of SBS-Modified Asphalt Mixture Reinforced with Eco-Friendly Basalt Fiber Based on Response Surface Methodology. **Materials**, v. 11, n. 8, p. 1311, 2018.

WONG, Y.; LING, S. An investigation of dynamical metal transfer in GMAW—Effects of argon shielding gas. **Journal of Materials Processing Technology**, v. 214, n. 1, p. 106-111, 2014.

XIE J. Dual beam laser welding. **Welding Journal**, v.81, p. 223–230, 2002.

ZHAN, Y.; LI, Y.; ZHANG, E.; GE, Y.; LIU, C. Laser ultrasonic technology for residual stress measurement of 7075 aluminium alloy friction stir welding. **Applied Acoustics**, v. 145, p. 52-59, 2019.

ZHANG, H.; LIU, J.; FENG, J. Effect of auxiliary TIG arc on formation and microstructures of aluminium alloy/stainless steel joints made by MIG welding-brazing process. **Transactions of Nonferrous Metals Society of China**, v. 24, n. 9, p. 2831-2838, 2014.

ZONG, R.; CHEN, J.; WU, C. A comparison of TIG-MIG/MAG hybrid welding with conventional MIG welding in the behavior of arc, droplet and weld pool. Journal of Materials Processing Technology, v. 270, p. 345-355, 2019.

ZUO, W., MA, L., LU, Y., LI, S., JI, Z. AND DING, M.. Effects of Solution Treatment Temperatures on Microstructure and Mechanical Properties of TIG–MIG Hybrid Arc Additive Manufactured 5356 Aluminium Alloy**. Metals and Materials International**, v. 24, n. 6, p. 1346-1358, 2018.

APPENDIX A

OPTIMIZATION MODEL

Figure 48 illustrates the optimization schema built in Microsoft Office Excel®.

Models

	Max	Max	Min	Min	Min	coded variables
	W	R	P	θ	D	α [-1.41;1.41]
Constant	10.71	2.61	2.14	35.29	40.34	1.00
h2 (mm)	0.24	- 0.03	0.09	1.08	- 0.25	- 0.53
d (mm)	0.58	- 0.08	0.08	- 3.46	1.79	- 0.39
θ1 (º)	- 0.22	0.02	- 0.07	0.73	- 0.73	0.44
TC (A)	0.09	- 0.03	0.23	0.14	2.60	- 1.17
h2 (mm)*h2 (mm)	0.28	- 0.04		- 1.06	0.55	0.28
d (mm)*d (mm)	0.23	- 0.04		0.41	1.03	0.15
θ1 (º)*θ1 (º)	- 0.16	0.07		3.20	- 1.12	0.19
TC (A)*TC (A)	0.01	0.04		0.52	- 0.24	1.37
h2 (mm)*d (mm)	0.19	- 0.01		- 0.74	- 0.59	0.21
h2 (mm)*θ1 (º)	- 0.07	- 0.04	0.04	- 0.98	1.53	- 0.23
h2 (mm)*TC (A)	0.24	- 0.04		0.16	1.28	0.62
d (mm)*θ1 (º)	- 0.28	0.04		0.75	0.43	- 0.17
d (mm)*TC (A)	0.55	- 0.10		- 5.09	2.33	0.46
θ1 (º)*TC (A)	- 0.01	0.02		1.36	- 0.46	- 0.51

Restrictions

g(x)	2.00	<=	2.00

Results

	W	R	P	θ	D
Objective Funcion	10.76	2.68	1.76	34.34	37.72
Target	**12.65**	**2.75**	**1.76**	**27.16**	**35.22**

Pay-off

	W	R	P	θ	D
W	**12.65**	2.35	2.43	28.75	46.16
R	10.68	**2.75**	2.02	40.05	36.88
P	10.76	2.68	**1.76**	34.38	37.72
θ	12.26	2.38	2.42	**27.16**	47.86
D	10.81	2.73	1.96	37.87	**35.22**

Normalization

	W	R	P	θ	D
d_mod	4%	82%	100%	44%	80%
w	0.05	0.05	0.8	0.05	0.05
F(x)_mod	0.90535648				

Figure 48 – Spreadsheet built to calculate the optimization of the parameters for the TIG-MIG/MAG hybrid welding applied on weld overlay on steel plates (SAE 1020).

Source: (Author).